DOCTOR OF PHILOSOPHY

A study of chromatin dynamics during transcription by fluorescence light microscopy

Dickerson, David

Award date:
2010

DOCTOR OF PHILOSOPHY

A study of chromatin dynamics during transcription by fluorescence light microscopy

David Dickerson

2010

University of Dundee

A Study of Chromatin Dynamics during Transcription by Fluorescence Light Microscopy

David Dickerson

A thesis submitted for the degree of Doctor of Philosophy
Supervisor: Professor Tom Owen-Hughes
University of Dundee
October 2010

TABLE OF CONTENTS

ABSTRACT

The genes of eukaryotes exist as DNA-RNA-protein complexes known as chromatin. The structure of chromatin fluctuates to allow controlled access to genetic information while maintaining its important packaging function. Recent improvements in optics, image acquisition electronics, and live imaging techniques, as well as the introduction of fluorescent fusion proteins, have made it possible to use fluorescence light microscopy to study the dynamic nature of chromatin compaction in cells. Here we report the application of advanced fluorescence microscopy to characterize the effects of transcription on chromatin compaction in living yeast cells. Repressor protein-GFP fusion proteins which recognize specific operator sequences were used to fluorescently tag specific gene loci, and an OMX fluorescence light microscope was then used to track their positions in three dimensions. It was determined that image acquisition with the OMX microscope is rapid enough to track fluorescently tagged genomic loci in live yeast cells in 3D, and that it does so with a root mean squared (RMS) measurement error of 162 nanometers (nm). It was also determined that the OMX microscope can distinguish between strains with fluorescent spots separated by 40 or 70 kb genomic distances. Additionally, it was found that chromatin compaction of a 15 kb gene driven by the Gal1 promoter is correlated with the carbon source on which the cells are fed, and that three different carbon sources produce three different transcription-dependent chromatin structures. Reversible changes in end-to-end distance of ~500 nm within two seconds were detected in the induced strain. These findings indicate that improvements in light microscopy enable chromatin to be studied in living cells on a scale not previously possible.

LIST OF FIGURES AND TABLES

ABBREVIATIONS

3C	Captures the Conformation of Chromatin
3D	3-dimensional
AFM	Atomic Force Microscope
ATP	Adenosine TriPhosphate
CENP-A	CENtromere Protein A
CFP	Cyan Fluorescent Protein
CHD1	Chromodomain-Helicase-DNA-binding protein
ChIP	Chromatin ImmunoPrecipitation
CHO	Chinese Hamster Ovarian
CTD	C-Terminal Domain
DHFR	DiHydroFoliate Reductase
DLC1	Dynein Light Chain 1
DNA	DeoxyriboNucleic Acid
DNMT3B	DNA (cytosine-5)-MethylTransferase 3B
dNTPs	Deoxynucleotide TriPhosphates
EM	Electron Microscopy
FACT	FAcilitates Chromatin Trancription
FISH	Fluorescence In Situ Hybridization
FJC	Freely Jointed Chain
FLIP	Fluorescence Loss In Photobleaching
FRAP	Fluorescence Recovery After Photobleaching
GFP	Green Fluorescent Protein
H3K4me2	Histone H3 Lysine 4, di-methyl
HAT	Histone AcetylTransferase
HDAC	Histone DeAcetylase Complex
HP1	Heterochromatin Protein 1
HSF	Heat Shock Factor
HSP70	Heat Shock Protein 70
IFM	ImmunoFluorescence Microscopy
ISWI	Imitation SWItch
LCR	Locus Control Region
NCP	Nucleosome Core Particle
NFR	Nucleosome Free Region
OMX	Optical Microscope eXperimental
ORF	Open Reading Frame
PCR	Polymerase Chain Reaction
PHD	Plant HomeoDomain
PIC	Pre-Initiation Complex
RNA	RiboNucleic Acid
RSC	Remodels the Structure of Chromatin
SAGA	Spt-Ada-Gcn5-acetyltransferase complex
SANT	Swi3, Ada2, N-Cor, TFIIB
SNF	Sucrose Non-Fermenting
SPM	Scanning Probe Microscopy
SWI	Homothallic switching
SWP	SWI/SNF complex Protein
TBP	TATA Binding Protein
TFIIB	RNA Polymerase II Transcription Factor complex IIB
TOP1	TOPoisomerase I
TSS	Transcriptional Start Site

ACKNOWLEDGEMENTS

Many thanks to Tom Owen-Hughes, Triantafyllos Gkikopoulos, Hilary Dewar, Vijender Singh, Elisa Garcia-Wilson, Andrew Bowman, Nicola Wiechens, Ramasubramanian Sundaramoorthy, Daniel Ryan, Maik Engeholm, and Helder Ferreira for their help with cloning and for lively discussions. Also many thanks to Joost Zomerdijk, Mike Stark, Gyurgy Hutvagner, Iestyn Whitehouse, and David Lilley for lively discussions. We thank Kevin Struhl's lab for generously providing the Yiplac204-GAL1-MDN1 plasmid, and the Grunstein Lab for generously providing yeast H3 and H4 tail truncation strains. Thanks to Tomoyuki Tanaka, Toyoaki Natsume, Jean-Francoise Maure, Matt Renshaw, Sapan Gandhi, and Etsushi Kitamura of the Tanaka Lab for help and for generously providing the yeast strains 1200, 1201, and 1252. Thanks to Jason Swedlow, Emma King, Markus Posch, Alexia Ferrand, and Michael Porter for assistance with tracking and training on the OMX microscope. We thank Khuloud Jaqaman and Gaudenz Danuser for their software programming efforts, providing their tracking software, and assistance in its use. Also thanks to Sam Swift, Paul Appleton, Alan Prescott, and Callum Thomsom for their help with microscopy. We thank Marek Gierlinski of the Data Analysis Group of the University of Dundee for help with fitting the Porod-Kratky chain equation to our data set and advice on histogram analysis. The OMX microscope of the University of Dundee was provided for by the Scottish Universities Live Sciences Alliance (SULSA), a strategic partnership between the Universities of Aberdeen, Dundee, Edinburgh, Glasgow, St Andrews and Strathclyde, and the Scottish Funding Council (SFC). We thank the people of Applied Precision for their help with the OMX and Deltavision microscopes. We thank DNA Sequencing & Services (MRCPPU, College of Life Sciences, University of Dundee, Scotland, www.dnaseq.co.uk) for DNA sequencing. Many thanks to the members of the Wellcome Trust Biocentre Media Kitchen. And I would especially like to thank Dr. Gail Miller for all of her support.

DECLARATION

I, David Dickerson, declare that I am the sole author of this thesis, that the research presented here is my own unless there is a clear statement otherwise. None of this research has previously been accepted for a higher degree.

David Dickerson

I certify that David Dickerson has spent the equivalent of at least nine terms in research work at the University of Dundee Wellcome Trust Centre for Gene Regulation and Expression and that he has fulfilled the conditions of the Ordinance General No. 14 of the University of Dundee and is qualified to submit the accompanying thesis in application for the degree of Doctor of Philosophy.

Tom Owen-Hughes

CHAPTER 1

Introduction

1.1 Chromatin structure

1.1.1 DNA

The genetic element of living organisms and some viruses is DNA. Within eukaryotes, DNA exists in a condensed form known as chromatin (Becker and Horz 2002) whose fundamental subunit is the nucleosome (Phillips and Johns 1965). Nucleosomes consist of pairs of four basic histone proteins wrapped by 146 base pairs of DNA (Kornberg 1974).

1.1.2 Histones

Histones are alkaline proteins which package DNA and are the major protein component of chromatin (Kornberg and Lorch 1999). There are five major classes of histones in eukaryotes: the core histones H2A, H2B, H3, and H4, and the linker histone H1 (Phillips and Johns 1965). Variants exist within the histone classes which have roles in various nuclear processes including transcription (Talbert and Henikoff 2010). The post-translational modification of histones has been shown to alter chromatin structure and has roles in a variety of cellular processes, including transcription, as will be discussed in section 1.1.4. (Strahl and Allis 2000).

The core histones share a globular structural motif known as the histone fold, and also have relatively unstructured N-terminal and C-terminal extensions or tails which make up approximately 25% their masses (Arents, Burlingame et al. 1991; Zheng and Hayes 2003). All four core histone N-terminal tails are associated with histone-DNA interactions and the formation of higher order chromatin structure (Zheng and Hayes 2003) primarily through protein-protein interactions dependent on post-translational modifications (Hansen, Tse et al. 1998), although the majority of chromatin fiber formation is attributed to the H4 tail (Dorigo, Schalch et al. 2003).

Linker histone H1 is a chromatin architectural protein that plays a role in the formation and maintenance of higher order chromatin structure through the binding of nucleosomes (discussed below) at DNA entry and exit sites (McBryant, Lu et al. 2010). The globular domain of the histone contains two DNA binding domains, and thus H1 may bridge different DNA molecules, and in this manner stabilize nucleosomal arrays to form higher order fibers (McBryant, Lu et al. 2010). In higher eukaryotes H1 is an abundant protein that is found in stoichiometric ratios of almost 1:1 with nucleosomes (Bates, Butler et al. 1981; Woodcock, Skoultchi et al. 2006). The yeast histone H1, Hho1p, plays a minor role in a subset of genomic loci where it functions as a negative regulator of transcriptional silencing through interactions with histone H4 (Yu, Kuzmiak et al. 2009). Deletion strains show no detectable growth, viability or mating phenotypes (Ushinsky, Bussey et al. 1997).

1.1.3 The histone octamer

Histone folds act as dimerization interfaces which enable histones to form dimer pairs (Arents, Burlingame et al. 1991). Two dimers of H3 and H4 bind via H3-H3 interactions to form a tetramer (Arents, Burlingame et al. 1991; White, Suto et al. 2001; Wood, Nicholson et al. 2005), while two H2A/H2B dimers sandwich the H3/H4 tetramer through interactions between H2B and H4 to form the octamer (Wood, Nicholson et al. 2005). The structure of the histone octamer has been solved via x-ray crystallography at a resolution of 1.90 Angstroms (Wood, Nicholson et al. 2005).

1.1.4 The nucleosome

The fundamental unit of chromatin is the nucleosome core particle (NCP) which consists of 146 bases of DNA wrapping 1.67 times around a histone octamer, the whole forming a left-handed helix with lateral dimensions of 11 nm (Phillips and Johns 1965; Kornberg and Thomas 1974; Luger, Rechsteiner et al. 1997). Through wrapping of DNA around the 6.5 nm diameter octamer, a 6-fold minimum compaction of the DNA is achieved (Arents, Burlingame et al. 1991).

Atomic resolution structures for the NCP have been solved by x-ray crystallography (Richmond and Davey 2003), and they indicate that the nucleosome contains over 120 contact points between the positively charged histones and the negatively charged DNA (Luger and Richmond 1998). This explains the stability of the complex, which resists denaturation at temperatures up to ~65^{o}C in 10 mM NaCl (Van Holde, Allen et

al. 1980). Although the NCP is stable to dissociation, it can be repositioned laterally as there are no sequence specific contacts between the histones and the DNA.

The N-terminal tails of the core histones flank the DNA gyres and extend beyond the nucleosome core structure (McBryant, Lu et al. 2010). These domains are not resolved in crystal structures and are thought to be relatively unstructured (Luger 2006).

1.1.4.1 Nucleosome positioning

Nucleosomes are typically separated by short sequences of linker DNA (Spadafora, Bellard et al. 1976), and in yeast are spaced roughly every 160-165 bases to form nucleosomal arrays (van Holde 1988). The deformation of DNA is energetically costly (Trifonov 1980; Satchwell, Drew et al. 1986; Widom 2001), and it has been demonstrated that there is a large sequence-dependent difference in free energy for nucleosome assembly (Thastrom, Lowary et al. 2004). As a result formation of nucleosomes is more favorable on some DNA sequences than others (Kunkel and Martinson 1981; Drew and Travers 1985; Fitzgerald D. 1999; Whitehouse and Tsukiyama 2006) (Lee, Tillo et al. 2007; Valouev, Ichikawa et al. 2008). A hallmark of DNA sequences that favors nucleosome deposition is a periodicity in A/T and G/C sequences. X-ray crystallography, solution studies, analysis of the free energies of different DNA sequences interacting with octamers, DNA arrays, and ChIP-seq studies indicate that A/T dinucleotides tend to face inward while short poly-G or poly-C runs tend to face outward in nucleosomes, and that, *in vivo*, these sequences tend to have a periodicity of 10 base intervals, consistent with the periodicity of helical twist

of B-form double stranded DNA (Drew and Travers 1985; Thastrom, Lowary et al. 1999). Other sequences are known to be inhibitory to the formation of nucleosomes. These sequences tend to be poly-A or poly-T rich, and are evolutionarily conserved (Yuan, Liu et al. 2005). The Weng Lab has developed an algorithm based on whole-genome *S. cerevisiae* nucleosome binding affinities which calculates the nucleosome formation potential of an input sequence (Peckham, Thurman et al. 2007). This study found that nucleosome inhibitory signals often span nucleosome length stretches of genomic DNA (Peckham, Thurman et al. 2007).

Recent high throughput sequencing and DNA array data indicate that nucleosomes tend to occupy conserved positions within the genomes of different organisms (Lee, Tillo et al. 2007; Valouev, Ichikawa et al. 2008). These studies revealed prominent patterns such as nucleosome depletion at transcriptional start sites (TSSs) and ordered nucleosome positioning at promoters (Segal, Fondufe-Mittendorf et al. 2006). Nucleosome numbering convention places the +1 nucleosome at transcriptional start sites (TSSs), with nucleosome number increasing through the open reading frame (ORF), while nucleosome numbers, starting with the -1 nucleosome, decrease upstream of the TSS. Tiled microarray analysis of nucleosome positioning indicated that many yeast genes have nucleosome free regions (NFRs) ~200 bases upstream of TSSs, and different explanations for this have been proposed. It was initially proposed that such NFRs are associated with rapid transcription initiation (Yuan, Liu et al. 2005). However, more recently, it has been shown that nucleosome positioning is retained in the absence of transcription (Fan, Moqtaderi et al. 2010).

Currently, several different factors are proposed to contribute to nucleosome positioning genomewide. These include:

1. The underlying DNA sequence to which the octamer is bound (Kunkel and Martinson 1981; Fitzgerald D. 1999; Segal, Fondufe-Mittendorf et al. 2006; Whitehouse and Tsukiyama 2006)
2. Sequence-specific transcription factor or repressor binding and forming positional barriers at promoter regions (Tirosh, Sigal et al. ; Zhang, Moqtaderi et al. 2009).
3. Nucleosomal sliding and eviction activities of various ATP-dependent chromatin remodeling enzymes (Flaus, Martin et al. 2006)

The relative contributions of these factors to nucleosome positions *in vivo* are a matter of debate (Kaplan 2010; Pugh 2010; Zhang 2010).

While nucleosomes fulfill packaging roles they also act as an impediment to genetic processes including transcription, replication, DNA repair, and recombination (Knezetic and Luse 1986; Lorch, LaPointe et al. 1987; Workman and Kingston 1998). All eukaryotes have evolved a series of strategies to contend with chromatin, including post-translational modification of histones, histone variant incorporation, and the alteration of chromatin structure via ATP-dependent chromatin remodeling enzymes.

1.1.4.2 Histone post-translational modifications

Histone post-translational modifications include acetylation, methylation, ubiquitination, phosphorylation, ADP-ribosylation, sumoylation, de-imination, and

proline isomerization (Kouzarides 2007). Additionally, methylation of lysines and arginines may take one of several different forms, including mono- or di-methyl for arginines, and mono-, di-, or tri-methyl for lysines (Kouzarides 2007). Since all four nucleosomal histones, as well as linker histones, may be modified at various residues along their lengths (Li, Carey et al. 2007), the overall complexity of possible histone modification patterns is vast.

A subset of these modifications serve as recognition sites for various chromatin-binding proteins, and it has been proposed that the patterns of histone modifications, through interactions with these proteins, constitute a histone code that directs differential recruitment of various proteins which interact with and modify chromatin (Luger and Richmond 1998; Spencer and Davie 1999; Strahl and Allis 2000; Turner 2000; Mersfelder and Parthun 2006).

Some histone modifications are recognized by specific chromatin binding domains of a range of proteins, and by joining the domains with other enzymatic activities, the histone modifications are linked to downstream events. Examples of these binding domains include chromodomains, bromodomains, and PHD domains, which bind methylated histones, acetylated histone tails, and methylated lysines, respectively (Kouzarides 2007). The most-studied chromodomain-containing protein with such a binding activity is HP1, which binds tri-methylated histone H3 on lysine 9 in higher eukaryotes and links this modification with deacetylase and methyltransferase activities which are associated with the formation of higher order, repressive chromatin structure (Kouzarides 2007).

Other lines of evidence conflict with the histone code theory. For example, ING2, a subunit of the mSin3a-HDAC1 histone deacetylase complex, binds histone H3K4me2 and H3K4me3 at the promoters of a subset of proliferation genes, where it acts to deacetylate adjacent histone tails, repressing the genes (Shi, Hong et al. 2006). This finding was unexpected given that H3K4 di- and tri-methylation have historically been associated with active transcription. Examples of such dual roles for individual histone modifications implicate the binding proteins, rather than the modifications, in the coordination of downstream events.

Recently significant progress has been made mapping histone modifications genome wide in attempt to correlate different modification patterns with specific cellular functions. For example, histone H3 lysine 4 mono- and di-methylation, H3 lysine 79 methylation, H3 lysine 36 methylation, and acetylation at various residues along the H3 tail were mapped via chromatin immunoprecipitation followed by DNA microarray, and have all been shown to be positively correlated with transcription (Rando 2007). Specifically, lysine 4 dimethylation has been shown to associate with active promoters, and methylation of lysines 36 and 79, as well as histone tail acetylation, have been shown to associate with transcribing open reading frames (ORFs) (Rando 2007). Similar studies have been performed in other organisms, including humans. An emerging theme is that the combinations of modifications observed do not appear to be as high as theoretically possible. This reduces the potential for a histone code of high complexity.

Histone tail modifications are thought to affect higher order chromatin structure and have roles in various cellular processes such as transcription, DNA repair, formation

of centromeres, mitotic chromosomal condensation, recombination, and replication (Strahl and Allis 2000; Yu, Teng et al. 2005; Chen, Carson et al. 2008; Li, Zhou et al. 2008) (Zheng and Hayes 2003). A minority of histone modifications are thought to have direct effects on chromatin fiber structure through changes in charge, as in the case of histone tail lysine acetylation which is thought to neutralize positive charges on histone tails, and thus allow electrostatic repulsion between negative charges on the DNA backbone, which de-condenses the chromatin fiber (Fletcher and Hansen 1996; Knoepfler and Eisenman 1999; Strahl and Allis 2000). Histone H4 acetylation at lysine 16, which is present in 80% of yeast histones, inhibits cross-fiber interactions and the formation of compact 30 nm-like fibers (Shogren-Knaak, Ishii et al. 2006). Histone tail modifications are relatively easily detected via mass spectrometry, and for this reason they have been studied to a greater extent than modifications on the globular domains.

Histones are also modified within their globular domains (Hyland, Cosgrove et al. 2005) (Mersfelder and Parthun 2006). Globular domain modifications have greater potential for directly altering chromatin structure due to their location within the structural region of the nucleosome. Structural analysis reveals that globular histone modifications may be categorized as either affecting the solute accessible face, the histone lateral surface, or the histone-histone interfaces (Cosgrove, Boeke et al. 2004; Freitas, Sklenar et al. 2004), but the functional implications of modifications at these sites have not been determined. An example of a globular domain histone modification is acetylation of histone H3 on lysine 56 (Donaldson 2005), which is a residue found on the histone-lateral surface (Cosgrove, Boeke et al. 2004). This modification is catalyzed by Rtt109 (Fillingham, Recht et al. 2008), and increases the

affinity of H3 with chaperone proteins CAF-1 and Rtt106. This modification has been shown to be associated with newly synthesized DNA as well as newly incorporated nucleosomes at the site of repaired double strand breaks (Chen, Carson et al. 2008; Li, Zhou et al. 2008), and is associated with correct positioning of a subset of chromosomal domains within the nucleus (Hiraga, Botsios et al. 2008).

In yeast, the Spt7, Ada2, Gcn5 acetyltransferase (SAGA) complex exemplifies the variety of effects which may be linked by one complex which contains a histone modification-binding domain. This complex contains a bromodomain, which allows it to interact with acetylated histone tails, contains a histone acetyltransferase (HAT) activity which allows it to further acetylate histone tails, which is associated with the formation of an open, extended chromatin conformation. The complex combines this with an ability to recruit transcriptional activators and basal transcription machinery (Grant, Sterner et al. 1998; Sterner, Grant et al. 1999). Additionally, the SAGA complex is thought to play a role in the recruitment of specific genomic loci such as the Gal1 locus to the nuclear periphery during transcription where it interacts with nuclear pore proteins and upregulates Gal1 transcription rates (Cabal, Genovesio et al. 2006). By linking histone tail modifications with enzymatic activities through binding domains such as the bromodomain, a single protein complex such as SAGA can thus have an effect on multiple downstream pathways, ranging from effects on local histone acetylation, with concurrent decondensation of local chromatin structure, to transcription, which can alter the chromatin structure of a specific open reading frame, and finally, to large-scale translocations of chromatin within the nucleus.

1.1.4.3 Histone variants

In addition to the four canonical core histones, a series of minor variants are also encoded in eukaryotes which provide the means of altering the functions of a subset of nucleosomes within a given genome (Boulard, Bouvet et al. 2007; Zlatanova, Bishop et al. 2009; Talbert and Henikoff 2010). The most common among these are variants of H2A and H3 (Talbert and Henikoff 2010). Nucleosomes containing variants have been proposed to exhibit differences in their stability, DNA wrapping, and post-translational modifications, compared to the canonical histones H2A, H2B, H3 and H4. These variants can be enzymatically exchanged for their canonical counterparts, leading to site-specific alterations in nucleosome biophysical properties and can ultimately facilitate a number of cellular processes, such as chromosome segregation, transcriptional regulation, DNA repair, and sperm packaging (Talbert and Henikoff 2010). Many histone variants are deposited throughout the cell cycle, as opposed to the majority of conventional histones which are deposited behind the replication fork during S-phase (Henikoff 2009).

The histone variant Htz1 (H2A.Z) is associated with the regulation of a number of biological processes in yeast, including transcription, cell cycle progression, heterochromatin silencing, and chromosome segregation (Guillemette and Gaudreau 2006). It is enriched at the 5' ends of both active and inactive genes in euchromatic promoters (Raisner, Hartley et al. 2005), where its deposition is Swr1-dependent (Krogan, Keogh et al. 2003; Mizuguchi, Shen et al. 2004; Zhang, Roberts et al. 2005). It has been shown to inhibit the ectopic spreading of heterochromatin into euchromatic regions (Abbott, Ivanova et al. 2001; Meneghini, Wu et al. 2003). *In*

vitro experiments show that Htz1 is released from chromatin under conditions where H2A and H3 remain associated, (Zhang, Roberts et al. 2005), and that NCPs which have incorporated Htz1 are substantially destabilized, implicating it in a role of transcriptional activation (Abbott, Ivanova et al. 2001). Furthermore, deletion of the gene increases the requirement for chromatin remodeling enzymes during transcriptional activation of a subset of loci (Santisteban, Kalashnikova et al. 2000), perhaps because canonical histones are more stable, and thus more difficult to slide or evict during initiation.

Other histone variants include the H3 centromeric histone variant CENP-A, which in yeast is known as Cse4, the H3 variants H3.1, H3.2, and H3.3, and H2A.X (Talbert and Henikoff 2010).

1.1.4.4 ATP-dependent chromatin remodeling enzymes

ATP-dependent chromatin remodeling enzymes share a catalytic core with homology to helicases which is thought to act as an ATP-dependent DNA translocating motor (Flaus and Owen-Hughes 2001). These proteins are related to the yeast Snf2 protein and thus are referred to as Snf2 family proteins. This family encompasses 24 distinct subfamilies which catalyze a variety of different activities, most of which are broadly conserved among species. Many subfamilies are linked to roles relating to chromatin and catalyze a range of distinct transitions in chromatin structure. For example, CHD1 and ISWI have been shown to catalyze the establishment of ordered nucleosomal spacing, and SWI/SNF and RSC are associated with the disruption of nucleosome structure and the displacement of histones (Clapier and Cairns 2009).

The Swr1 protein has recently been implicated in implicated in the deposition of histone variant H2A.Z at boundaries of heterochromatin in yeast in order to establish and maintain an anti-silencing activity (Zhou, Wang et al. 2010). Other members of this family perform roles which do not pertain to chromatin; for example, Mot1 and SWI/SNF have been demonstrated to be associated with transcription factor eviction (Auble, Wang et al. 1997; Kia, Gorski et al. 2008), while the SSO family are found in microbial species which do not code for histones, indicating a difference in function with respect to eukaryotes (Flaus, Martin et al. 2006).

The process of transcription is strictly controlled and under certain circumstances must be initiated rapidly (Jin, Zang et al. 2009; Floer, Wang et al. 2010), and in this regard several chromatin remodeling enzymes are known to perform remodeling roles at promoters. The +1 nucleosome, which often contains the histone variant H2A.Z as a result of a dimer exchange activity of the ATP-dependent chromatin remodeling complex Swr1 (Wu, Wu et al. 2009), is thought to be unstable due as a result of the presence of this variant. This instability has been proposed to facilitate its eviction during transcription initiation (Jin, Zang et al. 2009). ATP-dependent chromatin remodeling enzymes also have roles in the exposure of underlying regulatory regions such as TATA boxes during transcription initiation in a process called DNA site exposure (Havas, Flaus et al. 2000; Saha, Wittmeyer et al. 2005). For example, the RSC complex associates with a specific nucleosome at the Gal1 promoter, where it positions it such that it is partially unwound, with the Gal4 binding site exposed (Floer, Wang et al. 2010). Nucleosomes have been shown to be generally well-ordered at TSSs (Segal, Fondufe-Mittendorf et al. 2006), and this has been attributed to the activities of a number of ATP-dependent chromatin remodeling enzymes. For

example, ISWI and CHD1 have been shown to catalyze the even-spacing of nucleosomes within ORFs and promoters (Xella, Goding et al. 2006).

Nucleosome remodeling activities have been detected during transcriptional elongation as well. SWI/SNF has been shown to catalyze the eviction of nucleosomes ahead of elongating Pol II in a subset of ORFs, including the Gal10 gene (Schwabish and Struhl 2007), and histone depletion has been independently observed at this gene (Govind, Zhang et al. 2007). Such activity could result in changes in chromatin structure on a scale which are detectable by the fluorescence light microscope.

Most chromatin remodeling enzymes bind DNA non-specifically (Quinn, Fyrberg et al. 1996), and are either recruited to their site of action through interactions with transcription factors which do have sequence specificity and can bind nucleosomal DNA (Taylor, Workman et al. 1991; Cote, Quinn et al. 1994; Adams and Workman 1995; Utley, Cote et al. 1997; Sudarsanam and Winston 2000; Neely, Hassan et al. 2002), or through interactions of their binding domains with specific histone modifications (Hassan, Prochasson et al. 2002).

1.1.4.5 Other factors which alter chromatin structure

Chromatin structure is also subject to dynamic alteration through the activities of various proteins and complexes such as facilitates chromatin transcription (FACT), heat shock factor (HSF), GAGA factor (GAF), histone chaperones, and poly(ADP)-ribose (PARP) ; and various motor proteins such as nuclear actin, nuclear myosin, condensins, topoisomerases, dynein, and Pol II itself (Thrash, Bankier et al. 1985;

Schwabish and Struhl 2004; Schwabish and Struhl 2006; Weake and Workman 2008; Gong, Kakihara et al. 2009)(reviewed in (Gasser, Laroche et al. 1986; Morse 1992; Hirano and Mitchison 1994; Studitsky, Clark et al. 1994; Freeman, Aragon-Alcaide et al. 2000; Champoux 2001; Swedlow and Hirano 2003; Maeshima, Eltsov et al. 2005; Chuang, Carpenter et al. 2006; Carmo-Fonseca 2007; Hizume, Araki et al. 2007; Nunez, Kwon et al. 2008; Roca 2009; Durand-Dubief, Persson et al. 2010; Visa and Percipalle).

1.3 Higher Order Chromatin Structure

Studies of chromatin structure have characterized chromatin fibers of various sizes ranging from naked DNA (Spring and Franke 1981; Olins, Olins et al. 1986) to mitotic chromosomes. The basic subunit of chromatin, the NCP, can be arranged into nucleosomal arrays that are dynamically and reversibly compacted into higher order chromatin fibers (Becker and Horz 2002). In addition to the 11 nm nucleosomal DNA fiber mentioned previously, observed chromatin fibers of sizes and estimated compaction ratios are presented in Table 1.1.

Fiber Name	Fiber Size (nm)	Compaction Ratio	Reference
Naked DNA	2	1	(Felsenfeld and Groudine 2003)
Nucleosomal DNA	10 to 11	6 to 7	(Felsenfeld and Groudine 2003)
30 nm fiber	30	40	(Felsenfeld and Groudine 2003)
Chromonema	60 to 80	160	(Belmont and Bruce 1994)
Chromonema	100 to 130	1,000	(Belmont and Bruce 1994)
300 nm fiber	300	1,000	(Felsenfeld and Groudine 2003)
Metaphase chromosome	700	10,000	(Felsenfeld and Groudine 2003)

Table 1.1. Chromatin fiber sizes and their corresponding compaction ratios.

Nucleosomes are, for the most part, identical repeating structures, which renders it very difficult to distinguish them from one another in intact nuclei using microscopic means, and thus it is difficult to gather structural data directly *in vivo*. Recently, techniques have been devised for estimating chromatin compaction directly in living nuclei, although to date this has only been used to examine changes during mitosis (Lleres, James et al. 2009). Historically, researchers have resorted to *in vitro* characterization, which introduces the potential for measurement artifacts, and light microscopy techniques, which are limited by resolution of roughly 200 nm.

1.3.1 The 30 nm fiber

The 30 nm fiber has been studied extensively in biophysical and biochemical assays (Thoma, Koller et al. 1979; Bednar, Horowitz et al. 1998; Woodcock and Dimitrov 2001; Hansen 2002; Dorigo, Schalch et al. 2004), but no consensus regarding its structure has been reached (Robinson and Rhodes 2006; Tremethick 2007). An early model for the 30 nm fiber based on EM data is the solenoid model, which proposes that nucleosomes and linker DNA follow a path describing a left-handed helix or spring (Finch and Klug 1976). EM data on polynucleosome arrays of varying repeat lengths indicate that a solenoidal 30 nm fiber would contain ~11 nucleosomes per 11 nm turn of the fiber (McBryant, Lu et al. 2010). Later models based on the results of nuclease protection assays of disulfide cross-linked nucleosomal arrays include the two-start supercoiled model and the two-start twisted model, depicted in Figure 1.1, or perhaps a combination of the two (Dorigo, Schalch et al. 2004; Robinson and Rhodes 2006). Two-start helical 30 nm fiber is estimated to contain 5-6 nucleosomes per 11 nm helical rise (McBryant, Lu et al. 2010). Linker histones are believed to

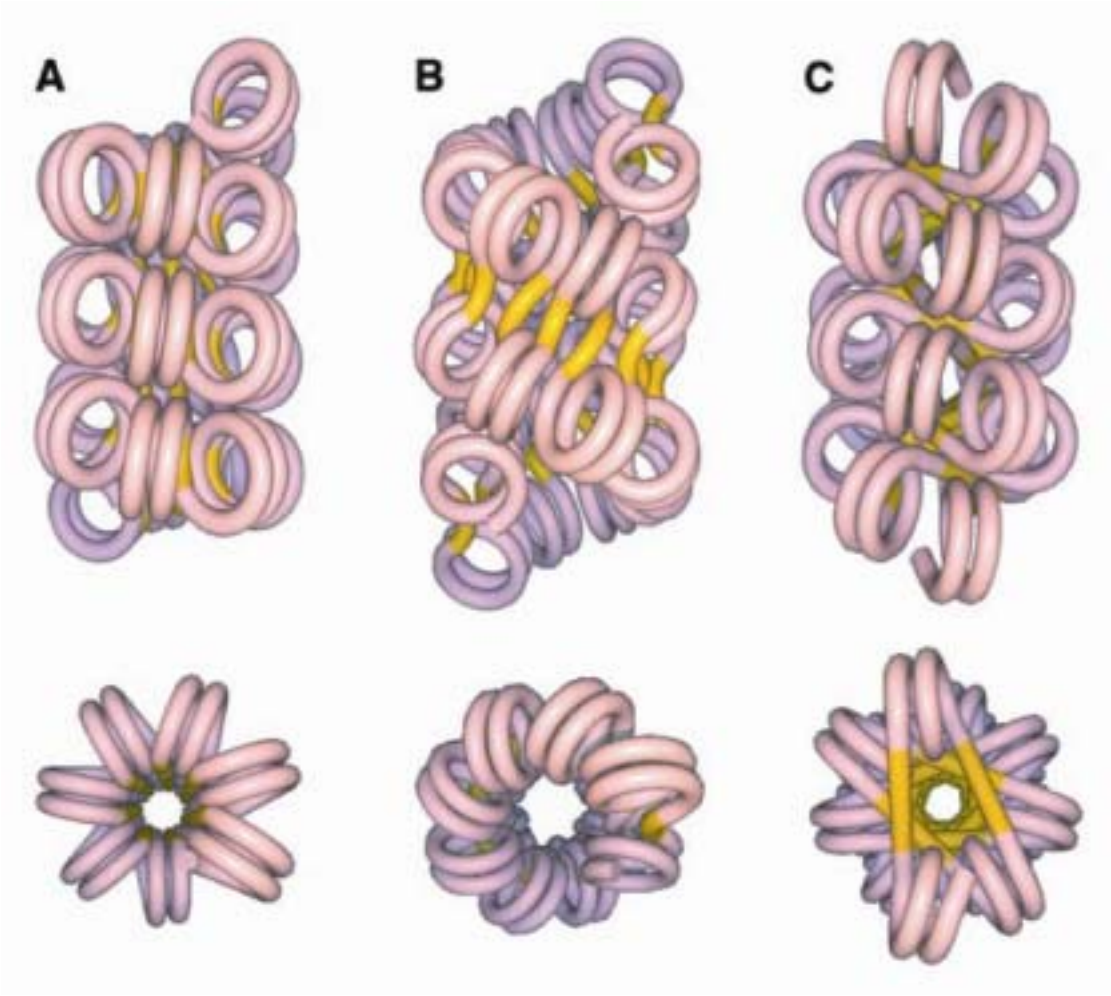

Figure 1.1 Three models for the 30 nm fiber: the one-start solenoid model consisting of nucleosomes immediately following one another along a helical path (A), and a pair of two-start models including the two-start supercoiled, or helical ribbon model (B), and the two-start twisted, or crossed-linker model (C). Double stranded nucleosomal DNA is shown in pink, linker DNA is shown in yellow. (Taken from Dorigo, Schalchet al. 2004)

promote the formation of the 30 nm fiber through the stabilization of intramolecular folding (Carruthers, Bednar et al. 1998), and studies have suggested that the 30 nm fiber is the predominant form of chromatin in the interphase nucleus of higher eukaryotes (Staynov 2008).

Detailed biochemical systems are not easily applicable to the study of chromatin fibers larger than the 30 nm fiber, and as a result of this the characterization of chromatin organization at levels beyond this rely heavily on experimental techniques used to measure compaction *in vivo*.

1.3.2 Measurement of chromatin compaction

Chromatin structure has been characterized using a variety of techniques, including in situ chemical fixation followed by 3C (Dekker, Rippe et al. 2002), fluorescence in situ hybridization (FISH) (Bystricky, Heun et al. 2004), and IF microscopy (Scheer 1987). Alternate strategies include the isolation of chromatin from nuclei followed by the introduction of mono- and/or divalent cations and subsequent analysis with EM (Kornberg and Thomas 1974; Belmont and Bruce 1994), AFM (Ohniwa, Morikawa et al. 2007), sedimentation studies (Thoma, Koller et al. 1979), or neutron scattering (Gerchman and Ramakrishnan 1987). These studies measure the end-to-end distance between fluorescently labeled chromosomal loci, as in the cases of fluorescence microscopy and FISH, directly measure chromatin fiber sizes as in the case of EM, or analyze regions in the genome which come in close proximity by 3C.

These data can be used to model a number of properties of chromatin, including persistence length, mass density, number of nucleosomes per 11nm turn, and compaction ratio. Results of a subset of these studies are presented in Table 1.2.

However, *in vitro* techniques such as these which rely on chemical fixation, 2D imaging, or the introduction of salts to the sample may result in artificial distortion of

	Persistence Length (nm)	Mass Density (bp/nm)	10kb distance (nm/10kb)	Nucs/11nm turn	Compaction Ratio	Method
Hahnfeldt, P 1993	220					FISH
Ostashevsky, J 1994	98 to 136					FISH
Bystricky K, 2004	170 to 220	110 to 150	67-91	7 to 10	40-fold	FISH
Dekker J, 2002	28		110	1.2 to 2.4		3C
Bressan D, 2004			60 to 80			Lac Tet system
Guacci V, 1994			42.5		80-fold	FISH
Hansen J, 2002				1 to 2		*In vitro*
Bednar J, 1998				6		EM

Table 1.2. *In vitro* measurements of chromatin characteristics.

chromatin structure. For example, mono- and divalent cations such as sodium and magnesium are associated with the condensation of 30 nm fibers into a higher order of structural organization in solution in a concentration-dependent manner (Paulson and Laemmli 1977; Marsden and Laemmli 1979; Thoma, Koller et al. 1979).

As can be seen from the table, there are discrepancies among the different measurements from the different techniques. The majority of the data comes from mammalian chromatin samples, which may have different compaction strategies than yeast. The Bystricky and Dekker studies, which examined yeast chromatin, also give conflicting results.

1.3.3 The chromonema fibers

The chromonema model introduced by the Belmont Lab describes progressive decondensation and straightening of post-mitotic Chinese hamster ovarian (CHO)

chromatin from initially helically or irregularly coiled structures into increasingly smaller chromonema fibers during G1 (Belmont and Bruce 1994; Robinett, Straight et al. 1996). These efforts resulted in the characterization of two different fiber sizes, the 60-80 nm and the 100-120 nm chromonema fibers, through light microscope and EM studies (Belmont and Bruce 1994). They report an initial appearance of the 100-120 nm fiber in early G1, with a later predominance of the 60-80 nm fiber in late G1 to early S phase, with an associated progressive uncoiling and straightening of these fibers during this portion of the cell cycle, as well as local formation of 30 nm fibers at junctions between larger fibers (Belmont and Bruce 1994). Fluorescent tagging of multiple chromosomal loci in chemically fixed CHO cells revealed an irregularity of mitotic chromosomal folding at one or multiple levels over tens of mega-base pairs (Strukov and Belmont 2009).

A fiber with dimensions between the two chromonema fibers has also been described in the literature. Scanning probe microscopy (SPM), atomic force microscopy (AFM), and immunofluorescence microscopy (IFM) studies of stretched human mitotic chromosomes by the Kawabata lab detected linearly linked 90 nm chromatin beads which stained for scaffold proteins and were structurally stable (Ikeda, Mizutani et al. 2010). This finding is intriguing in that it falls in the 20 nm window between two previously characterized chromonema fiber sizes, and thus, given the possibility of a slight measurement error from one technique or the other, perhaps provides independent verification of one or both of them.

Little else is known about the structure and formation of the chromonema, 300 nm, and mitotic chromosome fibers apart from their size, despite efforts from different

cytological and biochemical approaches. Nevertheless, models have been proposed which address their formation and structure.

1.3.4 Models of higher order chromatin structure

Large chromatin fibers have been variously modeled as radially oriented loops (Paulson and Laemmli 1977; Marsden and Laemmli 1979; Adolph 1980; Gasser, Laroche et al. 1986; Maeshima, Eltsov et al. 2005), a hierarchy of helical structures (Sedat and Manuelidis 1978), or a combination of the two (Rattner and Lin 1985; Boy de la Tour and Laemmli 1988), largely based on analysis of EM measurements. Chromatin looping is predicted to minimize entanglement effects during recondensation of mitotic chromosomes (Holm 1994). A mathematical example of this type of model is the Everaers Lab's Molecular Dynamics-based parameter-free minimal model of decondensing chromosomes, which predicts that, due to generic polymer effects, the chromatin of interphase nuclei behaves like concentrated solutions of ring polymers which never fully equilibrate into smaller structures, and thus are unlikely to entangle neighboring chromosomes (Rosa and Everaers 2008). In situ hybridization data indicates that chromatin folds according to a random walk model for scales of 100-1,000 kb, while looping predominates for scales over 1,000 kb (van den Engh, Sachs et al. 1992; Yokota, van den Engh et al. 1995). None of the various models characterize chromatin structure beyond general terms.

1.4 Nuclear organization

Various nuclear bodies have been characterized through cell biology and biochemical techniques which perform a range of cellular functions and have roles in the structural organization of chromatin within the nucleus. These include the nucleolus, Cajal or nucleolar bodies, and the inner surface of the nuclear envelope (Andrulis, Neiman et al. 1998; Gasser 2001; Carmo-Fonseca 2002; Wang, Haeusler et al. 2005). Additionally, transcription and replication factories are thought to have roles in determining interphase chromosomal organization.

1.4.1 Nuclear bodies

Cajal bodies are non-membrane bound nuclear structures composed of threads of the coilin protein, snRNAs, and scaRNAs which modify and assemble pre-mRNA splicing machinery subunits as well as 2'-O-methyl modify snRNAs (Carmo-Fonseca 2002). Cajal bodies are found in higher eukaryotes, while the corresponding structure in yeast is called the nucleolar body (Carmo-Fonseca 2002).

The nucleolus houses the rDNA repeats, which in yeast are primarily found within chromosome XII (Duan, Andronescu et al. 2010). The major function of the nucleolus is to transcribe 45 S rRNA and produce pre-ribosomal subunits (Faro-Trindade and Cook 2006). The outer surface of the nucleolus is associated with transcriptionally silent, condensed chromatin (Wang, Tegenfeldt et al. 2005), and through interactions with this region the nucleolus can organize surrounding chromatin (Wang, Haeusler et al. 2005).

The nuclear periphery of yeast has been identified as a zone which can be associated with transcriptional silencing, and several genes have been identified which rely on recruitment to the nuclear periphery as a means of regulation. The Sternglanz lab demonstrated that perinuclear localization helps to establish transcriptionally silent chromatin of the HM locus (Andrulis, Neiman et al. 1998). Telomeres and centromeres are also recruited to the nuclear periphery and are heavily silenced (Gasser 2001). This regulation is achieved through concomitant establishment of transcriptionally repressive heterochromatin at the nuclear periphery (Andrulis, Neiman et al. 1998).

Not all genes which relocate to the nuclear periphery are silenced, however, and several instances have been reported where genomic interactions with nuclear pore proteins result in upregulation of transcription (Cabal, Genovesio et al. 2006; Taddei, Van Houwe et al. 2006; Sarma, Haley et al. 2007; Ahmed, Brickner et al. 2010).

In higher eukaryotes chromatin is anchored to a central chromosomal scaffold made up of condensin, topoisomerase II, and histone H1 (Bode, Schlake et al. 1995; Maeshima, Eltsov et al. 2005; Hizume, Araki et al. 2007) through their association with scaffold attachment regions, providing a mechanism for stabilizing interphase chromatin structure (Bode, Benham et al. 2000). This structure appears to be lacking in yeast, where histone H1 and topoisomerase II have not been shown to associate with a scaffold structure, although topoisomerase II have been shown to be necessary for chromatin condensation (Yanagida 1990).

1.4.2 Factories

1.4.2.1 Transcription factories

Transcription factories are clusters of RNA polymerases and associated transcription factors which, through high local concentration and proximity, are believed to upregulate transcription and transcript maturation from multiple templates (Faro-Trindade and Cook 2006). Transcription factories are relatively immobile and must recruit and maintain proximity with the DNA templates which they transcribe, and as they typically interact with multiple templates, they introduce an organizational effect on chromosomal territories (Faro-Trindade and Cook 2006).

1.4.2.2 Replication factories

Replication factories are immobile nuclear foci where the bulk of DNA replication occurs through the simultaneous synthesis and extrusion of multiple loops of DNA (Hozak and Cook 1994). Subunits of replication factory machinery include DNA polymerase α, DNA polymerase ε, and PCNA (Baker and Bell 1998; Waga and Stillman 1998; Johnson and O'Donnell 2005). Similar to transcription factories, replication factories can interact with several DNA templates at a time and thus introduce an organizational effect on chromosomal territories (Kitamura, Blow et al. 2006).

1.4.3 Chromosomal territories

Interphase chromosomes are organized within the mammalian nucleus into distinct, non-random, preferred conformations called chromosomal territories (Heun, Laroche et al. 2001) (Cremer and Cremer 2001; Bystricky, Laroche et al. 2005) (Heard and Bickmore 2007) which are thought to be spatially defined by several variables. These include the spatial arrangement and orientation of the mitotic chromosomes from which they arise (Rosa and Everaers 2008), the association of disparate elements into functionally defined aggregates such as transcription (Iborra, Pombo et al. 1996; Osborne, Chakalova et al. 2004) (Faro-Trindade and Cook 2006) and replication factories (Hozak and Cook 1994), the association of centromeres at the spindle pole body and telomeres with the nuclear matrix (Spector 2003), and, in higher eukaryotes, the association of lamina-associated domains (LADs) with the nuclear lamina (Guelen, Pagie et al. 2008) and associations with the chromatin scaffold (Bode, Benham et al. 2000). The result is a spatial orientation known as the Rabl configuration (Rabl 1885).

Some similar observations have been made in yeast, although many of the structures found in mammalian nuclei are absent in this organism. A 3D model of the yeast genome during interphase based on 3C data has recently been published which estimates the relative orientations of the chromosomal territories within a nucleus (Duan, Andronescu et al. 2010).

1.4.4 Chromatin loop formation

Formation of loops within chromatin serves various purposes in a variety of cellular processes, such as transcription and chromatin condensation. As such, it occurs at different scales within different chromatin fiber sizes, appropriate to the cellular process in question.

3C is a method for analyzing the looping of chromatin which involves in situ fixation of cells, fragmentation of the chromatin, ligation of resulting DNA ends in dilute conditions, and sequencing across the ligated ends. It has confirmed that distant chromosomal loci can physically associate with one another (Dekker, Rippe et al. 2002). This technique has been used in conjunction with high throughput sequencing or hybridization to a microarray to analyze genome-wide chromosomal interactions to create a new method called 4C (Ohlsson and Gondor 2007), and can also be modified to screen for all potential interaction patterns within a limited region in a process called 5C (Gondor and Ohlsson 2009). Such methods have been used to confirm the existence of chromatin loops in a variety of circumstances.

Looping was first characterized in histone depletion studies of human cells using EM, which revealed that chromatin associates with the chromatin scaffold as a series of 10-30 μm loops (Paulson and Laemmli 1977). It was observed by the Cook lab that DNA is constrained loops which prevent its relaxation, and this constraint requires both RNA and protein for its integrity (Jackson, McCready et al. 1984). The Krawetz lab also confirmed that chromatin associates with a scaffold in a manner which selectively binds chromatin loops (Heng, Goetze et al. 2004).

Looping interactions associated with the regulation of transcription are detected during both the induction and the repression of individual promoters, in processes which bring different regulatory elements into close proximity. For example, 3C analysis demonstrates that looping at the B-globin locus brings the locus control region (LCR) into close proximity with the B-globin genes during the induction of transcription in mouse (Schoenfelder, Sexton et al. 2010). ChIP-Seq experiments in mouse have shown that the mediator complex, cohesin, and the cohesin loading factor Nipbl all occupy the same enhancer and promoter regions in a subset of genes (Kagey 2010). Furthermore, co-immunoprecipitation and co-purification data indicate that the three proteins likely form physical interactions with one another, while 3C analysis indicates that looping exists between specific enhancers and promoters in a mediator and cohesin-specific manner (Kagey 2010). It is hypothesized that the role of cohesin in this regard is to form rings which connect two DNA segments, thus forming a loop (Kagey 2010).

Looping which results in the physical association of promoters and terminators in a TFIIB-dependent manner associated with transcriptional memory has been described in a subset of genes, including the Gal10 gene (Singh and Hampsey 2007; Laine, Singh et al. 2009). This looping effect is dependent on subunits of the pre-mRNA 3'-end processing machinery, including Ssu72 and Rna15 (Singh and Hampsey 2007; El Kaderi, Medler et al. 2009).

Additionally, cohesin has been implicated in a role in transcriptional regulation in metazoans through its colocalization with the CTCF binding protein, possibly through

the stabilization of repressive chromatin loops organized by CTCF (Carretero, Remeseiro et al. 2010; Wood, Severson et al. 2010).

1.4.5 Relocalization of chromosomal domains

Relocalization of chromatin domains away from their chromosomal territory in response to transcriptional initiation was first described by the Sheer Lab through the use of FISH to study the effects of interferon on the major histocompatibility complex region of chromosome 6 in human (Volpi, Chevret et al. 2000). The Bickmore lab also used FISH to demonstrate that local gene density and transcription can result in the relocalization of a gene to the outside of its chromosomal territory in mouse (Mahy, Perry et al. 2002). Other relocalization events associated with transcription were confirmed through studies of the Gal1 locus in yeast by the Nehrbass Lab using live cell 3D microscopy (Cabal, Genovesio et al. 2006). It was shown that this recruitment is dependent on subunits of the SAGA complex, the nuclear pore protein Nup1, as well as the mRNA export factor Sac3 (Cabal, Genovesio et al. 2006). The Silver lab also demonstrated relocalization of the Gal1 locus in yeast using live cell 2D microscopy (Drubin, Garakani et al. 2006). They confirmed that this recruitment is dependent on Sac3, and proposes that relocalization to the nuclear periphery is due in part to random diffusion (Drubin, Garakani et al. 2006).

Relocalization of chromatin domains as a means of silencing has also been described in the literature. As mentioned previously, perinuclear localization helps to establish transcriptionally silent chromatin of the HM locus (Andrulis, Neiman et al. 1998),

while telomeres and centromeres are recruited to the nuclear periphery where they are heavily silenced (Gasser 2001).

The picture of chromatin which has been emerging for the past several years is that of a molecule which dynamically self-assembles into higher order structure, decondenses into smaller fibers, and rearranges itself as necessary during various cellular processes, such as transcription. Very little is known about the changes in structural conformations which occur during these transitions.

1.5 Pol II Transcription

Messenger RNA (mRNA) transcription in yeast is regulated by promoter and enhancer DNA elements which under appropriate conditions recruit gene-specific transcription factors, RNA polymerase II (Pol II), and the general transcription factors to the 5' end of a gene, and aid in pre-initiation complex (PIC) formation, transcription initiation, promoter clearance, and elongation (Lee and Young 2000). In the course of these events, chromatin structure can be altered considerably as a means of facilitating the process, both in ORFs, as well as in promoters (Eberharter and Becker 2002; Li, Carey et al. 2007; Schwabish and Struhl 2007; Weake and Workman 2010).

Yeast promoters typically extend ~200 bases upstream from the genes they regulate and contain binding sites for a variety of sequence specific transcription factors; and the nature, number, and location of these sites vary from one gene to another (White 2001).

The regulation of transcription factor localization within, or outside of, the nucleus, and the interplay between activators and repressors have been shown to be major factors in the control of access of transcription factors to their binding domains, and thus, the control of transcription initiation (Lee and Young 2000).

Examples of these regulatory methods include the nuclear importation of cell-cycle specific transcription factors, permitting access to constitutively accessible binding sites at promoters or enhancers, and the post-translational modification of promoter- or enhancer-bound repressor proteins, causing their release from the DNA, and thus exposing binding sites for access by constitutively expressed transcription factors (Hunter and Karin 1992; Lee and Young 2000). The binding sequences for these transcription factors and repressors vary greatly from promoter to promoter, as do the corresponding DNA binding domains of the transcription factors and repressors which bind them. Additionally, there are a wide variety of covalent modifications and transcription factor modification sites, and a wide variety of ways that transcriptional activators and repressors can interact. As a result there are many distinct mechanisms for regulating transcription from individual promoters.

Many eukaryotic promoters contain basal or core elements known as TATA boxes or initiators, one of which is usually present in any given gene. These DNA elements are consensus sequences which are recognized by specific proteins involved in transcriptional initiation. TATA boxes are present in over 20% of all Pol II-driven genes in yeast (Basehoar, Zanton et al. 2004), and are located upstream of the TSS, while initiators are located at the TSS (White 2001). TATA-less and initiator-less

promoters are transcribed inefficiently and often from multiple, cryptic start sites (Lee and Young 2000).

Enhancers typically contain binding sites for one or more sequence specific transcription factors and regulate expression remotely. The classical definition of an enhancer is a cis-acting element which drives high level expression in transient transfection assays (as opposed to an LCR, which drives high level expression in stable transfection assays, regardless of integration site) (Bulger and Groudine 1999).

The initial events in transcription induction may be followed by a variety of promoter-specific events, including, although not necessarily in this order, the recruitment of ATP-dependent chromatin remodeling enzymes such as SWI/SNF which alter local chromatin topography, the recruitment of histone covalent modifiers such as SAGA-subunit Gcn5p, which acetylate local histone tails resulting in further local chromatin decondensation, and the recruitment of transcription factor complexes such as Mediator or Compass, which in turn recruit subunits of the pre-initiation complex (PIC) (Weake and Workman 2010). The PIC is made up of transcriptional scaffold proteins (Yudkovsky, Ranish et al. 2000), general transcription factors, and subunits of Pol II occurs at the promoter, typically 40 to 120 bases upstream of the TSS in yeast (Hampsey 1998). The exact makeup of the PIC varies from promoter to promoter, but contains at least 60 subunits, although this is likely to be an underestimate due to the difficulty in characterizing complexes of this size. Initiation of transcription is also regulated through the phosphorylation of serines 2 and 5 of the c-terminal domain (CTD) of Pol II, which play roles in promoter clearance and elongation, respectively (Phatnani and Greenleaf 2006).

Two models regarding the procession of Pol II along DNA have been verified: either the polymerase is immobilized, as in a transcription factory, and the DNA is pulled through it in a ratchet-wise fashion, or the polymerase is not immobilized and is allowed to process along the DNA template (Faro-Trindade and Cook 2006). If Pol II or the DNA ends are immobilized, this unwinding introduces positive superhelical torsion in the DNA ahead of the processing polymerase, and negative superhelical torsion behind, which must be relieved in order for transcription to proceed efficiently. Relaxation is catalyzed by topoisomerases which nick one strand of the DNA, allowing one strand to unwind with respect to the other (Thrash, Bankier et al. 1985).

Elongation by Pol II has been reported to occur at a rate of roughly 1.1-2 kb/minute in yeast and drosophila (Ardehali and Lis 2009). Studies in yeast which attempt to count mRNA transcripts indicate that rates of message production are generally low, probably as a result of energy conservation, and that many genes are typically only transcribed only a single time during a cell cycle (Bon, McGowan et al. 2006). Other transcription frequency studies indicate that there is a great deal of variability in the transcription rates of individual genes, that abortive transcripts are frequent, and that transcription often occurs in pulses (Chubb, Trcek et al. 2006). The average Pol II density in mammalian somatic diploid nuclei has been shown to be <1 per gene (Jackson, Pombo et al. 2000).

Transcription in yeast is regulated at the 3' end of the ORF by DNA elements called terminators, which signal for transcriptional termination, and recruit subunits of the 3' end-processing complex (Russo and Sherman 1989).

1.5.1 Previous studies of the effects of transcription on chromatin compaction

Various experimental results show an association with transcription and the decondensation of chromatin. The traditional model of transcription, based on EM and nuclease digestion data, holds that with transcription comes a 6-fold decondensation in chromatin fiber size, from the 30 nm fiber to the 10 nm fiber (Hu, Kireev et al. 2009). In situ hybridization, FISH and scanning confocal microscopy data indicate higher levels of chromatin compaction, consistent with the presence of a 30 nm fiber or higher, even during transcription (Lawrence, Singer et al. 1990; Yokota, van den Engh et al. 1995; Munkel, Eils et al. 1999; Tumbar, Sudlow et al. 1999).

Recently the Belmont Lab described the results of live cell fluorescence microscopy of chromatin in 2D which found that arrays of endogenous CHO chromatin interspersed with lac operator repeats and inducible DHFR, HSP70, or MT genes adopt a linear arrangement which changes its compaction ratio 1.5-3-fold upon induction (Kireev, Lakonishok et al. 2008; Hu, Kireev et al. 2009). Other experiments performed by the Lis Lab using a high-resolution MNase scanning assay demonstrate that transcription of HSP70 in drosophila is activated within seconds during heat shock, and is correlated with a visible decondensation of local chromatin (Petesch and Lis 2008). Monoallelic decondensation has also been demonstrated to

be possible in mouse, as shown by the LaSalle Lab using FISH experiments on the imprinted snoRNA gene cluster on 15q11-13 (Leung, Vallero et al. 2009).
The inhibition of transcription causes recondensation of chromatin which is also measurable by various techniques. For instance, in the Balbiani ring puffs of *Chironomus tentans*, transcriptional inhibition by the inhibitor DRB results in reduction in polymerase occupancy and rapid chromatin condensation (Andersson, Mahr et al. 1982), while recovery from alterations in nucleosome topology during transcription has been shown to occur on a time scale of <5 minutes at a subset of genomic loci in yeast using MNase and DNaseI digestion (Pederson and Morse 1990). ChIP time course data indicates that re-deposition of histones at the transcribed Gal10 locus takes place on the order of <1 minute in yeast (Schwabish and Struhl 2004).

1.6 Thesis objectives

1.6.1 Characterize the effects of ATP-dependent chromatin remodeling enzymes on chromatin structure

In order to determine if the ATP-dependent chromatin remodeling enzyme SWI/SNF catalyzes an increase in the motion of chromosomal loci to which it is recruited in yeast, we propose to analyze the motion of a fluorescently tagged genetic locus which shows differential recruitment of the enzyme in mother and daughter nuclei. Motion controls for this project include fluorescently tagged nuclear pore proteins and fluorescently tagged spindle pole body proteins, both of which serve as immobile reference points which can be used to control for drift. An additional control would be the disruption of the catalytic function of SWI/SNF to determine if it results in a

loss of a motion phenotype. Motion will be recorded with the fluorescent light microscope, and tracking and motion analyses will be performed. An alternate strategy which will be pursued is to recruit large numbers of SWI/SNF molecules to a given fluorescently tagged chromosomal locus to increase the likelihood of detecting a motion phenotype.

To investigate the effects of SWI/SNF on the interaction of sequence specific DNA binding proteins with their binding sites *in vivo*, we propose to generate a yeast strain which artificially recruits SWI/SNF to a fluorescently tagged chromosomal locus and perform photobleaching experiments to analyze the off-rate of the fluorescent proteins, thus determining if the fluorescent tags were evicted by the enzyme.

1.6.2 Establishment of a system for tracking chromosomal loci in 3D *in vivo* with the OMX microscope

In effort to expand the application of the fluorescence light microscope to the study of chromatin structure *in vivo* in 3D, we propose to establish a system for measuring chromatin compaction based on the tracking of syntenic fluorescent chromosomal loci in yeast. Strains with fluorescent tags flanking different genomic distances will be generated, imaged with the OMX microscope, and the data will be modeled with the Porod-Kratky chain equation to estimate persistence length, linear mass density, and the compaction ratio.

1.6.3 Characterize the effects of transcription on chromatin structure in 3D *in vivo* with the OMX microscope

In effort to expand the application of the fluorescence light microscope to the study of the effects of transcription on chromatin structure *in vivo* in 3D, we propose to generate a yeast strain containing an inducible 15 kb gene flanked with GFP-tagged loci. Live cell 3D fluorescence video microscopy of the strain with and without induction will be performed with the OMX microscope, and the results will analyzed to determine if transcription-dependent changes in chromatin compaction can be measured in real time.

CHAPTER 2

Materials and Methods

2.1 Materials

2.1.1 Chemicals

Chemicals were purchased from Invitrogen, Sigma-Aldrich, Amresco, Fisher, BDH, and Calbiochem, and solutions were made up with Millipore filtered water.

2.1.2 Bacterial Strains

MAX Efficiency Stbl2 Competent Cells (Invitrogen 10268-019)

SCS110 competent cells (Stratagene 200247)

XL10-Gold Ultracompetent Cells (Stratagene 200314)

GM2929 (Yale 7080)

Dh5α Competent Cells (Invitrogen 18265-017)

2.1.3 Sources of Enzymes

Alpha factor (Zymo Research y1001)

Concanavalin A (Sigma-Aldrich C-2631)

M-MLV Reverse Transcriptase (Promega 9PIM170)

Restriction Endonucleases (NEB, Takara, Promega)

Rapid DNA Ligation Kit (Roche 11 635 379 001)

Platinum Taq (Invitrogen 10966-018)

Zymolyase (Seikagaku Biobusiness 120493)

2.1.4 Antibodies

Anti-GFP antibody (Roche 1-814-460)

Mouse anti myc 9E10 antibody (Sigma-Aldrich M4439)

Anti mouse Cy3-labelled secondary antibody (Sigma-Aldrich C2181)

2.1.5 Equipment

Eppendorf Mastecycler PCR machine

Eppendorf 5417C tabletop centrifuge

Eppendorf 5417R tabletop centrifuge

Fujifilm FLA-5100 fluorescent image analyzer

Novex Minicell Electrophoresis Chamber (Invitrogen)

Varian Cary 50-BIO UV spectrophotometer

Xcell 2 Blot Module (Invitrogen)

2.1.6 Buffers

MES Buffer	Invitrogen NP0002
NuPAGE LDS Sample buffer	Invitrogen NP0007
Rapid screening buffer	20% sucrose, 200 mM NaOH, 120 mM KCl, 10 mM EDTA, 0.5% SDS, pinch bromophenol blue
TBE	89 mM Tris-borate pH 8.3, 2 mM EDTA
TES	10 mM Tris-HCl pH 7.5, 10 mM EDTA, 0.5% SDS
Western blot block buffer	1x PBS, .05% Tween-20, 1-3% milk
Yeast protein extraction buffer	100 mM Tris pH 7.9, 250 mM ammonium sulphate, 1 mM EDTA, 10% glycerol. Add fresh DTT (0.5 mM final) and 1X yeast protease inhibitors.
1X DNA loading buffer	Invitrogen
Sorbitol, 1.2 M plus Potassium Phosphate, 0.1 M pH6.6 buffer	2.186 g sorbitol plus 762 µl 1M K_2HPO_4 plus 1238 µl 1M KH_2PO_4, bring to final volume 10 mls with dH_2O
Block buffer	1X PBS, 30 mg/ml BSA, 0.1% Tween-20, bring to final volume of 20 ml with dH_2O
Spheroplast buffer	400 µl 10 mg/ml zymolase, 100 µl fresh B-Mercaptoethanol, 0.762 ml 1M K_2HPO_4, 1.238 ml 1M KH_2PO_4, final volume 20 ml with dH_2O
1X protease inhibitors from the following stock solutions:	0.1 M PMSF (100x) 16 mg/ml Ethanol; Store at -20 °C
	Benzamidine (100X); 31 mg/ml H2O; Store at -20 °C
	Leupeptin (500X); 0.15 mg/ml Ethanol; Store at -70 °C for less than 6 months
	Pepstatin (200X); 0.28 mg/ml methanol; Store at -20 °C.
	Chymostatin (2,500X); 5 mg/ml DMSO; Store at -20 °C

Table 2.1. Buffers used during the course of this work

2.1.7 Miscellaneous supplies

1 kb plus ladder (Invitrogen 10787-018)

Ariad Argen Regulated Transcription Kit Version 2.0

Bioptechs 40 mm coverslips no. 1 (Bioptechs, 40-1313-0319-1)

Immobilon-P^{SQ} PDVF transfer membrane (Millipore PRO2532)

Multimark Protein Ladder (Invitrogen LC5725)

QIAfilter Plasmid Maxiprep Kit (Qiagen 12263)

QIAprep Spin Miniprep Kit (Qiagen 27106)

QIAquick Gel Extraction Kit (Qiagen 28706)

QIAquick PCR Purification Kit (Qiagen 28104)

Salmon sperm DNA, sonicated, single stranded, 10 mg/ml (Invitrogen 15632-011)

Seeblue Plus 2 protein ladder (Invitrogen LC5925)

2.1.8 Media

All media were prepared by the Wellcome Trust Biocentre Media Kitchen. Media for *E. coli* strains were prepared according to the standard recipes of Sambrook and Russell (Sambrook, Fritsch et al. 1989). Media used for yeast strains were made according to standard recipes of Burke et al. (Burke 2000).

Yeast-Peptone-Adenine (YPA) medium	(1 % (w/v) yeast extract, 2 % (w/v) Bacto-peptone, 0.004 % (w/v) adenine)
Synthetic dropout media (DOA)	((0.67 % (w/v) yeast nitrogen base minus amino acids, 2 % (w/v) glucose), 0.2 % drop out mix containing all amino acids and other synthetic growth factors (synthetic complete or SCD medium).
Sporulation agar (SPO)	VB sporulation medium (0.82 % (w/v) sodium acetate, 0.19 % (w/v) KCl, 0.035 % (w/v) MgSO4, 0.12 % (w/v) NaCl and 1.5 % (w/v) Bacto agar (Difco)
Luria-Bertani (LB) medium	(1 % Bacto peptone (Difco), 0.5 % Bacto yeast extract (Difco), 1 % NaCl pH 7.0) supplemented with 100 µg/ml ampicillin

Table 2.2. Media used during the course of this work

2.2 Methods

2.2.1 Molecular biology methods

2.2.1.1 Agarose gel electrophoresis

DNA fragments were resolved by agarose gel electrophoresis (Sambrook, Fritsch et al. 1989) using 0.8 to 1.5% agarose (Invitrogen), 1X TBE buffer, 1 kb plus ladder (Invitrogen), 1X DNA loading buffer (Invitrogen), and 10,000x SYBR Safe gel stain (Invitrogen) at 110 V for 40 to 70 minutes. DNA was visualized with a UV light box.

2.2.1.2 Bacterial transformations

Transformations of XL10-Gold Ultracompetent Cells (Stratagene) were performed according to manufacturer's protocol. 0.5 μl of sample or control ligation was transformed into 12.5 μl of cells per transformation, colonies were selected over night on LB + 100 μg/ml ampicillin plates.

Transformations of dam-/dcm- SCS110 competent cells (Stratagene) were performed according to manufacturer's protocol. 1 μl of 1 ng/μl plasmid was transformed into 50 μl of cells per transformation, colonies were selected over night on LB + 100 μg/ml ampicillin plates.

Transformations of plasmids with multiple repeat sequences into MAX Efficiency Stbl2 Competent Cells (Invitrogen) were performed according to manufacturer's

protocol. 0.5 μl of sample or control ligation was transformed into 50 μl of cells per transformation, colonies were selected over night on LB + 100 μg/ml ampicillin plates.

Transformations of plasmids with multiple repeat sequences into dam-/dcm- strain 7080/GM2929 (CGSC, Yale University) were performed by thawing cells 10' on ice, aliquoting 1 μl of 1 ng/μl plasmid into 30 μl cells, mixing gently, incubating on ice for 30', heat-shocking at 42^{o}C for 30 sec, incubating on ice for 2 minutes, rescuing in LB at 37^{o}C for 1 hr with shaking, and selecting over night on LB + 100 μg/ml ampicillin + 12.5 μg/ml chloramphenicol plates at 30^{o}C.

2.2.1.3 Colony preps

Colony preps for the rapid isolation of genomic yeast DNA were performed via the Hahn Lab protocol by transferring single colonies to 30 μl 0.2% SDS, vortexing 15 sec, incubating at 90^{o}C for 4 minutes, vortexing 1 minute, centrifuging at 14,000 rpm in an Eppendorf 5417C tabletop centrifuge, and transferring the supernatant to a new 1.5 ml tube on ice.

2.2.1.4 DNA ligation

DNA ligation was performed with a Rapid DNA Ligation Kit (Roche) as per the manufacturer's instructions.

2.2.1.5 DNA purification from agarose gels

DNA purification from agarose gels was performed with a QIAquick Gel Extraction Kit (Qiagen) as per the manufacturer's instructions.

2.2.1.6 DNA sequencing

DNA sequencing was performed by DNA Sequencing & Services (MRCPPU, College of Life Sciences, University of Dundee, Scotland, www.dnaseq.co.uk) using Applied Biosystems Big-Dye Ver 3.1 chemistry on an Applied Biosystems model 3730 automated capillary DNA sequencer.

2.2.1.7 Ethanol precipitation of DNA

Ethanol precipitation of DNA was performed as per Sambrook (Sambrook, Fritsch et al. 1989). The precipitation step was facilitated by incubating samples in liquid nitrogen for 3 minutes.

2.2.1.8 Genomic DNA extraction from yeast cells

Genomic DNA extraction from yeast cells was performed as per Linda Hoskins' protocol (Hoskins 1997).

2.2.1.9 Glycerol stocks

Glycerol stocks of log-phase yeast or bacterial cultures were made by adding 800 µl 30% filtered glycerol to 800 µl cells in growth media and freezing at -80^{o}C for long term storage.

2.2.1.10 PCR amplification of DNA

PCR methods varied, but generally followed the protocol outlined in Sambrook (Sambrook, Fritsch et al. 1989) using an Eppendorf Mastecycler PCR machine, and Platinum Taq (Invitrogen).

2.2.1.11 PCR purification

PCR Purifications were performed with a QIAquick PCR Purification Kit (Qiagen) as per manufacturer's instructions using an Eppendorf 5417C tabletop centrifuge.

2.2.1.12 Phenol-chloroform purification of DNA

Phenol-chloroform purification of aqueous DNA samples was performed by adding one volume saturated phenol pH 7.9 (Amresco), vortexing 15 sec, centrifuging 15 sec in an Eppendorf 5417C tabletop centrifuge, transferring the top (aqueous) layer to a new 1.5 ml tube, adding one volume 24:1 chloroform:isoamyl alcohol (Amresco), vortexing 15 sec, centrifuging 15 sec, and transferring the top layer to a new 1.5 ml tube.

2.2.1.13 Plasmid purification from E. coli cells

Plasmid purification from E. coli cells was performed using a QIAprep Spin Miniprep Kit or a QIAfilter Plasmid Maxiprep Kit (Qiagen) as per manufacturer's instructions.

2.2.1.14 Rapid screening for correct bacterial clones

Rapid Screening of transformed bacterial colonies for correct clones was performed by picking single colonies into 30 µl of warmed rapid screening buffer (20% sucrose, 200 mM NaOH, 120 mM KCl, 10 mM EDTA, 0.5% SDS, pinch bromophenol blue), mixing, incubating at 37^{o}C for 5 minutes, and performing agarose gel electrophoresis. Lanes with band sizes larger than the control were screened by restriction digest for correct inserts.

2.2.1.15 Restriction enzyme digestion of DNA

Restriction enzyme digestion of DNA was performed as per manufacturers' instructions.

2.2.1.16 RT-PCR

RT-PCR was performed as per manufacturers' instructions using M-MLV Reverse Transcriptase (Promega).

2.2.2 Yeast methods

2.2.2.1 Alpha Factor Synchronization

Alpha Factor Synchronization of Mat a yeast cells was performed as per the Tomo Tanaka Lab protocol (personal communication). Cells were grown to A600 of 0.2, washed 3 times with dH_2O to remove Bar1p, and resuspended in YPAD medium. Alpha factor (Zymo Research) was added to a final concentration of 1.25 ug/ml, followed by incubation at 26 ^oC with shaking for 50 minutes. The same volume of alpha factor was again added, and the process was repeated at time intervals of 50 minutes, 30 minutes, and 20 minutes. Cells were observed under brightfield for shmooing, and a budding index was performed (number of cells budded/total cells). In some cases, cells were released from arrest in late G1 by washing four times with dH_2O.

2.2.2.2 Crossing yeast strains

Yeast strains of differing mating types were woken and the following day were patched together on a YPAD plate. The following day the patch was streaked to a double-selection plate and selected for three days. Single colonies were patched to sporulation plates and allowed to sporulate for five days. Sporulated cells were harvested by pipetting 1 ml dH_2O on the surface of the plate and then transferring it to a 1.5 ml tube. Cells were centrifuged at 10,000 rpm in an Eppendorf 5417C tabletop centrifuge and all but 200 μl of supernatant was removed. An equal volume of 1mg/ml Zymolyase (Seikagaku Biobusiness) in 1 M sorbitol was added the cells,

mixed, and incubated at 25°C. At intervals of 10 minutes, 2 µl of cells were taken and mixed with 2 µl of 0.2% sarkosyl on a microscope slide to check for spheroplasting. When 75% of cells were spheroplasted they were resuspended in 150 µl dH_2O, 150 µl mineral oil was added and the tube was vortexed for 2 minutes and centrifuged for 30 sec at 10,000rpm. 100 µl of oil containing the haploid spores was plated on double-selection plates and selected for two days.

2.2.2.3 Total cell lysates for extraction of yeast protein

Total cell lysates for extraction of yeast protein were prepared following the Hahn Lab adaptation of the Horvath protocol (Horvath and Riezman 1994). Grow 100 ml yeast cells to A600 of 0.6 to 1.2, wash with cold extraction buffer (100 mM Tris pH 7.9, 250 mM ammonium sulphate, 1 mM EDTA, 10% glycerol) in a 50 ml tube. Resuspend cells in 0.5 ml extraction buffer containing fresh DTT (0.5 mM final) and 1X protease inhibitors in a 1.5 ml tube with a locking top. Add 500 µl glass beads. In cold room vortex at top speed for 1 minute. Transfer to ice for 1 minute. Repeat for a total of 10 minutes vortexing. Briefly microcentrifuge to remove all liquid and leave behind most of the glass beads. Centrifuge at top speed at 4°C for 15 minutes and remove supernatant, being careful to avoid any glass beads. Freeze extracts and store at -80 °C.

2.2.2.4 Total yeast RNA purification

Total RNA was purified from yeast by washing 5 mls cells at A600 0.8 1x in ice-cold deionized water, then adding 50 µl TES (10 mM Tris-HCl pH 7.5, 10 mM EDTA,

0.5% SDS), followed by snap-freezing in liquid nitrogen. Cells were then thawed briefly on ice and 50 µl 65°C saturated phenol pH 4.5 (Amresco) was added and samples were vortex at maximum speed for 15 seconds. Samples were incubated at 65 °C for one hour, with vortexing every 10 minutes for 10 seconds, followed by a two-minute incubation in liquid nitrogen. Samples were then centrifuged at 14,000 rpm for 10 minutes at RT in an Eppendorf 5417C tabletop centrifuge and supernatants were then transferred to a new 1.5 ml tube. Samples were then phenol-extracted 4x with 65 °C saturated phenol pH 4.5 followed by incubation in liquid nitrogen and centrifugation, extracted once with 24:1 chloroform:isoamyl alcohol (Amresco), and ethanol precipitated. Sample concentrations were determined with a Varian Cary 50-BIO UV spectrophotometer.

2.2.2.5 Yeast transformations

Yeast transformations were performed using a protocol based on Gietz (Gietz, St Jean et al. 1992). 5 mls log phase cells A600 1.0 were washed once with dH_2O, resuspended in 10 ml YPAD, and incubated at 26°C for 3.5 hrs. Cells were then washed three times with dH_2O, resuspended in 300 µl 100 mM LiOAc, split equally into two 1.5 ml tubes, and incubated at 30°C for 15 minutes. Cells were then pelleted by centrifuging at 10,000 rpm in an Eppendorf 5417C tabletop centrifuge and the supernatant was aspirated. In a separate tube, 125 µl 50% PEG4000, 18 µl 1 M LiOAc, 5 µl 10 mg/ml sonicated single stranded salmon sperm DNA (Invitrogen), and 10 µl transforming DNA (minimum 5 µg) or water (for mock) were vortexed. This was then added to the cells and vortexed. Transformations were incubated at RT from overnight to 3 days, then incubatedfor 5 minutes two times in 1 M sorbitol with 3,000

rpm centrifugation steps, and incubated once for 15 minutes in 1:1 1 M sorbitol:YPAD+2% glucose. Cells were then rescued for 4 hours at 26°C with shaking and plated on selective plates at two concentrations.

2.2.3 Microscopy preparatory protocols

2.2.3.1 Agarose Pads

Agarose Pads were made by boiling 5% TBE-agarose (Invitrogen) then allowing it to cool to 68°C in a heat block, then mixing 1:1 with synthetic complete media + 2% raffinose + 2% galactose, and pipetting 5 µl of this onto a microscope slide, then gently placing another slide atop for 1 minute. Pads were stored in a closed, humid container for 1 day before use.

2.2.3.2 Formaldehyde fixation of GFP-expressing yeast cells for microscopy

Yeast cells were fixed for microscopy using a modified version of Bressan's protocol (Bressan, Vazquez et al. 2004). To 1 ml of yeast cells at A600 0.2 in YPAD add 54 µl 37.5% formaldehyde (1.8% final concentration), mix, and incubate at RT for 10 minutes. Quench the formaldehyde with 1/20th volume 2.5 M glycine. Centrifuge at 10,000 rpm for 15 sec in an Eppendorf 5417C tabletop centrifuge and aspirate supernatant. Incubate at RT for 10 minutes in 1 ml 0.1 M Potassium Phosphate buffer pH 6.6 (381 µl 1 M K_2HPO_4 + 619 µl 1 M KH_2PO_4+9 mls dH_2O) + glycine. Centrifuge again, aspirate supernatant, and resuspend the cells in an appropriate

volume of 0.1 M Potassium Phosphate buffer pH 6.6, transfer to ice, observe under microscope.

2.2.3.3 Concanavalin A plate preparation

Concanavalin A (C2631, Sigma) is a lectin protein which interacts with specific terminal sugar proteins which are expressed on the outside of the yeast ascal wall, and can be used to immobilize yeast on cover slips and microscope slides. Add 100 µl/dish or cover slip or slide, 10' RT, aspirate, 2 hours RT air dry minimum. Treated dishes may be stored at RT for months. Concanavalin A stock: Dissolve at 0.2% in PBS, store at -20^{o}C.

2.2.3.4 Preparing glass coverslips for use in microscopy

Acid wash coverslips to aid cells and polyamino acids to stick to the glass. Heat the coverslips in a loosely-covered glass beaker in 1 M HCl at 50-60oC for 4-16 hrs. Cool.

Wash coverslips extensively in dH_2O, then ddH_2O. Rinse coverslips in ethanol and leave to dry between a folded sheet of whatman paper (dry as separate coverslips). Keep in a sterile tissue culture dish (can store for a year). Acid wash is optional, ethanol wash is not.

2.2.4 Experimental protocols

2.2.4.1 Strain construction

2.2.4.1.1 Naming convention for strains with two syntenic fluorescent spots

Several of the strains in this study have been stably transformed with a tet operator array, a lac operator array, a fluorescently tagged tet repressor fusion gene, and a GFP-lacI fusion gene for the purpose of fluorescently tagging individual genomic loci. The operator arrays are integrated adjacent to one another in the clones, with various amounts of genomic DNA separating them. The amount of genomic DNA flanked by the fluorescent spots ranges from 15 kb to 30 kb to 60 kb, depending on the strain. Naming convention includes the length of the intervening genomic DNA as well as half of the lengths of the operator sequences in strain names. Therefore, a strain with 60 kb genomic distance flanked by ~10 kb of lac operator array and ~10 kb of tet operator array is referred to as a 70 kb strain, as 60 + ½(10 kb) + ½ (10 kb) is 70 kb. It should be noted that the fluor included in the tet repressor fusion may be different for a given 70 kb strain, as tetR-GFP, -3xGFP, -mCherry, and -3xCFP 70 kb strains were all generated.

Several strains generated during this work include syntenic lac operator and tet operator arrays, the GFP-lacI fusion protein, and a tetR fusion protein fused to either GFP, 3xGFP, mCherry, or 3xCFP. These various strains are all referred to as two-spot strains.

2.2.4.1.2 Cloning strategy for GFP-tagged HO locus

Dr. Triantafyllos Gkikopoulos of the TOH lab generated strain 1115 which contained a tetOx224 operator array stably integrated upstream of the *HO* promoter, expressed the tetR-GFP fusion protein from a copy of the URA3 promoter, and contained a deletion of the CDC20 gene which was rescued with a GAL1:CDC20 construct, permitting the expression of Cdc20p in a galactose-dependent manner. The last two modifications permitted cell-cycle synchronization through withholding galactose. The strain was verified by PCR using primers 1487 and 1488. This strain was used to create strain 1114 which has *ash1* deleted. This deletion was verified by PCR using primers 1790 and 1791.

Attempts were made to introduce a point mutation into the catalytic domain of the *SNF2* gene, or to delete the *SNF2* ORF entirely in strain 1115, but they were not successful. Attempts were made to tag the nuclear pore protein *NUP49* and the spindle pole body protein *SPC42* with GFP to be used as a motion control for MSD analysis, but these attempts were not successful. It was observed that strains transformed with the *cdc20* deletion and the GAL1:CDC20 construct are difficult to transform and cross (personal communication, personal observation).

2.2.4.1.3 Cloning Strategy for tetR-GFP-activation domain fusions

A yeast strain with a 112-copy tet operator tandem array stably integrated between 166,500 bp and 169,500 bp on chromosome XV, and a NLS-tetR-GFP fusion construct stably integrated at the *LEU2* locus was previously generated by Matt

Renshaw of the Tanaka Lab. This strain was well suited for the present study and the Tanaka Lab graciously made it available as a generous gift. This strain, 1154, will be referred to as MRtetGFP.

The SWI/SNF subunit Snf5 was tagged with the 13Xmyc tag in strain MRtetGFP by homologous recombination to facilitate immunofluorescence microscopy (IFM) of subsequent strains. Primers 1587 and 1610 were used to amplify across 13Xmyc in the pFA13mycHIS3 plasmid for this purpose. This new strain, 1160, was verified by PCR across the integration site using primers 1588 and 1589, and was then named strain MRtetGFPmyc.

The SWI/SNF subunits Snf6p and Snf11p, which are relatively small at 37.6 and 18 kiloDaltons, respectively, which are both present in the complex in two copies, and which are known to interact with relatively few proteins other than SWI/SNF subunits, were cloned downstream of, but in frame with, tetR-GFP in this strain. The cloning strategy is presented in Figure 2.1, with the SWI/SNF subunit SNF6 used as an example.

2.2.4.1.4 Cloning strategy for the chromatin remodeling deletion strains

The Tanaka Lab had previously generated two yeast strains with fluorescently tagged syntenic loci which were well suited for the present study and which they made available for this study as generous gifts. The first, strain 1200, is a 70 kb strain (see Materials and Methods for naming convention) (Kitamura, Blow et al. 2006). The operator arrays include an 11,100 bp tet operator array containing 224 repeats is

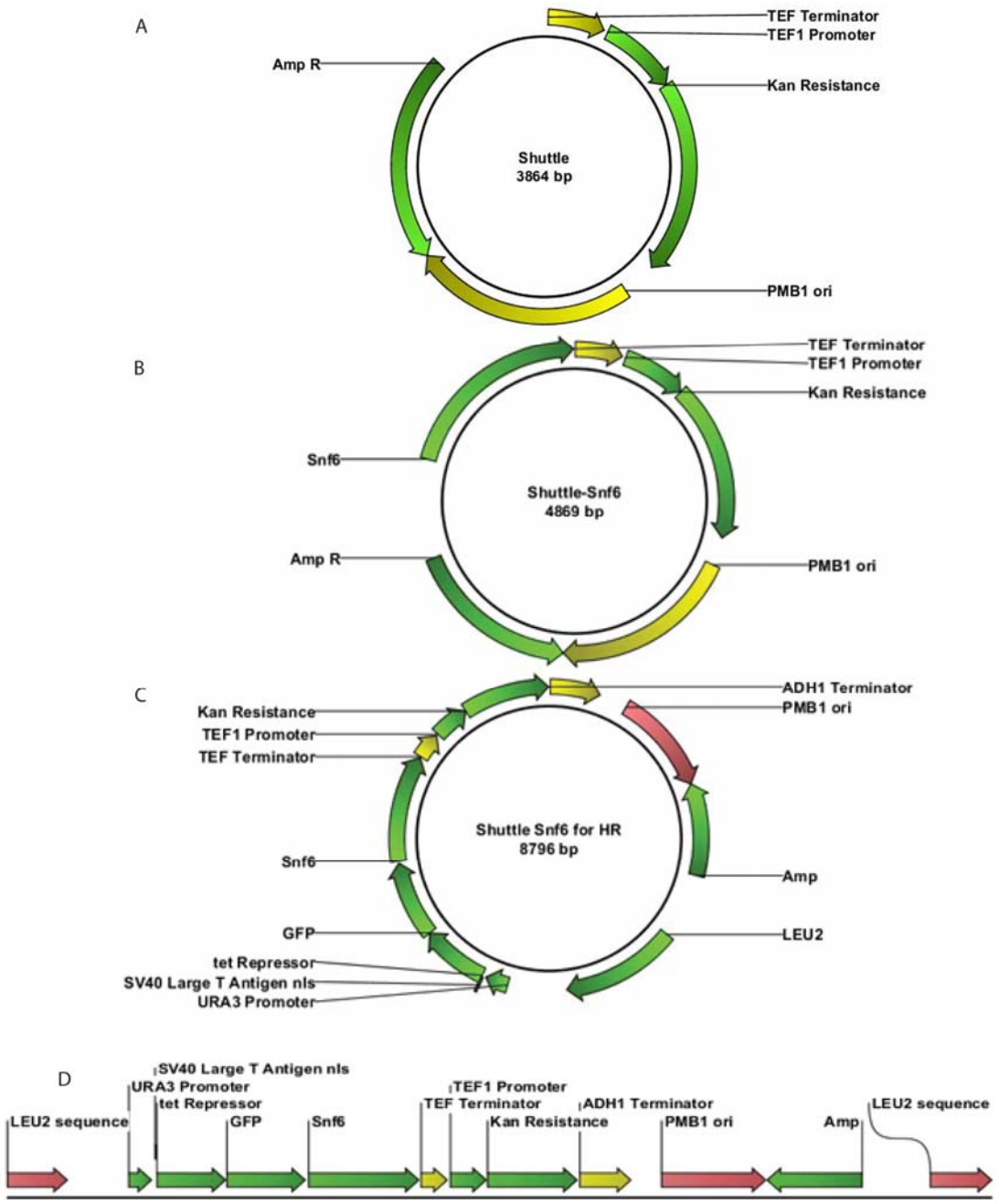

Figure 2.1 Cloning of SWI/SNF recruitment strains. Primers 1516 and 1517 were used to amplify SWI/SNF subunit Snf6 and flank it with restriction sites. Primers 1518 and 1519 were used to similarly amplify Snf11. A shuttle vector (A) was utilized to place Snf6 or Snf11 adjacent to the kanamycin resistance gene, generating Shuttle-Snf6 or Shuttle-Snf11 plasmids (B, Snf6 used as example). Snf6- or Snf11-KanR was then cloned into a pre-transformation vector (C). The transforming constructs were isolated via restriction digest and gel extraction before transformation. The construct is shown integrated at the *LEU2* locus in S. cerevisiae chromosome III in D. PCR was performed across integration sites using primers 1524 and 1526 to verify correct integration. Strains 1170 and 1168 were named TetR-GFP-Snf6 and –Snf11, respectively. The resulting fusion proteins recruited the SWI/SNF complex to a tet operator array of 112 tandem repeats, which was localized with the GFP tag, on chromosome XV.

integrated at 298 kb on chromosome IV, and a 10,000 bp lac-operator array containing 256 repeats was integrated at 358 kb, also on chromosome IV. The strain also expresses the lacI-GFP and tetR-3xCFP fusion proteins, which fluorescently tag the operators with a green and a blue spot, respectively. The two fluorescent tags in this strain flank a genomic distance of 60 kb and 36 open reading frames. The second strain, 1252, has the same lac operator array integration site as strain 1200, but the tet operator array is integrated at 340 kb in chromosome IV (unpublished). Thus, the two fluorescent tags flank a genomic distance of 30 kb and 18 open reading frames. This strain also expresses GFP-lacI and tetR-3xCFP. A list of genes flanked by the fluorescently tagged loci in the two strains is presented in the appendix.

The chromatin remodeling enzyme deletion strains *chd1*, *fun30*, *irc5* (lsh), and *ris1*, as well as the histone chaperone protein deletion strain *asf1*, were crossed into the 70 kb background individually, and clones were isolated on appropriate selective plates. Strains were verified by PCR across integration site juctions. Primers used for checking integration site junctions are presented in Table 2.3. Attempts to introduce a snf2 point mutation into the 70 kb strain which would cripple its SWI/SNF catalytic activity failed. Attempts were made to cross histone H3 and H4 tail truncations into the 70 kb strain, but no crosses were successful and it was determined that there was a duplication of a crucial selectable marker in the 70 kb strain (strain 1200).

Deletion	5' junction Primers	3' junction Primers
chd1	1523 and 1796	1795 and 1797
fun30	1523 and 1799	1795 and 1800
irc5	1523 and 1802	1795 and 1803
ris1	1523 and 1805	1795 and 1806
asf1	1523 and 1808	1795 and 1809

Table 2.3. Primers used to verify chromatin remodeling enzyme and asf1 deletions in the 70 kb strain.

2.2.4.1.5 Cloning strategy for the Gal1p-MDN1 strain

The cloning strategy adopted to create this strain is presented in Figure 2.2. Briefly, a copy of the 15 kb ribosomal *MDN1* gene, driven by the inducible Gal1 promoter and flanked by Lac and Tet operator arrays, was stably integrated at the URA3 locus of yeast strain 1261 which contains stably integrated GFP-LacI and TetR-GFP fusion genes.

Three plasmids were generated in order to establish this system. The first, plasmid 202, was constructed by first PCR amplifying across the Cyc1 terminator using primers 1957 and 1958. These primers introduced restriction sites flanking the terminator. This PCR product, as well as the pRS416 plasmid, were then digested with XbaI and BamHI restriction enzymes, PCR- or gel-purified, and ligated together, and the resulting plasmid was called pRS416-Cyc1t. The 3' end of the *MDN1* gene was then amplified by PCR using primers 1959 and 1960, which flank the gene fragment with restriction sites. This PCR product, and the pRS416-Cyc1t plasmid were then digested with SacI and BclI, PCR- or gel-purified, and then ligated together to produce the pRS416-Cyc1t-MDN1 3' plasmid. This plasmid was digested with PmlI and PfoI, the 4701 bp fragment was gel isolated away from the 619 bp fragment, then treated with Klenow, and blunt-end ligated to make the pRS416-Cyc1t-MDN1 3'-noCEN6 plasmid. This plasmid and the pRS306TetOx224 plasmid were digested with BamHI and HindIII, either gel purified or Qiagen PCR purified, and both large fragments were ligated together to make plasmid 202, which was transformed into the MAX Efficiency Stbl2 bacterial cell line (Invitrogen 10268-019).

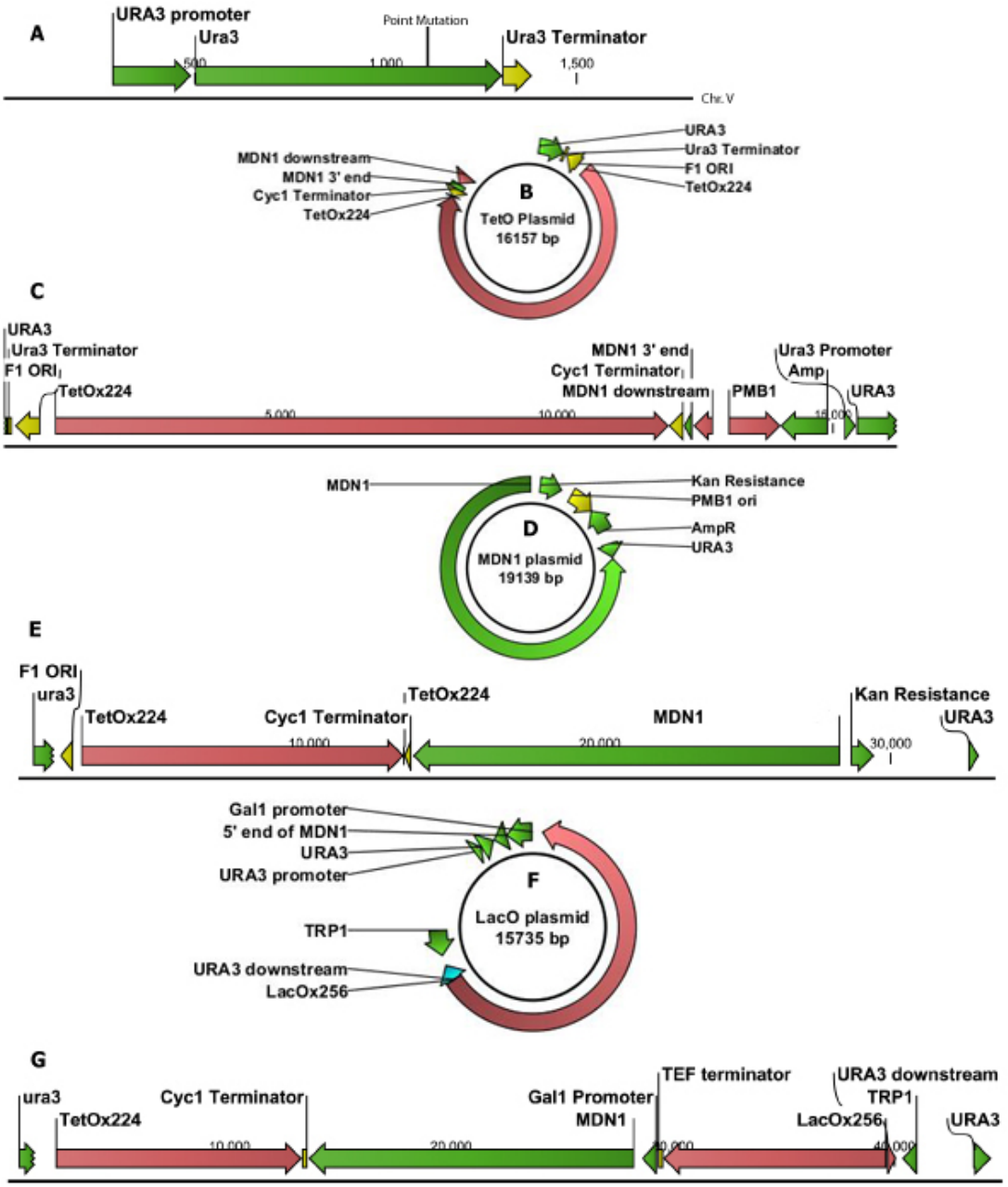

Figure 2.2 Cloning the Gal1p-MDN1 strain. A. The *ura3* locus. Yeast strain 1160 contains a point mutation at *URA3* (shown) and has been stably transformed with the tetR-GFP and GFP-LacI constructs. This strain was transformed successively with a tet operator array, the MDN1 gene, and the lac operator array to generate the Gal1p-MDN1 strain. First, a tet operator array of 224 tandem repeats was cloned into a plasmid (B) containing the wild type URA3 gene. This was linearized via restriction digest within URA3 and transformed into strain 1160, where it stably integrated at the URA3 locus (C). The MDN1 gene was cloned into a plasmid (D), restriction digested, and transformed into the strain shown in C, generating the strain shown in E. The lacOx256 array was cloned into a plasmid (F), restriction digested, and transformed into the strain shown in E to generate the Gal1p-MDN1 strain (G).

The second plasmid, 206, was constructed by PCR-amplifying the 5' end of the *MDN1* gene with primers 2004 and 2008, digesting it and the pFA6-KanMX6 plasmid with SacII and SacI, Qiagen PCR purifying, and ligating the large fragments to make the pFA6-KanMX6-MDN1A plasmid. Primers 2005 and 2048 were used to amplify across the 3' end of the *MDN1* gene. This product and the pFA6-KanMX6-MDN1A plasmid were then digested with NruI and BssHII, and the large fragments were ligated together to make the pFA6-KanMX6-MDN1A+C plasmid. This plasmid and the pYCG-YLR106c (EUROSCARF P20368) plasmid (196) were digested with SacI and SacII and the large fragments were ligated together to make plasmid pFA6-KanMX6-MDN1ABC. PCR amplification across the URA3 promoter using primers 1996 and 1997, with plasmid pRS416 as template, generated a URA3 promoter PCR product. This product, as well as the pFA6-KanMX6 plasmid (124), were digested with BstEII, then SalI, Qiagen PCR purified, and the large fragments were ligated together to make the pFA6-KanMX6-URA3pro plasmid. The pFA6-KanMX6-URA3pro plasmid and the pFA6-KanMX6-MDN1ABC plasmid were both digested with BspHII and SphI, the large fragments were gel extracted, and then ligated together to make the pFA6-KanMX6-URA3pro- MDN1ABC plasmid (206).

The third plasmid, 207, was constructed by first transforming the Yiplac204-Gal1Pro-MDN1 5' plasmid (190)(Struhl Lab) into dam- bacterial strain SCS110 (Invitrogen). PCR amplification of the URA3 promoter was done using primers 1993 and 2105, with the pRS416 plasmid as template. Plasmid 190 and the PCR product were digested with HindIII and BclI, either Qiagen PCR purified or gel extracted, and the large fragments were ligated together to create Yiplac204-Gal1Pro-URA3pro. PCR amplification of the URA3 downstream region was done using primers 1994 and

1995, using yeast genomic DNA as template. This PCR product and the Yiplac204-Gal1Pro-URA3pro plasmid were digested with NarI and NdeI, either Qiagen PCR purified or gel extracted, and the large fragments were ligated together to create Yiplac204-Gal1Pro-URA3pro-URA3down. This plasmid was then digested with SacI and NarI, while the LacOx256 plasmid was digested with SacI and AccI, both large fragments were gel extracted and then ligated together to make the Yiplac204-Gal1Pro-URA3pro-URA3down -LacO plasmid. This plasmid was transformed into Stbl2 competent bacteria (Invitrogen). PCR amplification of the TEF1 terminator was performed with primers 2013 and 2014 using the pAG32 plasmid as template. This PCR product, as well as the Yiplac204-Gal1Pro-URA3pro-URA3down -LacO plasmid, were digested with XhoI and SacI, the large fragments were isolated via Qiagen PCR purification or gel extraction and ligated together to create plasmid 207. The plasmid was transformed into competent bacterial strain GM2929 (Yale), which is dam-, dcm-, and recombination deficient as it has the recJ deletion.

Plasmids 202, 206, and 207 were digested individually with at least three different restriction enzymes, each of which cut the respective plasmid five times, in order to verify correct clones.

Plamid 202 was digested with Bpu10I and transformed into yeast strain 1279 to make strain 1280. Correct clones were selected with –ura plates. Plasmid 206 was digested with PmlI and transformed into strain 1280 to make the TetO-MDN1 strain. Correct clones were selected with G418 plates. Plasmid 207 was digested with BtgI and BclI and transformed into strain TetO-MDN1 to make strain 1295, the Gal1p-MDN1 strain. Correct clones were selected with –trp plates.

Genomic DNA was isolated from strain 1295 and the Gal1 promoter and 5' end of the *MDN1* gene were sequenced. A deletion mutation was detected at base 241, resulting in a frame shift across the majority of the gene. The plasmid was corrected, and several colonies from a newly transformed yeast strain were isolated recently, but as of the time of this writing these strains have not been screened to determine if the point mutation was corrected. As the project aims to examine the effects of transcription on chromatin structure, as opposed to the transcript itself or the gene product, we decided to proceed with microscopy experiments on the deletion strain. PCRs across integration site junctions show that all three constructs integrated correctly at the URA3 locus. Microscopy confirmed that the intensity of both spots was >4-fold over background, indicating that copy number of lac and tet operators was preserved.

2.2.4.2 Experimental microscopy and analysis protocols

2.2.4.2.1 Single particle tracking

A plethora of software designed for tracking fluorescent point spread functions in microscopy videos has become available in recent years. These software programs include many similar features which are important for accurate spot tracking. Among these, background subtraction and thresholding increase the signal to noise ratios, aid in spot detection, and reduce localization error. Drift can be controlled for using methods mentioned above. Registration is a process which relies on pattern recognition software to identify at least two immobile structures in a series of images,

and then adjusts for drift by aligning these spots in all of the images. This allows for the subtraction of movement arising from the system and the accurate tracking of mobile structures within the system. Fitting a Gaussian curve to the pixels of a PSF can effectively locate its center of mass at sub-pixel resolution, and there are several types of Gaussian algorithms available in various software packages which perform this function. Estimations of the z-coordinate during 3D tracking are based on intensity measurements of spots visible in >1 image in a single stack. Once spots are detected, a variety of methods may be used to track the particles from image to image. These rely on various parameters such as maximum expected displacement during a given time interval, known particle trajectories, and intensity information which can be used to track specific spots that come in close proximity with one another and therefore have overlapping point spread functions. Most tracking programs allow user input to correct miss-tagged PSFs and eliminate false PSFs. A list of tracking software programs tested during the course of this project is included in the Tracking software tested section of the Materials and methods chapter.

2.2.4.2.2 Mean squared displacement (MSD) analysis and diffusion constants

Brownian motion is the random migration of particles due to their thermal energy, and the observed motion of such particles under no other external forces can be described as a random walk (Berg 1993). Fluorescently tagged chromosomal loci have been shown to follow similar diffusive patterns and their motion has been analyzed and characterized mathematically using MSD analysis (Qian, Sheetz et al. 1991). MSD curves of particles tracked microscopically can be calculated using the formula $MSD(\Delta t) = \langle d(t) - d(t + \Delta t) \rangle^2$, where MSD is in units $\mu m^2/sec$, and d(t) is the position

of the particle at time t (Marshall, Straight et al. 1997). The application of Monte Carlo calculations and percolation theory to the modeling of the motion of diffusing particles observed in solution mark an important step in the development of SPT analysis theory through the characterization of anomalous diffusion due to obstacle concentration (Saxton 1994). MSD analysis of the diffusion of particles over relatively long time scales has been used to show that particle motion can be characterized as exhibiting different types of diffusion (Figure 2.3), including diffusion with flow, simple or free diffusion, or diffusion in a box (constrained diffusion) (Qian, Sheetz et al. 1991; Cabal, Genovesio et al. 2006; Platani, Santarella-Mellwig et al. 2009). More recently this list has been appended to include a type of heavily constrained diffusion which follows the power law $<\Delta d^2> = c(\Delta t)^{\alpha}$ and is called subdiffusion (Figure 4j) (Cabal, Genovesio et al. 2006).

Fluorescence video microscopy of strains 1115 and 1114 was performed using a Deltavision inverted fluorescence microscope (Applied Precision). Strains were cultured overnight in YPA plus 2% raffinose at 26^{o}C with shaking. Media was inoculated such that the A600 would be 0.2 at the following morning. A budding index was performed to verify synchrony, and cells were washed three times with SC media plus 2% raffinose and plated on MatTek dishes (P35G-1.5-10C, Mattek) treated with Concanavalin A (C-2631, Sigma). Cells were allowed to adhere for 10 minutes at RT, were washed two times with SC plus 2% raffinose. Cells were released from cell cycle arrest with 2% galactose 20-50 minutes before imaging. 2D imaging consisted typically of 600 images with 25msec exposure times, 124x124 dimensions, utilizing the standard Quad filter set (FITC, RD-TR-PE, DAPI, Pol), acquisition with a Cascade 512 EMCCD camera, 100% ND filter setting, 1.514

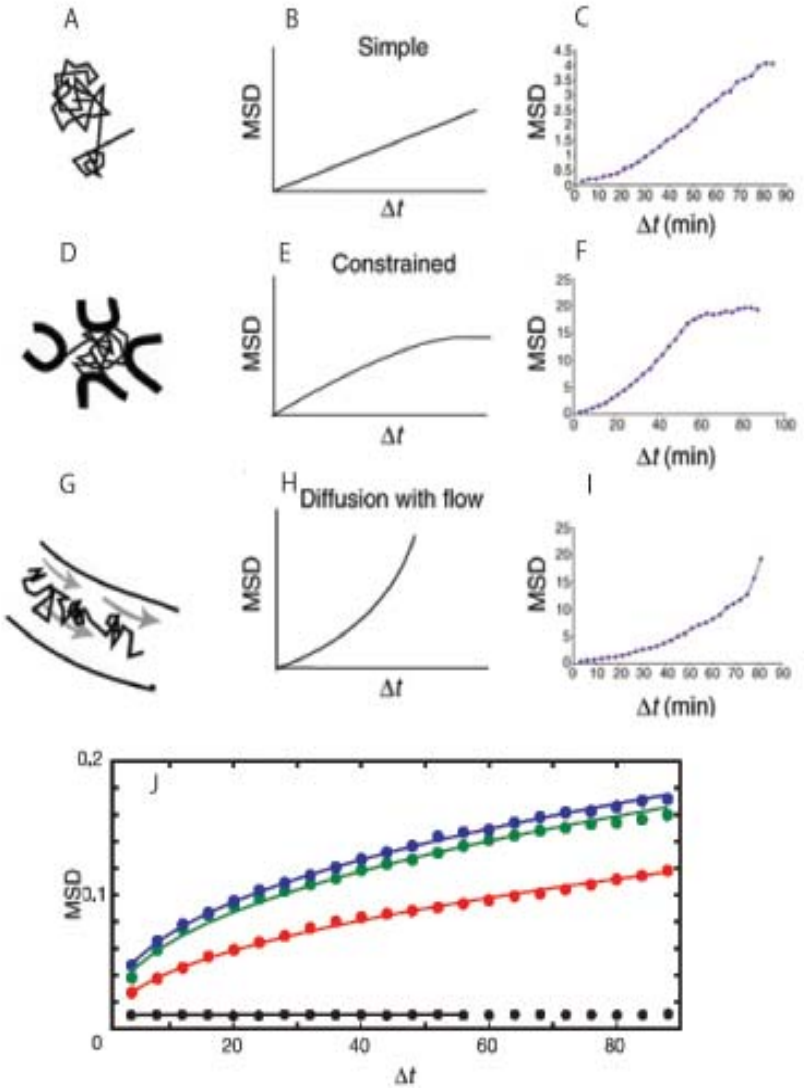

Figure 2.3 Classifications of diffusion. A. Random walk diagram showing simple diffusion. B. Idealized MSD graph of simple diffusion. C. Example MSD graph of simple diffusion. D. Random walk diagram showing constrained diffusion. E. Idealized MSD graph of constrained diffusion. F. Constrained diffusion. G. Random walk diagram showing diffusion with flow. H. Idealized MSD graph of diffusion with flow. I. Example MSD graph of diffusion with flow. J. Cabal et al. describe a classification of diffusion known as sub-diffusion, which occurs when the diffusing structure is constrained to diffuse along a surface, for example, along the inner lining of the nuclear envelope. Idealized MSD graph of sub-diffusion (red line). Green and blue dotted lines are examples of constrained diffusion, black is fixed control. Images taken from Platani et al 2002 and Cabal et al 2006.

immersion oil at 25°C or 1.516 at 30°C. Microscopy was limited to two videos per dish to avoid over-bleaching of samples. 3D imaging was performed with the same

settings but included a stack size of 3 μm and a step size of 200 nm.

Videos were filtered with Spot Enhancing Filter 2D, and spots were then tracked and diffusion paths were generated with Spot Tracker 2D, both produced in the Gasser Lab, and made available as ImageJ plugins. MSD analysis was performed on the resulting data. Videos with 600 time points were collected for a minimum of 10 pairs of mother/daughter nuclei per condition, and of these at least 400 time points were usable per video. Tracking of spots *in vivo* is typically performed with immobile controls for drift, as mentioned previously. As attempts to tag the nuclear pore protein Nup49, and the spindle pore body protein Spc42 with GFP failed in strain 1115, motion analysis was performed without these controls. Diffusion paths of all videos were examinedto rule out drift. Diffusion constants were calculated as the slope of the MSD curve at the second through fourth time increments (MSD/Δt). Time increment one is considered to be the time point most affected by noise and for this reason is not used in the calculation.

2.2.4.2.3 Immunofluorescence microscopy (IFM) of yeast cells

Polylysine-treat slides for 5 minutes at RT, then air dry for 2 hrs. Harvest 10 ml cells at A600 of 0.1 to 0.2. Wash 3x in dH_2O to remove Bar1p, then resuspend in 10 ml YPAD. Synchronize the cells using the Tanaka Lab alpha factor synchronization method, which arrests cells in late G1. Note budding index. Make a control sample that will receive no primary antibody. Fix 1 ml cells with 54 μl 37.5% formaldehyde (Sigma) for 10 minutes with shaking at 25^{o}C, quench with 1/20th volume 2.5 M glycine, ice 5 minutes, centrifuge at 10,000 rpm for 15 sec and aspirate supernatant.

Resuspend cells in 500 µl Sorbitol/Potassium Phosphate buffer, transfer to a 1.5 ml tube. Centrifuge at 10,000 rpm for 15 sec and wash again in Sorbitol buffer. To 10 mls Spheroplast buffer add 20 µl B-mercaptoethanol and 80 µl 10 U/ml Zymolyase. Centrifuge at 10,000 rpm for 15 sec and resuspend cells in 500 µl spheroplast buffer plus B-ME and Zymolyase. Incubate at 30^{o}C with shaking at 500 rpm for 10 minutes. Cells are fragile after zymolase treatment. Check spheroplasting by mixing 2 µl 2% to 2 µl cells on a microscope slide and compare to a no-sarkosyl control. Ideally, you want 70% of the cells to burst in the sarkosyl. Centrifuge at 10,000 rpm for 15 sec and wash 2x in Sorbitol buffer, then resuspend the cells in 10x pellet volume. Add 50 µl cells per slide or cover slip and incubate for 15 minutes at RT. Aspirate supernatant, dip slides in MeOH for 6 minutes, then acetone for 30 sec at RT in the fume hood. Air-dry completely. Add 100 µl block buffer and incubate for 30 minutes at RT, aspirate. Add 100 µl primary antibody diluted in blocking agent and incubate at 4^{o}C overnight in a humid, airtight chamber. Wash 5x in block. Add 5 µl secondary antibody diluted in block buffer and incubate for 1 hr in the dark at RT. Wash 5x in block buffer, add 50 µl DAPI (0.2 mg/ml in PBS), and incubate for 15 minutes at RT in the dark. Wash 5x in block buffer and air dry. Add mounting media (60% glycerol+10% AF3 Citifluor anti fade+30% dH_2O) and observe under the microscope.

2.2.4.2.4 Photobleaching

2.2.4.2.4.1 Fluorescence recovery after photobleaching (FRAP)

FRAP relies on a pulse of high-intensity light to irreversibly photobleach a population of fluorophores in a target region, and subsequent measurement of the recovery of fluorescence in the bleached region as bleached fluorophores are replaced by unbleached from elsewhere in the cell (Stavreva and McNally 2004). This allows quantification of the binding rate of a DNA binding domain protein with respect to its DNA binding sequence (Sprague, Muller et al. 2006) or the calculation of diffusion constants of diffusing fluorophores (Houtsmuller 2005).

The method involves the initial measurement of the pre-bleach intensity of the target region (F-), measurement just after the bleach event (F_0), the measurement of the target intensity at several time points following the bleach, the comparison of F_0 with the maximal intensity recovered post-bleach (F_{inf}), and the calculation of the half time of recovery, or $T_{1/2,}$ which is the time it takes for the target to regain half its post-bleach maximal intensity . The various intensity readings are plotted against time to generate a recovery curve. The half time is calculated from the bleach correction factor and Axelrod's time constant, which are calculated during the FRAP data curve fit (Axelrod 1976). The mobile fraction (MF) is the percentage of fluorescent molecules that are free to diffuse within the bleached region, and is presented in equation 1:

$MF = F_{inf} - F_0 / (F- - F_0)$

Equation 1. (Axelrod 1976)

The half-time of recovery, $T_{1/2}$, is given as equation 2:

$$½ MF = F(T_{1/2}) - F_0 / (F(-) - F_0)$$

Equation 2. (Axelrod 1976)

The 2-dimensional diffusion coefficient (D) of the fluorophore is given in equation 3:

$$D = W^2 / 4t_D$$

Equation 3. (Axelrod 1976)

Where W is the laser spot radius and t_D is Axelrod's time constant. The bleaching effect due to image acquisition must be established beforehand for normalization purposes.

2.2.4.2.4.2 Fluorescence loss in photobleaching (FLIP)

FLIP relies on a pulse of high-intensity light to irreversibly photobleach the unbound fraction of fluorescently tagged DNA binding domain proteins within a target region, and the subsequent measurement of the loss of fluorescence from the DNA binding domain as unbleached proteins are replaced by bleached. The half-life time of decay of the fluorescence intensity of the DNA binding domain allows us to estimate the off rate of the DNA binding protein. Normalized FLIP decay curves may be fitted by the exponential function (Rino, Carvalho et al. 2007) given by equation 4:

$F(t) = e^{-kt}$

Equation 4. The term k is the rate of fluorescent decay. The bleaching effect due to image acquisition must be established beforehand for normalization purposes (Rino, Carvalho et al. 2007).

2.2.4.2.4.3 Photobleaching experiments

Fluorescence video microscopy of strains 1160, 1168, and 1170 was performed using a Deltavision inverted fluorescence microscope (Applied Precision). Strains were cultured overnight in YPA plus 2% glucose at 26^{o}C with shaking. Sufficient media was inoculated such that the A600 would be 0.2 the following morning. Cells were washed three times with SC media plus 2% glucose and plated on MatTek dishes (P35G-1.5-10C, Mattek) treated with Concanavalin A (C-2631, Sigma). Cells were allowed to adhere for 10 minutes at RT, were washed two times with SC plus 2% glucose.

Imaging was typically performed with 100% ND filter setting, 1.514 immersion oil, at 25^{o}C using 124x124 image dimensions, utilizing the standard Quad filter set (FITC, RD-TR-PE, DAPI, Pol), and acquisition was done with a Cascade 512 EMCCD camera. Microscopy was limited to two videos per dish to avoid over-bleaching of samples. 3D imaging was performed with the same settings but included a stack size of 3 μm and a step size of 200 nm. FRAP experiments were carried out using the Deltavision microscope fitted with a laser and a beam expander, as described. FLIP experiments were carried out using the Deltavision microscope fitted with a laser and a beam expander, and a Zeiss LSM 510 confocal microscope.

2.2.4.2.5 Establishment of a system for tracking chromosomal loci in live cells with OMX

The lac operator is a specific DNA 8-mer sequence which is recognized and bound by the lac^{i} repressor protein. Multi-copy tandem arrays of the lac operator stably integrated into the yeast genome and bound by green fluorescent protein (GFP)-lac repressor-nuclear localization signal (NLS) fusion proteins have previously been shown to localize specific DNA sequences *in vivo* as point spread functions via fluorescence light microscopy (Robinett, Straight et al. 1996; Straight, Belmont et al. 1996). Single-molecule studies relying on integrated photon molecular counting (IPMC) of lacOx256 arrays bound by GFP-lacI fusions indicate that an average of 13 tagged fusion proteins are bound to the array at a given time (Wang, Tegenfeldt et al. 2005). Similar fluorescent localization may be done with the Tet operator arrays bound by tet repressor-GFP-NLS fusion proteins (Michaelis, Ciosk et al. 1997). GFP-lacI-bound lac operator arrays and tetR-GFP-bound tet operator arrays are known not to interact *in vivo* (Aragon-Alcaide and Strunnikov 2000). When two loci on the same chromosome are tagged in this manner, the distance between the spots can be measured microscopically and the results from many such measurements may be used to model chromatin compaction.

Previous comparisons of strains with stably integrated lacOx256 arrays and either no lacI, with lacI, or with lacI-GFP fusions, examined by IF microscopy with a fluorescent primary antibody recognizing lacI, by immunostaining of the lacO array using purified lacI followed by an anti-lacI antibody, or by live cell fluorescence microscopy, indicated that lac repressors do not substantially alter local chromatin

structure when bound to a lac operator array (Robinett, Straight et al. 1996). Similarly, nuclease and functional analysis performed on repressor-bound stably integrated lac operon arrays indicate that they do not substantially alter local chromatin structure (Heun, Laroche et al. 2001).

2.2.4.2.5.1 Collection of data from the 25, 40, and 70 kb strains

Strains were grown overnight in YPAD, or YPA plus appropriate carbon source, and then pelleted, washed twice, and resuspended in synthetic complete media plus 2% appropriate carbon source (University of Dundee media kitchen) followed by incubation on ice. Cells were plated on Concanavalin A (C2631, Sigma)-treated coverslips (Bioptechs, 40-1313-0319-1) and allowed to adhere for 10 minutes, and were washed with synthetic complete media plus 2% appropriate carbon source. Cells were incubated at room temperature (23^{o}C) for at least 20 minutes before observation with the OMX microscope (Applied Precision). Live cell 3D fluorescence video microscopy was performed, typically with 10 msec exposures, 10% ND, stack heights of 4 μm, a step height of 400 nm, a field of view of 128x128 pixels, and 50 time points. Under these conditions, individual images were 40 msec apart, and each stack, and thus each time point, was 539 msec apart. Illumination was provided by a 488 nm laser, and imaging was performed with a back-illuminated EMCCD camera (Photometrics) set in conventional mode for analysis with the Danuser tracking software. Cultures were asynchronous, but G1-phase cells were identified by the relative sizes of the mothers and daughters, and only these cells were imaged. Videos from cells which had proceeded to S-phase, i.e. cells with spots observed to split briefly in two, were dropped.

2.2.4.2.5.2 Root mean squared (RMS) measurement error determination

A method for the estimation of microscope measurement error proposed by the Sedat Lab relies on the tracking of immobilized fluorescent spots. First, a sample with a fluorescent spot of dimensions known to be smaller than the resolution of the microscope is chemically fixed. Such a fluorescent spot is detected as a PSF. Fluorescence video microscopy is performed on the sample using the most rapid acquisition settings of the microscope, and a Gaussian curve is then fit to the pixels of the PSFs in the different time points of the video to locate their centers of mass at sub-pixel resolution. Ideally, since the sample is fixed, the spot should not appear to move during the video. However, fluctuations in pixel intensities due to background or drift, as well as real diffusive movement which cannot be completely dampened by chemical fixation, result in a displacement, though small, from image to image in the video. Spot displacement per time point may be calculated using the Pythgorean Theorum. Measurement error is simply the detected motion of the spot when it is known that motion is minimal, which in this case is simply the RMS displacement of the spot per time point (Marshall, Straight et al. 1997).

Similar analysis may be performed in live cells in 3D where two adjacent chromosomal loci are fluorescently tagged. In this instance, the distance between the two spots is calculated in each stack using their location information. Drift is internally controlled for due to the fact that the motion of the two spots is relative to each other, not the system itself. The MSD at the smallest time increment is calculated as $<\Delta d\ (\Delta t_{min})^2>$, where d is the end-to-end distance between the two spots, and the RMS distance measurement precision is given as the square root of one-half

of this mean squared displacement (Marshall, Straight et al. 1997). Since the detected motion of the two spots is relative to one another, information about drift is ignored in this calculation. Thus, the RMS distance measurement error in the case of two spots in live cells does not additionally represent the effective resolution of the microscope as it does in the case of fixed, single spot analysis.

2.2.4.2.6 Modeling chromatin with the Porod-Kratky chain equation.

Chromatin may be modeled mathematically as a semi-flexible worm-like chain or flexible polymer using the Porod-Kratky equation (Equation 5), which uses modal end-to-end spot distance measurements to relate the persistence length (a measure of flexibility), the linear mass density, and the compaction ratio (Kratky and Porod 1949; Langowski 2004). This model assumes DNA has a homogeneous elasticity, although EM observations indicate that DNA kinking may occur more frequently than expected for a Gaussian distribution of bending angles (Wiggins, van der Heijden et al. 2006), and short DNA fragments have been shown to have a higher than expected cyclization probability for a homogeneously elastic worm-like chain (Cloutier and Widom 2004). An alternate method for determining characteristics of chromatin from 3C data combines the Porod-Kratky chain equation with the freely jointed chain (FJC) model (Ringrose, Chabanis et al. 1999; Rippe 2001). Marek Ghierlinski of the Data Analysis Group performed the fitting of the Porod-Kratky chain equation to the fixed-cell 40 kb and 70 kb data sets for this project.

$<r^2> = 2 \times Lp^2 \times (Lc/Lp - 1 + e^{-Lc/Lp})$

Equation 5. The Porod-Kratky chain equation. $<r^2>$ is the modal end-to-end distance squared, Lp is the persistence length, a measure of flexibility, Lc is the contour length, which is the genomic distance (d) divided by the linear mass density in base pairs per nm (c), and the compaction ratio is the observed linear mass density over the expected linear mass density of 2.94 for linear, B-form DNA .

2.3 Microscope specifications

2.3.1 Deltavision

Deltavision Olympus IX71 inverted fluorescence microscope (Applied Precision) fitted with a 100x PlanApo objective lens with a NA of 1.4, either a Coolsnap HQ charge coupled device (CCD) camera (Photometrics) or a Cascade 512 electron multiplying charge coupled device (EMCCD) camera (Cascade), an Olympus high pressure mercury lamp, a Nano-motion III precision control stage motor, a beam expander, and a standard Quad filter set (FITC, RD-TR-PE, DAPI, Pol). The Linux workstation is equipped with Resolve3D (Applied Precision) automated data collection software. The stage motor has an absolute accuracy < 0.6 *u*m per 13 *u*m Z scan, and an out-of-axis motion accuracy of < 0.6 *u*m per 13 *u*m Z scan (< 0.3 *u*m typical).

2.3.2 The *DeltaVision*|OMX® microscope

The *DeltaVision*|OMX® system is a new microscope format produced by Applied Precision which provides increased temporal and spatial resolution compared to conventional microscopes. The University of Dundee recently acquired one of only a handful of OMX microscopes in existence. The microscope is equipped with four

solid-state 200 mW lasers emitting at 405 nm, 488 nm, 593 nm, or 642 nm wavelengths for sample illumination. It is also equipped with four independent back-illuminated Cascade II EMCCD cameras with 16 micron pixels, 512x512 CCDs, and on-chip charge multiplication which provide simultaneous multi-channel imaging capabilities (Photometrics). It is equipped with a Piezo stage, an Olympus UPlanSpo 100X 1.4 NA oil lens, custom manufactured DAPI/FITC/Rhodamine/DIC and DAPI/FITC/A594/Cy5 emission filter sets (Semrock), a Bioptechs FCS2 live-cell chamber imaging system with temperature control. The Linux workstation is equipped with Resolve3D (Applied Precision) automated data collection software. The working specifications of the OMX are presented in Table 2.4. The OMX microscope of the University of Dundee was provided for by the Scottish Universities Life Sciences Alliance (SULSA), a strategic partnership between the Universities of Aberdeen, Dundee, Edinburgh, Glasgow, St Andrews and Strathclyde, and the Scottish Funding Council (SFC).

OMX specifications	Value in nm
Lateral Pixel Size Conventional Mode	79
Axial Pixel Size Conventional Mode	Varies with step size
Lateral Resolution Conventional Mode	350
Axial Resolution Conventional Mode	700
Deconvolved Lateral Resolution C.M.	250
Deconvolved Axial Resolution C.M.	500
Lateral Pixel Size S.I.	79
Axial Pixel Size S.I.	125
Post-reconstruction Lateral Pixel Size	40
Post-reconstruction Axial Pixel Size	125
Post-reconstruction Lateral Resolution	125
Post-reconstruction Axial Resolution	250

Table 2.4. Specifications of the OMX microscope. The resolutions are theoretical maxima, and in practice are slightly reduced, depending on the wavelength of the emitted light. C.M. is conventional mode, S.I. is structured illumination.

2.3.2.1 Structured illumination mode

The superior resolution of the OMX microscope is achieved on fixed cell samples through the application of the structured illumination mode. In this mode incident light passes through a fine mesh as well as the sample, producing a moire interference pattern containing positional information from both. The sample is imaged in 3D from three different angles, the known contribution of the mesh pattern is subtracted out, and the remaining interference pattern is deconstructed, producing an image of the sample at a resolution greater than possible with a simple glass objective.

2.3.2.2 Conventional mode

The conventional mode of the OMX microscope is optimized for speed in image acquisition. This is achieved through improvements in the light path, improvements in the electronics controlling the lasers, cameras, and the coordination of the two, and through the use of a Piezo stage, which relies on electrical impulses to Piezo-electric crystals to rapidly alter stage height with sub-micrometer precision. We tested the OMX in conventional mode using strain 1300 and found it can generate stacks of five images with exposure times of 10 msec and a temporal resolution of 30 msec per image with a 400 nm step size, and can acquire at this rate in 2 channels; or stacks of 9 images with exposure times also of 10 msec and a temporal resolution of 40 msec per image in a single channel.

2.3.3 Zeiss Confocal

Zeiss LSM Meta 510 Confocal Microscope (Carl Zeiss Ltd, UK) fitted with a 100× α PlanFluar/NA 1.45 objective. The workstation is equipped with LSM 510 acquisition software (Carl Zeiss, Inc.).

2.3.4 Axiovert

Inverted Axiovert 200 microscope (Zeiss) fitted with a DG4 lamp (Sutter), a GFP filter set (#41017, Chroma), a 0.60D ND filter (Chroma), an ImagEM EMCCD camera (C9100-13, Hamamatsu), and a Piezo stage, which relies on electrical impulses to Piezo-electric crystals to rapidly alter stage height with sub-micrometer precision. The workstation is equipped with Volocity acquisition software version 4.2 (Improvision).

2.4 Tracking software tested

Several different tracking software programs were tested during the course of this project for comparative purposes. Criteria for useful software centered on the degree of automation of the analysis, with the intent of minimizing analysis time, while maintaining accurate tracking capability. The software programs tested are presented in Table 2.5.

Softworx	Applied Precision (Issaquah, WA)
Imaris	Bitplane (St. Paul, MN)
Volocity	Perkin Elmer
Kalaimoscope Motion Tracker	Kalaimoscope
Irfanview	Irfanview
Tracking software	K. Jaqaman/Danuser Lab
StackReg	D. Sage/Gasser Lab/ImageJ
TurboReg	D. Sage/Gasser Lab/ImageJ
Spot Enhancing Filter 2D	D. Sage/Gasser Lab/ImageJ
Spot Tracker 2D	D. Sage/Gasser Lab/ImageJ
Image5D	D. Sage/Gasser Lab/ImageJ
View5D	R. Heintzmann Lab /ImageJ
TikalPro	Eils Lab
Omero Spot Tracker	Swedlow Lab/Omero website

Table 2.5. Tracking software tested during the course of this work. The StackReg, TurboReg, Spot Enhancing Filter 2D, and Spot Tracker 2D programs developed by the Gasser Lab are used together as a package for 2D filtering and spot tracking.

The Softworx program allows for manual tracking only, while all others listed are meant to be automated. Two software packages of note were fully or nearly-fully automated and produced location data that was in good agreement with data generated manually with the Softworx spot tracking function. These software packages were Bitplane's Imaris and the Spot Tracker 2D package from the Gasser Lab/ImageJ.

The Danuser spot tracking software provided the best automated 3D spot tracking capabilities in terms of ability to track two spots of the same color when in close proximity. It utilizes a mixture model fitting algorithm which analyzes 4D image data by employing the prior knowledge that detected spots are PSFs, and that a known number of spots are present, and then fits a number of tracking algorithms to the data, with statistical analysis of the fit of each algorithm to determine which is most accurate (Dorn, Jaqaman et al. 2005). The software relies on the fact that spot intensity, corrected for bleaching, is relatively constant over time, and uses least

squares multitemplate matching to estimate tag positions when they overlap. An interface allows the user to overrule any links which are obvious miscalls. This software requires raw image data as input and cannot be applied to the analysis of deconvolved images or images acquired with an EMCCD camera.

CHAPTER 3

Application of Fluorescence Microscopy to Study the Effects of ATP-dependent Chromatin Remodeling Enzymes on Chromatin Organization

3.1 Introduction

The compaction of DNA into higher order structures represents a key step in regulating access to genetic information. Eukaryotes rely on a selection of specialized ATP-dependent chromatin remodeling enzymes with roles in transcription, replication, DNA repair, and recombination to catalytically alter chromatin structure (Cote, Quinn et al. 1994; Kwon, Imbalzano et al. 1994; Utley, Cote et al. 1997; Flaus, Martin et al. 2006).

It has been established that ATP-dependent remodeling enzymes can alter the structure of chromatin at the level of the nucleosome *in vitro*. However, the activities relevant to the action of ATP-dependent remodeling enzymes *in vivo* are less clear. It is also not clear what the consequences of alterations to the structure of individual nucleosomes might be with respect to the macroscopic organisation of chromatin. Biochemical studies of remodeling enzymes have been dominated by the ease with which nucleosomal substrates can be prepared. It is more difficult to assess whether ATP dependent remodeling enzymes might have additional effects on higher order chromatin organization. For these reasons we were interested to study the organization of chromatin *in vivo*.

Perhaps the most direct way to study chromatin structure *in vivo* is observe it directly by microscopy. Recent developments make it practical to study the motion of individual genetic loci in fixed or living cells. Here we sought to apply cell based imaging to study the actions of ATP dependent chromatin remodeling enzymes.

The yeast Snf2 protein was the first ATP-dependent chromatin remodeling enzyme to be identified. It has been studied extensively and it is known that this complex is recruited to a subset of genes during the course of gene regulation. This made the SWI/SNF complex an attractive candidate for study.

In *Saccharomyces cerevisiae* SWI/SNF is a 1.14 megaDalton (Smith, Horowitz-Scherer et al. 2003), 11-subunit complex. The relative copy numbers of the SWI/SNF subunits, as well as their functions, are presented in Table 3.1. Overall, these are arranged as a globular structure possessing a cavity with the dimensions to accommodate a nucleosome (Smith, Horowitz-Scherer et al. 2003). More recent studies of SWI/SNF and the closely related RSC complex confirm that this cavity is occupied by a nucleosome (Dechassa, Zhang et al. 2008; Tang, Nogales et al. 2010). SWI/SNF is implicated in the regulation of transcription at a subset of yeast genes (Sudarsanam, Iyer et al. 2000). These genes relate to a variety of cellular processes

Subunit	Relative copy number*	Properties	
Swi1p	1.03	AT-rich ARID DNA binding domain and activation domain binding site	(Quinn, Fyrberg et al. 1996; Kortschak, Tucker et al. 2000; Prochasson, Neely et al. 2003)
Snf2p	1.00	DEAD/H helicase domain, catalytic subunit	(Cote, Quinn et al. 1994; Richmond and Peterson 1996; Flaus, Martin et al. 2006)
Swi3p	1.97	Implicated in complex assembly and H2A/H2B displacement	(Yang and Narlikar 2007)
Snf5p	1.17	Implicated in complex assembly and catalysis, contains activation domain binding site	(Prochasson, Neely et al. 2003)
Snf6p	2.12	Contains DNA binding domain, implicated in complex structural integrity	(Quinn, Fyrberg et al. 1996)
Arp7p	0.90	Purported nuclear scaffold protein and nuclear membrane interaction activities	(Cairns, Erdjument-Bromage et al. 1998; Rando, Zhao et al. 2000; Shen, Mizuguchi et al. 2000; Olave, Reck-Peterson et al. 2002)
Arp9p	0.66	Purported nuclear scaffold protein and nuclear membrane interaction activities	(Cairns, Erdjument-Bromage et al. 1998; Rando, Zhao et al. 2000; Shen, Mizuguchi et al. 2000; Olave, Reck-Peterson et al. 2002)
Snf11p	2.22	Contains transcriptional activator binding domain	(Treich, Cairns et al. 1995)
Swp29p	3.11	Required for efficient transcription in yeast, contains YEATS domain	(Kabani, Michot et al. 2005; van Vugt, Ranes et al. 2007)
Swp73p	1.19	Implicated in complex structural integrity, contains transcriptional activator binding domain	(Cairns, Levinson et al. 1996)
Swp82p	1.84	Uncharacterized	(Peterson, Zhao et al. 1998)

Table 3.1. Subunits of the SWI/SNF ATP-dependent chromatin remodeling enzyme (Smith, Horowitz-Scherer et al. 2003).

including the stress response (Ganster, McCartney et al. 1998), heat shock (Sullivan, Weirich et al. 2001; Corey, Weirich et al. 2003; Schwabish and Struhl 2007; Petesch and Lis 2008), phosphate starvation, (Santisteban, Kalashnikova et al. 2000; Sudarsanam, Iyer et al. 2000; Barbaric, Luckenbach et al. 2007; Wippo, Krstulovic et al. 2009), and carbohydrate metabolism (Neigeborn and Carlson 1984; Abrams, Neigeborn et al. 1986; Hirschhorn, Brown et al. 1992; Schwabish and Struhl 2007). SWI/SNF binds DNA non-specifically (Quinn, Fyrberg et al. 1996), but is recruited to

some promoters through interactions with transcriptional activators (Sudarsanam and Winston 2000; Neely, Hassan et al. 2002). An alternate mode of recruitment to acetylated histones is via bromodomains present in the Snf2p subunit (Hassan, Awad et al. 2006). These different pathways for recruitment provide a means of directing the relatively small number of SWI/SNF complexes present in a cell (estimated at 100-200 molecules) (van Vugt, Ranes et al. 2007) to the loci where they are required.

SWI/SNF has been observed to drive a range of chromatin transitions *in vitro* including nucleosome sliding (Whitehouse, Flaus et al. 1999; Jaskelioff, Gavin et al. 2000; Saha, Wittmeyer et al. 2002; Kassabov, Zhang et al. 2003; Zofall, Persinger et al. 2006) nucleosome eviction (Owen-Hughes and Workman 1996; Lorch, Zhang et al. 1999; Phelan, Schnitzler et al. 2000; Govind, Zhang et al. 2007; Gutierrez, Chandy et al. 2007), and H2A/H2B dimer exchange (Bruno, Flaus et al. 2003). *In vivo* SWI/SNF has been shown to catalyze the eviction of nucleosomes from open reading frames (ORFs) during transcription and there is evidence that the complex associates with elongating PolII (Schwabish and Struhl 2007). It has also been shown to generate alterations to chromatin structure within 5' gene regulatory elements (Hirschhorn, Brown et al. 1992). This latter activity can also involve the removal of nucleosomes, for example at the *HO* locus (Gkikopoulos, Havas et al. 2009), as well as at the Pho5 and Pho8 loci (Wippo, Krstulovic et al. 2009).

An elegant series of studies performed in the Nasmyth and Peterson laboratories established the budding yeast *HO* locus as a paradigm for studying the action of chromatin remodeling enzymes. The *HO* locus encodes a site specific nuclease required to direct site specific recombination events that result in changes in yeast

mating type (Jensen, Sprague et al. 1983). The *HO* locus is only expressed transiently in mother cells during the cell cycle, but is not expressed in genetically identical daughter cells and as a result can be considered as model epigenetically and temporally regulated gene.

The regulation of this gene is dependent on the sequence specific transcriptional activator Swi5p. Swi5p is normally phosphorylated by Cdk1p, which prevents it from entering the nucleus. Cytoplasmic levels of Cdk1p drop near the end of mitosis, resulting in reduced phosphorylation of Swi5p, enabling it to enter the nucleus (Brazas and Stillman 1993).

Swi5p binds cooperatively with Pho2p to the upstream promoter regions URS1 and URS2 of the *HO* locus, and together they recruit SWI/SNF (Brazas and Stillman 1993). Swi5p and SWI/SNF in turn recruit the Mediator complex to the URS2 region (Bhoite, Yu et al. 2001). SWI/SNF and Mediator cooperatively recruit the SAGA complex to URS2 (Takahata, Yu et al. 2009), where the SAGA-subunit Gcn5 is responsible for the acetylation of histone tails of H3 and H4 at the promoter (Sterner, Grant et al. 1999). After the binding of SWI/SNF, SAGA, and Mediator, nucleosomes are remodeled at the URS2 region, dependent on chaperone protein Asf1p and elongation factor FACT, which bind URS2 (Takahata, Yu et al. 2009). Others have demonstrated that five nucleosomes in the *HO* promoter are removed from URS1 and URS2 at roughly this time frame, and in a manner which is likely due to the activities of SWI/SNF and Asf1p (Gkikopoulos, Havas et al. 2009). The SBF complex, which is composed of the Swi4p and Swi6p subunits, is then recruited to the URS2 region (Cosma, Tanaka et al. 1999), which results in the recruitment of

Mediator to the TATA box. Following this, various subunits of the transcription pre-initiation complex, including TFIID, TFIIH, and PolII are recruited to the TATA box in a Cdc28-dependent manner (Cosma, Tanaka et al. 1999; Krebs, Kuo et al. 1999; Cosma, Panizza et al. 2001).

In daughter cells, Ash1p binds the URS1 region of the *HO* locus and represses transcription by blocking all steps beyond Swi5p (Cosma 2004). As a result, in *ash1* knockouts both mother and daughter cells transcribe from the *HO* locus and switch mating types (Bobola, Jansen et al. 1996).

3.2 Determination of whether SWI/SNF activity alters the mobility of a genomic locus to which it is recruited

The strict requirement for SWI/SNF in regulation of the *HO* promoter together with the fact that the timing of its recruitment was well characterized made this an attractive system for studying the action of SWI/SNF at a cellular level. The Einstein-Smoluchowski theory of Brownian motion in liquids relates linear mass density to diffusive motion (Bingham 1996). As ATP-dependent chromatin remodeling enzymes are thought to have marked effects on chromatin organization, it is possible that they could alter the linear mass density of chromatin and thus indirectly catalyze an increase in the motion of individual chromosomal loci. A preliminary investigation along these lines was initiated by Dr. Triantafyllos Gkikopoulos of the TOH Lab, who generated yeast strains containing fluorescently tagged *HO* loci using the tetO/tetR-GFP system, including an *ash1* strain. These strains were further modified using a GAL1:CDC20 construct to allow synchronization via withholding

galactose. Dr. Gkikopoulos performed 2D fluorescence video microscopy on the strains, manually tracked the fluorescent loci, performed MSD analysis, and compared the resulting MSD curves from a small number of mother versus daughter nuclei. The results of one such comparison are presented in Figure 3.1, and indicate that, in this pair of nuclei, the *HO* locus in the mother cell diffuses more than that in the daughter cell.

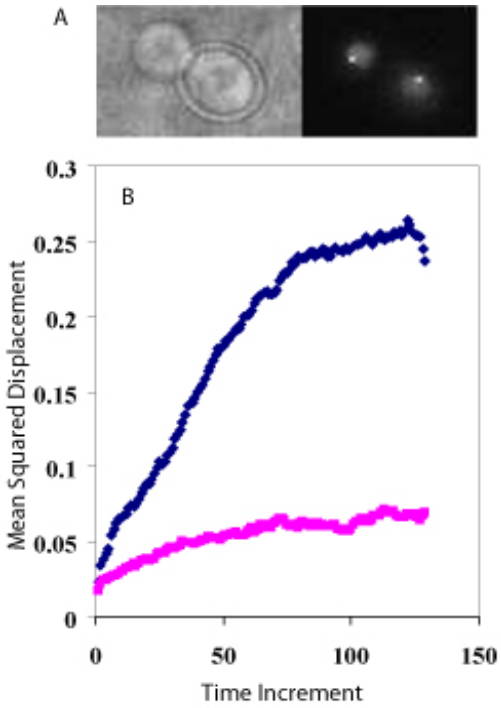

Figure 3.1. Mean squared displacement (MSD) analysis of GFP-tagged HO loci in mother and daughter yeast nuclei. A. Brightfield image shows larger mother cell at lower right, and smaller daughter cell at upper left. Corresponding UV image shows HO loci of mother and daughter as dots, and nuclei are also visible due to unbound nuclear tetR-GFP. B. MSD analysis was performed as described in the Materials and Methods, and indicates that the HO locus of the mother cell (blue line) has experienced greater motion than the locus in the daughter cell (pink line).

The data obtained in Figure 3.1 were based on a small number of measurements. With the aim of determining whether these preliminary observations were

representative, and to characterize any role for SWI/SNF, the motion of the HO promoter was studied in more detail.

Initial studies focused on strain 1115, in which the *HO* locus is tagged with a tet operator bound by tetR-GFP fusion proteins. As this strain encodes functional Ash1, SWI/SNF is expected to be recruited to the *HO* gene differentially in mother versus daughter cells 20-30 minutes following release from Cdc20 induced cell-cycle arrest (Bobola, Jansen et al. 1996). Fluorescent imaging was performed in 2D, and the tagged *HO* locus tracked using the ImageJ plugin Spot Tracker which was developed in the laboratory of Susan Gasser (Sage, Neumann et al. 2005). In order to quantitatively compare the motion of the HO locus in mother and daughter cells, MSD curves were then plotted as described in the materials and methods section. Figure 3.2A shows an MSD curve obtained over 200 time points using data from 6 mother and 8 daughter cells. The curves show overlapping standard error bars indicating that there is no significant difference between the motion of the mother and daughter loci. Additional repeats performed on different days also revealed no significant difference between mother and daughter cells (not shown), though this data is not directly comparable as background fluorescence from unbound tetR-GFP within the nuclei was inconsistent from day to day, necessitating changes in the microscope image acquisition settings.

This analysis was next performed at 30^{o}C rather than 25^{o}C as temperature has the potential to influence chromatin dynamics. Nine mother and eleven daughter cells were imaged and tracked as described, and the motion of the loci in daughter nuclei showed slightly higher motion.

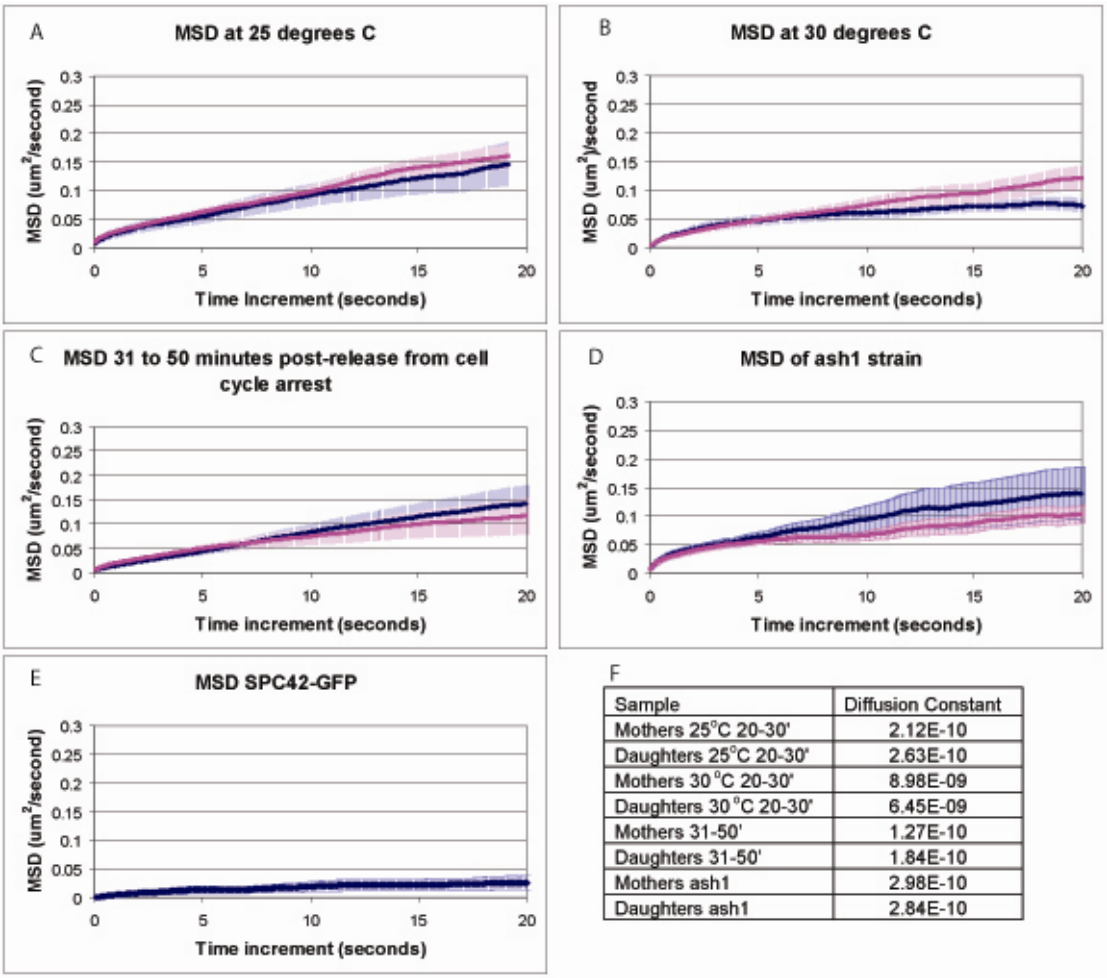

Sample	Diffusion Constant
Mothers 25°C 20-30'	2.12E-10
Daughters 25°C 20-30'	2.63E-10
Mothers 30°C 20-30'	8.98E-09
Daughters 30°C 20-30'	6.45E-09
Mothers 31-50'	1.27E-10
Daughters 31-50'	1.84E-10
Mothers ash1	2.98E-10
Daughters ash1	2.84E-10

Figure 3.2. MSD analysis of GFP-tagged *HO* loci under various conditions. Strains were cultured, images, and analyzed as described in the Materials and Methods. Blue line corresponds to the mean MSD of mothers, pink line corresponds to the mean MSD of daughters. Error bars show one standard error. A. Imaging was performed at 25 degrees Celsius and 20-30 minutes post-release from cell cycle arrest. B. Imaging was performed at 30 degrees Celsius 20-30 minutes post-release. C. Videos taken at 25 degrees Celsius 31-50 minutes post-release from cell cycles arrest. D. Analysis of ash1deletion strain. E. Analysis of GFP-tagged SPC42, a spindle pole body subunit which serves as an immobile control. F. Diffusion constants corresponding to the different conditions listed in A-D. Due to microscope setting changes necessitated by day-to-day inconsistencies in background nuclear unbound GFP levels, not all data was in a format that could be presented on the same graph. The graphs presented are representative of equivalent data sets from different days.

An alternative means of quantifying differences in motion involves the calculation of diffusion constants from MSD curves. This involves fitting a line to the data for the smallest time increments (performed as described in the methods). Given that there is

error associated with the MSD curves themselves there will be some error in the calculation of diffusion constants. None the less the calculation of diffusion constants provides values that are comparable to those reported previously. However, comparison of diffusion constants between mother and daughter cells showed only minor differences between mothers and daughters. For example, the higher diffusion constant obtained for daughter cells in comparison to mother cells at 25^{o}C (Figure 3.2F) was found not to be reproduced in data generated on different days (data not shown). The diffusion constants calculated were within an order of magnitude of previously published values (Bystricky, Laroche et al. 2005).

Strain 1115 was first analyzed at 25^{o}C looking in early G1 of the cell-cycle, at 20-30 minutes post-release from cell-cycle arrest. During this time frame SWI/SNF is thought to be recruited to the *HO* locus, which is expected to undergo remodeling, but not transcription (Bobola, Jansen et al. 1996). Analysis was next performed at 25^{o}C, 31-50 minutes post-release from cell-cycle arrest (Figure 3.2C). During this time the cell is expected to make the G1-S-phase transition, when *HO* locus is expected to be transcribing (Bobola, Jansen et al. 1996). No difference in MSD was detected, but the daughter nuclei showed higher diffusion constants. An *ash1* strain meant to serve as a control showed slightly increased motion of the *HO* loci in mother nuclei, although transcription of the locus is known to occur in both mothers and daughters in this strain (Figure 3.2D). This observation may be the result of low sample size (n=8). The spindle pole body is thought to be an immobile structure during the G1 phase of the cell cycle, and the MSD profile of a strain containing a SPC42-GFP fusion protein (strain 1196) is thought to be representative of the noise or sensitivity of the tracking system. The MSD curve of SPC42-GFP in Figure 3.2E shows a detected motion

which is roughly one-quarter to one-sixth that of many of the MSD curves of the *HO* loci. This noise is assumed to be present in all samples.

In all of the conditions listed, there were cases of individual *HO* loci in both mother and daughter nuclei which were observed to have MSDs which were exaggerated compared to those of the adjacent nuclei. These highly mobile outliers are responsible for the large standard deviations seen in the MSD graphs. The source of this increased mobility was not determined.

An attempt was made to assess 3D image acquisition of strain 1115 using the Deltavision microscope, however the rate of image acquisition in 3D was inadequate. Large deviations in position were detected from frame to frame during the acquisition of a single stack which resulted in an unacceptable degree of measurement error, and the approach was dropped. An attempt was also made to acquire images using an Axiovert 200 microscope fitted with a Piezo stage, but strain spot intensity was found to be insufficient for acquisition at a rate necessary for 3D analysis.

It was hypothesized that the ATP-dependent chromatin remodeling enzyme SWI/SNF might catalyze an increase in the motion of chromosomal loci to which it is recruited; however, analysis of loci under various conditions failed to detect a significant difference in MSD between these and control loci. One possible explanation for this is that there is insufficient change in the linear mass density of the *HO* locus to alter its diffusive properties on a scale which is detectable by light microscope. A second possible reason could be that the observed motion patterns of the mother and daughter *HO* loci are the result of random forces within the nucleus that are unrelated to

transcription from *HO*. Given either of these first two instances, it would not be plausible to continue with this project. A third possible reason could be related to low occupancy of SWI/SNF at the *HO* locus. Given this possibility, further experiments were justified.

3.3 A strategy for directing high occupancy recruitment of SWI/SNF to a locus

We reasoned that the relatively low SWI/SNF occupancy at the HO locus might not be sufficient for microscopic detection of a motion phenotype. In order to determine if high SWI/SNF occupancy at a given locus would have a measurable effect on the motion of the locus, yeast strains in which SWI/SNF was artificially recruited to a fluorescently tagged locus were generated. The strategy adopted involved modification of the tetO/tetR-GFP system through inclusion of domains which direct recruitment of SWI/SNF. The domains selected were the Snf6p and Snf11p proteins, which are relatively small at 37.6 and 18 kiloDaltons, respectively, which are both present in the complex in two copies, and which are known to interact with relatively few proteins other than SWI/SNF subunits (Smith, Horowitz-Scherer et al. 2003). These domains were cloned into the tetR-GFP fusion protein shuttle plasmid as illustrated in Figure 2.1. This plasmid was then integrated in a strain with a tet operator array stably integrated on chromosome XV, as described in the Materials and Methods. The recruitment strategy is presented in Figure 3.3.

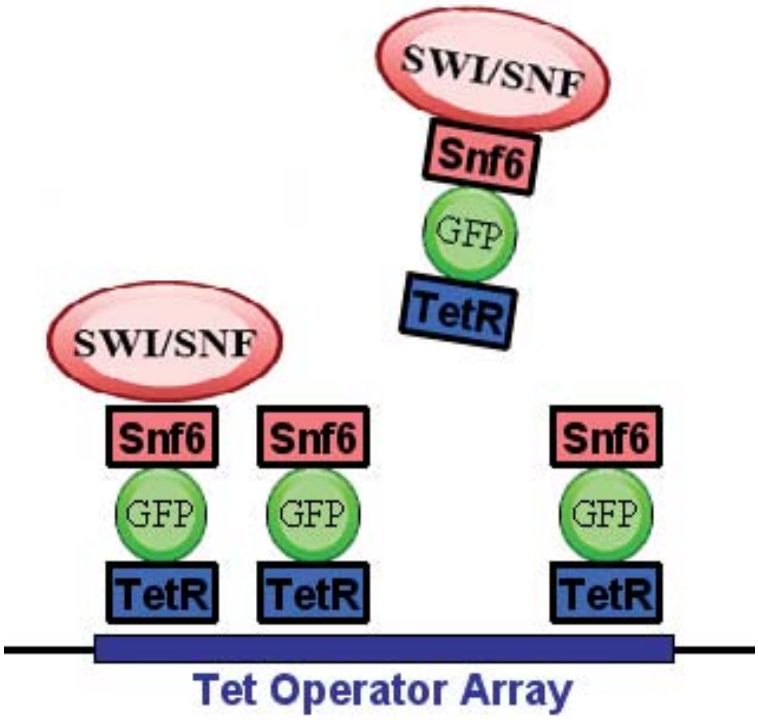

Figure 3.3. SWI/SNF recruitment strategy. The SWI/SNF complex is recruited to a tet operator array stably integrated on chromosome XV via tetR-GFP-Snf6 (or –Snf11) fusion proteins.

Western blotting was performed as described in Materials and Methods using an anti-GFP antibody (Roche 1-814-460) to verify correct fusion protein expression, and the results are presented in Figure 3.4. Bands with the mobility expected for the fusion

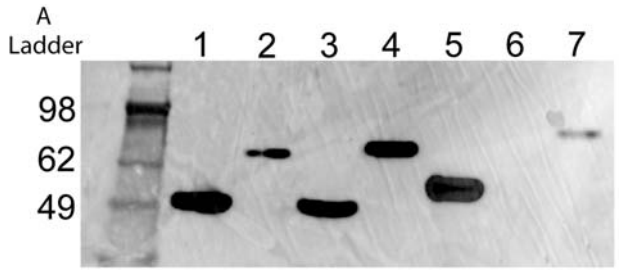

B

	Strain	kd
1	TetR-GFP (1160)	51.1
2	SPC42-GFP	69
3	NUP49-GFP	76.4
4	TetR-GFP-GCN4	69.5
5	TetR-GFP-deltaVP16	56.2
6	TetR-GFP-SNF11 (1168)	70.5
7	TetR-GFP-SNF6 (1170)	89.4

Figure 3.4 Western blot of tetR-GFP fusion proteins using an anti-GFP antibody. Samples and ladder were imaged separately without moving the blot or adjusting the focus using an LAS4000, and then overlayed in Photoshop. Ladder is Seeblue Plus2 (Invitrogen cat.# LC5925). A. Samples 1-7. Sample 6 (strain 1168) showed no band by western blot, however, this strain did show weak signal indicating colocalization of the tet operator array with SWI/SNF in immunofluorescence studies. The Nup49-GFP strain is incorrect. B. Legend.

protein could be detected in all strains except strain 1168 (tetR-GFP-Snf11).

In order to confirm that the GFP fusion proteins could direct the recruitment of SWI/SNF, IFM was performed on strains 1168 (tetR-GFP-SNF11) and 1170 (tetR-GFP-SNF6), as well as controls, using an anti-myc primary antibody against Swi5-myc and a Cy3-labelled secondary antibody. Colocalization of tetR-GFP and Swi5-13Xmyc signals was observed for strain 1168, as well as possible (faint) colocalization in strain 1170 (Figure 3.5). No-myc and no-primary antibody controls showed no colocalization, indicating that the myc signal was specific and that SWI/SNF was recruited to the tet operator array via the tetR-GFP fusions (Fig. 3.6).

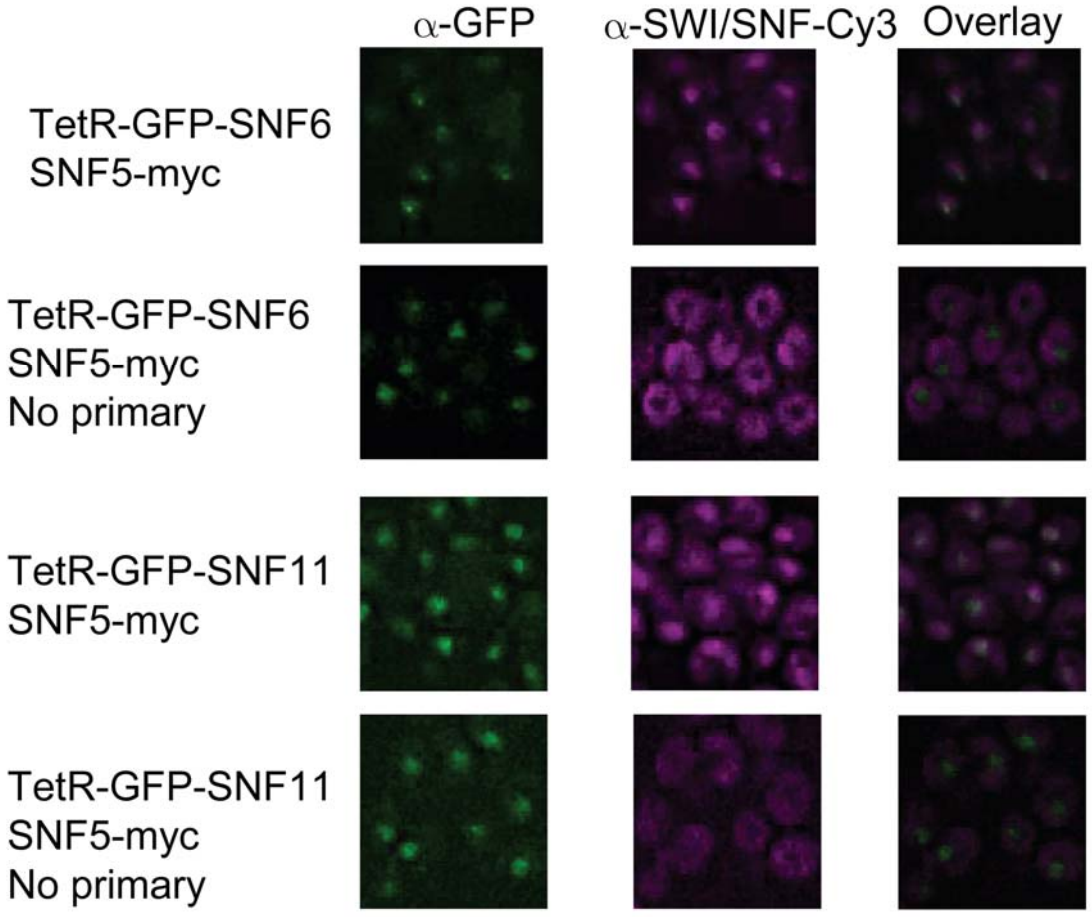

Figure 3.5. IFM of tetR-GFP fusion strains with anti-myc antibody to detect colocalization of the GFP-tagged tet operator array and SWI/SNF. The tetR-GFP fusion proteins recruit SWI/SNF to the tet operator array via SWI/SNF subunits Snf6 or Snf11 in rows 1 and 3, respectively, where punctate GFP and Cy3 (SWI/SNF) colocalization is observed. No primary antibody controls in rows 2 and 4 show non-specific Cy3 staining of the cytoplasm.

The IF protocol used was optimized to retain GFP signal.

2D fluorescence video microscopy of strains 1160 (the tetR-GFP control), 1168 (tetR-GFP-Snf11), and 1170 (tetR-GFP-Snf6) was performed, followed by spot tracking and MSD analysis as described previously, and the results are presented in Figure 3.7. No significant difference in motion was detected between strain 1168 (tetR-GFP-SNF11) and a control strain, indicating that the recruited SWI/SNF did not have a detectable effect on motion when tethered to the tet operator array in this manner. Strain 1170 (tetR-GFP-SNF6) showed a decrease in the motion of the tet operator

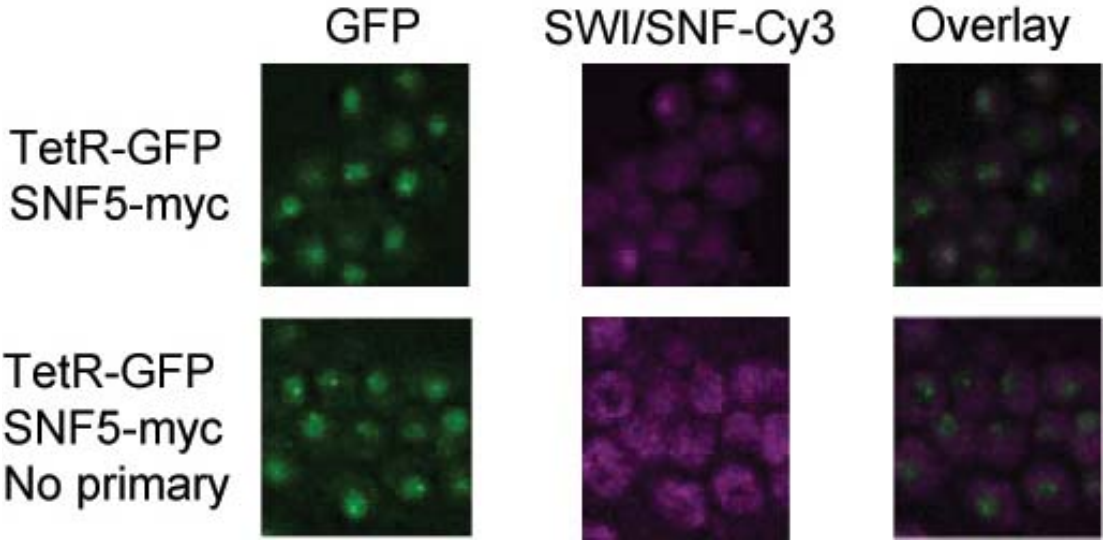

Figure 3.6. Immunofluorescence microscopy of tetR-GFP fusion control strains with anti-myc antibody to rule out non-specific antibody binding. The top row shows a TetR-GFP strain that should not recruit SWI/SNF to the tet operator array, and contains myc-tagged copy of SNF5. Cy3 staining localizes to the nucleus, but no punctate patterns are discernable, thus SWI/SNF is not recruited to the tet operator. Second row shows the same strain with no primary antibody. Cy3 non-specific staining is cytoplasmic and diffuse.

array compared to the control strain, possibly due to the increase in mass of the locus from the recruited SWI/SNF molecules.

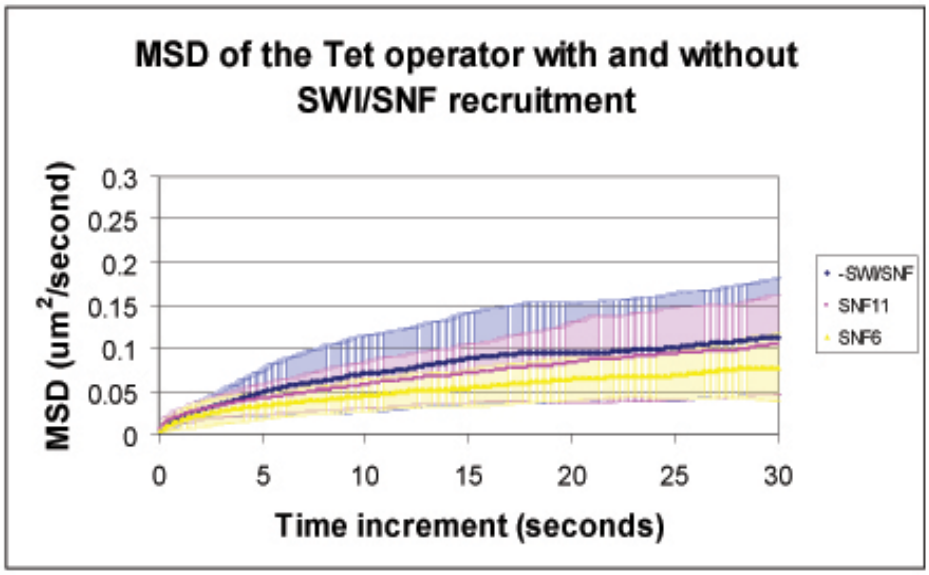

Sample	Diffusion Constant
-SWI/SNF	2.20E-06
SNF6	2.00E-06
SNF11	2.30E-06

Figure 3.7 A. MSD analysis of tet operator array on chromosome XV with and without artificial recruitment of SWI/SNF via tetR-GFP-SNF6 (yellow line) or tetR-GFP-SNF11 (red line) fusion proteins, compared to a control (blue line). No increase in motion in the tet operator array is seen upon SWI/SNF recruitment. B. Diffusion constants of the three strains. Error bars show standard deviation.

This strategy aimed to recruit large numbers of myc-tagged SWI/SNF molecules to a tet operator array integrated on chromosome XV. However, the IF microscopy results showed that punctate Snf5-myc signal was barely detectable above background in the tetR-GFP-Snf11 strain, and it was only slightly more intense in the tetR-GFP-Snf6 strain. As this technique is fairly sensitive, this possibly indicates low levels of recruited SWI/SNF. We hypothesized that artificial recruitment of the SWI/SNF complex to a given locus would catalyze an increase in the mobility of the locus, but increased motion was not detected through MSD analysis of two independent strains where such artificial recruitment had been confirmed. As Snf6p and Snf11p are both present in the SWI/SNF complex in two copies (Smith, Horowitz-Scherer et al. 2003), there are four possible orientations in which the complex may be tethered to the DNA. However, it is possible that none of these orientations are permissive for catalytic

activity by the complex, and therefore these experiments do not rule out the hypothesis, but we saw no evidence that SWI/SNF catalyzes an increase in the motion of chromosomal loci to which it is recruited.

3.4 Applying the directed recruitment of SWI/SNF to study its effects on binding of the tet repressor to DNA.

While Snf2 proteins are best known for their roles in altering the structure of chromatin, it is also known that in some cases members of this protein family act to alter the interaction of non-histone proteins with DNA. For example, SSO proteins are found in two-thirds of microbial genomes, and as these do not encode histone proteins, it begs the question as to their function (Flaus, Martin et al. 2006). The Snf2 family protein Mot1p acts to remove TBP from DNA in an ATP-dependent reaction (Auble, Wang et al. 1997), and Rad54 has been proposed to influence the association of Rad51 with DNA (Shah, Zheng et al. 2010). Of more direct relevance to SWI/SNF, it has been found that human SWI/SNF influences the occupancy of the PRC1 and PRC2 silencers, as well as the de novo DNA methyltransferase DNMT3B at the $p15^{INK4b}$ and $p16^{INK4a}$ loci in living cells (Kia, Gorski et al. 2008). *In vitro* it has been found that binding of GR the glucocorticoid receptor to chromatin occurs in cycles that are dependent on the presence of hSWI/SNF *and ATP* (Fletcher, Xiao et al. 2002). These observations raise the possibility that SWI/SNF acts to destabilize the association of transcription factors with DNA in yeast *in vivo,* ultimately resulting in their eviction.

The yeast strains generated in the previous section which recruit SWI/SNF to a tet operator array via tet repressor fusion proteins provide a potential means to study whether the complex catalytically alters tetR-DNA binding (Figure 3.3). The strategy adopted relies on FRAP and FLIP, which utilize pulses of high-intensity light to irreversibly photobleach populations of fluorophores in a target region, and subsequent measurement of the recovery or loss of fluorescence of, correlating this recovery rate with the duration the fluorophores remain associated with the target region. This can be used in live-cell imaging to compare on/off rates of transcription factors, or in this case, to determine whether SWI/SNF evicts the tetR-GFP-SWI/SNF-recruitment domain itself. This could be detected by a difference in spot recovery rates when SWI/SNF is recruited versus a control. Photobleaching experiments were carried out as described in Chapter 2.

Initial FRAP experiments were performed in 2D using the Resolve3D FRAP program with the expected recovery time set to 25 seconds; however, acquisition was problematic in several regards. Fluorescently tagged chromosomal loci in yeast have been observed to diffuse >200 nm within half a second and to diffuse about a substantial volume of the nucleus. As there was a ~5 second time delay between aiming the laser and the bleach event when performing photobleaching experiments with the Deltavision, spots were most often observed to have diffused out of the path of the laser by the time the bleach occurred. Spot fluorescence recovery was not observed to be consistent, as some spots were detectable almost immediately after the bleach while others were not detectable until after several seconds later. During the recovery period spot intensities varied greatly from image to image, indicating that they were perhaps diffusing in and out of the plane of focus, and the resulting

recovery curves were not reproducible (Figure 3.8).

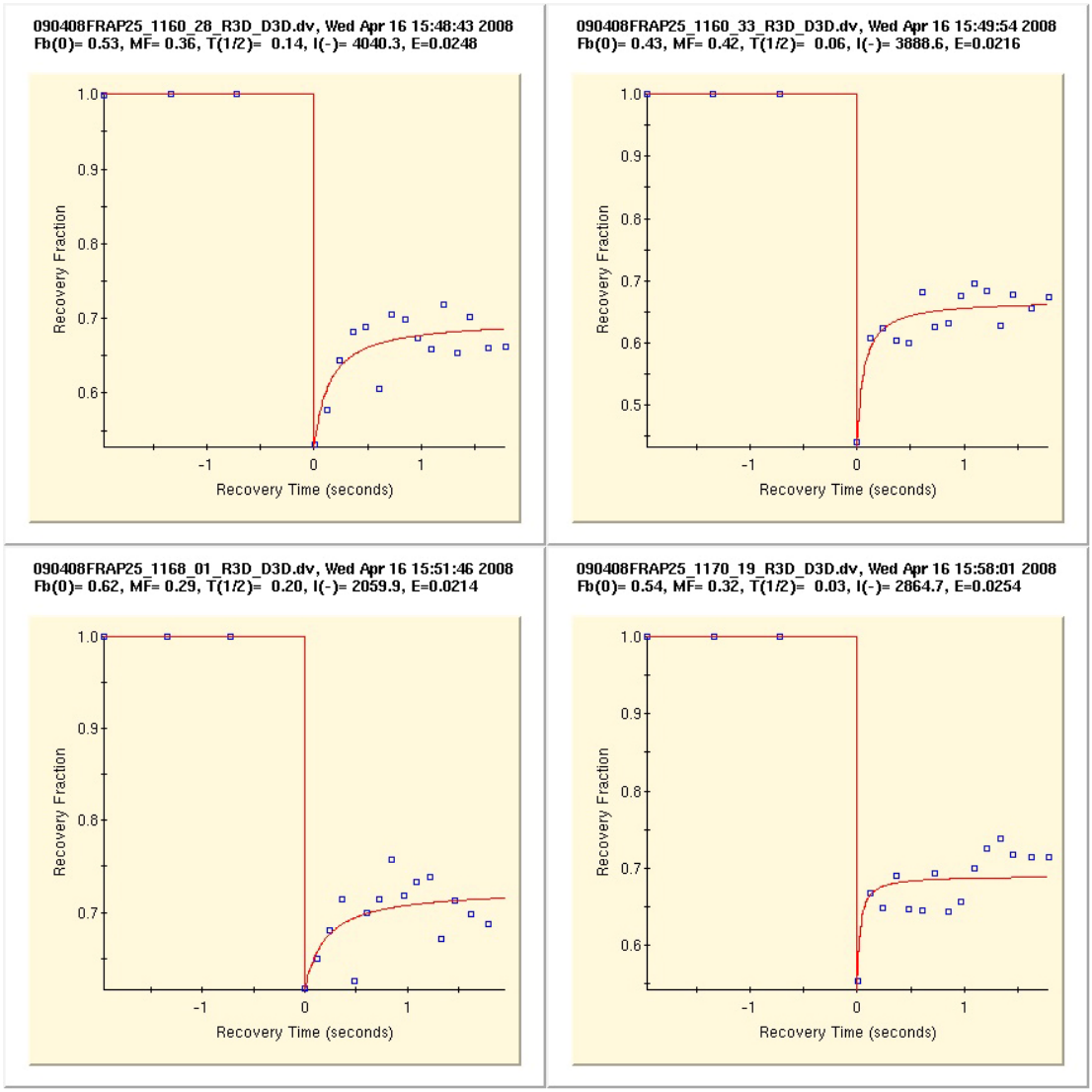

Figure 3.8. Example FRAP recovery curves. Top row: TetR-GFP control. Bottom row: TetR-GFP-SNF6. Spot diffusion during image acquisition prevented accurate intensity measurement in 2D analysis.

A switch was made to 3D post bleach acquisition in effort to address the problem of spot diffusion in and out of the plane of focus. Signal intensity recovery times were observed to be >5 minutes. Large variations in spot intensity resulted in low R^2 values (<.25) when curve fitting, and the recovery curve slopes were inconsistent. An example 2-minute recovery curve is presented in Figure 3.9.

FLIP experiments were performed on strains 1168, containing the tetR-GFP-Snf11 fusion, and 1170, containing the tetR-GFP-Snf6 fusion. These two strains were observed to have relatively high nuclear background fluorescence. FLIP experiments

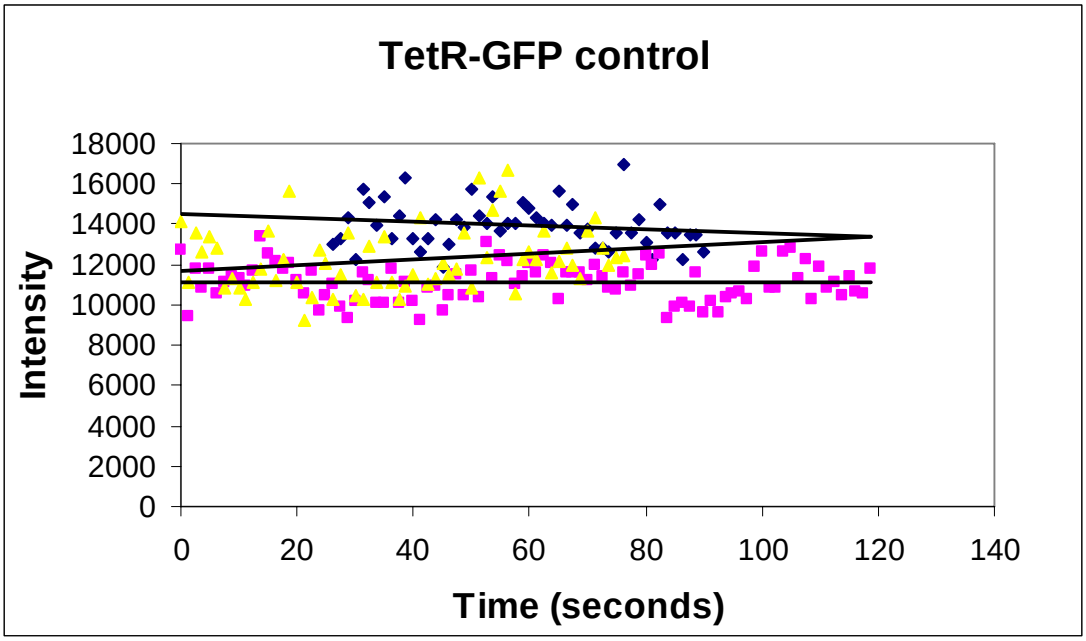

Figure 3.9. Two minute 3D FRAP recovery curves from the control sample showed inconsistent slopes and low R^2 values.

performed with either the Deltavision or the Zeiss LSM 510 confocal microscope were not able to generate consistent recovery curves (Figure 3.10). Attempts were made to fit the curves with various trendlines, and it was determined that fitting with a line generated the highest R^2 values. Recovery curves within a given sample were inconsistent with respect to slope, both within individual experiments and between experiments performed on different days. No meaningful difference in fluorescent recovery was detected based on comparison of the TetR-GFP-SNF6 and –SNF11 strains with the control.

In this chapter three different approaches were used to investigate the effects of the SWI/SNF complex on chromatin organization. In the first, the motion of the HO locus which is known to be regulated by SWI/SNF was studied. Despite some preliminary findings to the contrary, no evidence could be obtained to indicate that this locus was reorganized on a microscopic scale either during times when it was

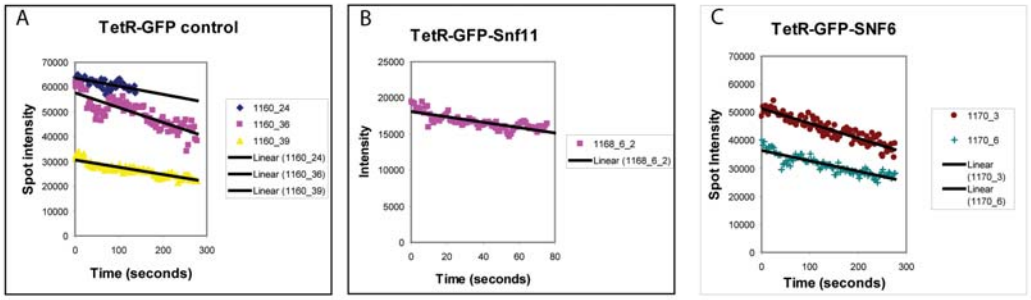

D	Slope
TetR-GFP Control 36	-167
TetR-GFP Control 39	-82
TetR-GFP-SNF6 3	-148
TetR-GFP-SNF6 6	-104
TetR-GFP-SNF11	-99

Figure 3.10. Flip results. FLIP experiments were performed on strains 1160 (TetR-GFP control, A), 1170 (TetR-GFP-SNF6, B), and 1168 (TetR-GFP-SNF11, C). The slope of the recovery curves are recorded in D. Off rates were not internally consistent based on slope of intensity loss, and no change in off-rate was detected in strains where SWI/SNF was recruited to the tet operator array.

subject to SWI/SNF-directed remodeling, or to transcription. One possible explanation for this is that the remodeling events occurring do not affect the motion of the locus. However, an alternative is that the frequency with which the HO promoter is activated is low. This would mean that any changes in motion occurring upon activation could be obscured by a large background of promoters in the inactive state.

In an attempt to circumvent this issue, SWI/SNF was artificially recruited to operator binding sites with high efficiency. Using this scheme, no effects of the SWI/SNF complex on chromatin organization could be detected. This adds further support to the possibility that the action of this complex is insufficient to alter chromatin

organization at this scale. However, it could also be the case that the context of the artificial recruitment scheme did not permit SWI/SNF to function normally. At endogenous genes there is interplay between different types of chromatin alteration, such as histone modification and ATP-dependent chromatin remodeling (Li, Carey et al. 2007). It is possible that recruitment of SWI/SNF within the context of the tet operator array does not permit this interplay.

Finally we used the strains we had generated in an attempt to investigate whether SWI/SNF influences the interaction of tet repressor with DNA. To do this an approach based on FRAP and FLIP analysis was adopted. This has been successfully applied to obtain on and off rates describing the association of other DNA binding proteins with their binding sites (Lippencott-Schwartz 1998). However, the diffusion of fluorescently tagged genomic loci in yeast occurs at a rate which is prohibitively rapid for FRAP and FLIP analysis with the Deltavision microscope, and no instrumentation was available with the potential to overcome this limitation. As a result, it was not possible to determine whether SWI/SNF evicts transcription factors from chromatin *in vivo* using this system. It is possible that the FLIP experiments would have detected a SWI/SNF-dependent loss of GFP at the tetO array if the nuclear background GFP signal had been lower. This might have been remedied by cloning in an alternate promoter to drive expression of the fusion protein. However, the decision was taken not to pursue this further. Interestingly, it was recently reported that human SWI/SNF destabilizes the association of the PC1, PC2, and DNMT3B proteins (Kia, Gorski et al. 2008). This makes it seem likely that SWI/SNF related complexes do indeed have functions that involve altering the interactions of

non-histone proteins with DNA in addition to the complexes better characterised effects on chromatin.

CHAPTER 4

The Study of Chromatin Compaction with the OMX Microscope

4.1 Introduction

Previous chapters include studies where a single genomic locus was fluorescently tagged and studied. An alternative approach involves the tagging of two adjacent, syntenic loci, subsequent microscopic analysis of the distance between the fluorescent spots, and the extrapolation of this type of data using polymer models such as the Porod-Kratky chain equation to estimate chromatin characteristics (Bystricky, Heun et al. 2004). This approach has an advantage over single-spot tracking in that drift is internally controlled. The only relevant measurement is the distance between two tagged loci, therefore all other motion is considered drift, and no other steps to control for drift such as tagging immobile nuclear structures are necessary.

Improvements in the field of fluorescent light microscopy have made it possible to acquire live 3D videos at a rate such that individual fluorescently tagged genomic loci diffuse minimally during acquisition of a single stack. This type of analysis precludes the artefacts introduced by chemical fixation and non-physiological conditions, which have been issues in previous studies of chromatin compaction, and facilitates the acquisition of large data sets compared to fixed cell experiments. These factors improve confidence in measurements in one respect, but as the observed loci are still capable of diffusing during the acquisition of single stacks, confidence is lowered in other respects, namely in microscopic measurement error. Regardless, such a live-cell

3D approach, when applied to fluorescently tagged chromosomal systems such as that described by Bystricky et al., should lead to an improved understanding of chromatin structure.

4.2 Current 3D live cell fluorescence microscopy techniques

Freely diffusing fluorescently tagged chromosomal loci, when recorded via video fluorescence microscopy, display a random walk pattern which has its origins in Brownian motion (Marshall, Straight et al. 1997). In order to accurately track a fluorescently tagged chromosomal locus in 3D, imaging must be rapid enough that the spot does not have time to diffuse during the acquisition of a single stack of images. The majority of 3D live-cell fluorescence microscopy techniques in use today rely on exposure rates and stack acquisition rates which do not meet this criterion.

When the 3D image acquisition rate is slower than the rate of diffusion, a tagged locus will have time to diffuse from image to image within a stack, which affects the intensity reading of the spot in a given image as well as its lateral position. It can not be determined if the spot is diffusing up or down from image to image, and given this and the fact that there is some intensity variation inherent to fluorescent image acquisition, slow acquisition rates therefore increase measurement artifact in z as well as x an y.

The pharmaceutical company Lab-on-a-Chip has developed a shaped, mirrored microscope slide which reflects samples from two directions and which, through trigonometric analysis, permits precision localization of lateral and axial coordinates

simultaneously from videos made on conventional microscopes (Hajjoul, Kocanova et al. 2009). With this technology they claim to be able to acquire images with 10 ms exposures and error of 27 nm per axis. It has yet to be determined whether this approach has any drawbacks or is amenable for strains with multiple fluorescent spots in the same cell.

4.2.1 Resolution

When light is emitted from a point source, it scatters in a well-defined pattern. Viewed from the side, this pattern produces a non-punctiform intensity distribution called the point spread function (PSF). The PSF may be modelled as a 3-dimensional (3D) volume (Figure 4.1) (Davidson 2010).

When viewed through a microscope, PSFs are observed to have central Airy disks comprising 86% of the total intensity of the light from the point source which is collected by the objective, surrounded by concentric rings of light known as Airy rings. PSFs are Gaussian in nature and may be mathematically fit to individual Gaussian curves to estimate the lateral coordinates of their central maxima.

The resolution limit, or the ability of a microscope to distinguish two adjacent PSFs of equal intensity, depends on the degree of overlap of the two disks. This measurement, known as the Raleigh Criterion, is roughly the distance from the maximum of one PSF to the first minimum of the second, though this distance may vary if the intensities of the two PSFs differ (Davidson 2010). The theoretical maximum resolution for a given objective is defined by Abbe's equation.

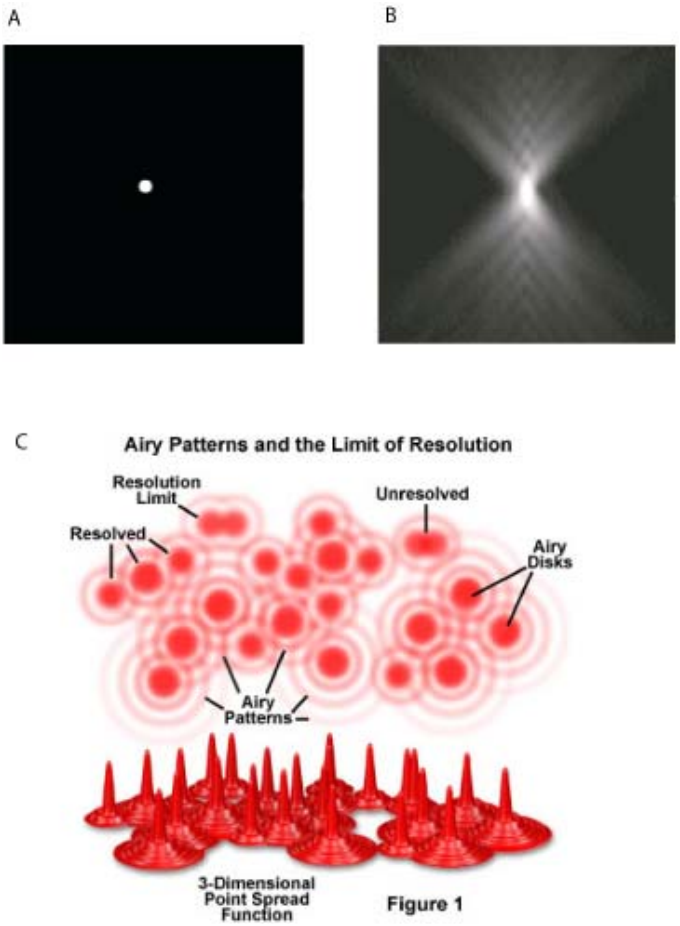

Figure 4.1. The point spread function. (A) 100 nm point source. Imaging from a point source produces a non-punctiform distribution called the point spread function (PSF) which, when viewed from the side resembles the diffraction pattern in (B). When viewed from above PSFs are detected as Airy patterns (C). (Davidson 2010, used with permission.)

$$R=NA/(0.61\lambda)$$

Equation 6. Abbe's equation. Numeric aperture (NA) is equal to $\eta \sin(\alpha/2)$ where η is defined as the index of refraction of the objective and α is the acceptance angle of the lens aperture, while λ is the wavelength of the emitted light (Swedlow 2010).

When determining the resolution of a given microscope objective one may simply refer to Equation 6 for the theoretical value; however, there are other considerations to be made which influence resolution and which render Abbe's equation merely an estimate. For example, the signal to noise ratio places limits on the resolution. The signal to noise ratio is the intensity contrast between a fluorescent signal and the

background noise, and is calculated as the number of standard deviations between the signal intensity as compared to background (Goldman, Swedlow et al. 2010). Noise, or background, arises from several sources, including detector flaws, fluctuations in illumination, Poisson or shot noise, autofluorescence, non-specific fluorochrome staining, and stray light (Goldman, Swedlow et al. 2010), and is expressed as the square root of the sum of the variances of contributing noise sources. Another factor which may affect resolution is drift. Drift is any kind of motion in microscopy that arises from the system, as opposed to motion of the observed structure of interest, and may originate from several sources, including motion of the microscope relative to the sample, temperature differentials within the system, inadequate anchoring of the sample to the microscope slide, or deformations of the sample. Drift may be accounted for mathematically in some cases (Thomann, Dorn et al. 2003), controlled for through comparison with tagged, immobile structures within the sample (Heun, Laroche et al. 2001), or controlled for by analyzing the relative distance between two or more tagged structures rather than the motion of a single structure (Marshall, Straight et al. 1997). In this last instance, diffusive motion of the locus as a whole is considered to be drift, and the only motion measured is that of the spots relative to one another.

The amount of inherent noise varies from microscope to microscope. Because of this, the resolution of a given objective and microscope should be tested if one wishes to determine its exact value. This may be done by imaging fluorescent beads with dimensions known to be smaller than the theoretical maximum resolution, and using spot-finding software to calculate the minimum distance by which they may still be resolved.

Microscopic images are not limited to the resolution of the microscope and objective, however, as software is available which may be used to improve on the raw data. An iterative deconvolution algorithm may be applied to a given image to correct for out of focus light, and this can increase resolution. Additionally, Gaussian curve algorithms may be fitted to a given 2D PSF to locate its central maximum at sub-pixel resolution. Both of these methods may increase resolution significantly.

Analysis in 3D adds additionally complexity to the problem of resolution. Intensity fluctuations during stack acquisition can have a significant effect on z-resolution as the z-coordinate is determined by an algorithm based on spot intensity measurements on several images from a stack. These fluctuations can arise from various sources, including spot movement in or out of the focal plane, fluctuations in the light source, camera faults, or stray light. Excessive bleaching during stack acquisition can artificially shift the apparent location of a spot in z, eliminate the signal altogether, or kill the cell. In order to limit the amount of bleaching during 3D analysis it is best to use a microscope system optimized for sensitivity and speed.

4.2.2 The OMX microscope

In October 2008 the University of Dundee College of Life Sciences acquired an OMX microscope. This system utilizes four independent lasers and cameras, as well as a Piezo stage, all optimized for rapid acquisition, and offers the potential for performing live cell, 3D tracking of rapidly diffusing cellular structures (see Materials and Methods). In this chapter we sought to determine whether this microscope could be

applied to the measurement of the end-to-end distances separating syntenic chromosomal loci in yeast as a means of characterizing chromatin structure.

4.3 Selection of yeast strains

In order to carry chromatin compaction analysis, yeast strains were needed in which chromosomes were tagged with operator sites separated by a defined distance in base pairs. As many of the sequence specific DNA binding dimerize, it was important to use two different operator sequence to reduce the possibility of artefacts arising from operator induced looping. Fortunately, the Tanaka Lab had previously generated two yeast strains with fluorescently tagged syntenic loci which were well suited for the present study and which they made available for this study as generous gifts. The first has two such fluorescently tagged loci flanking 60 kb of endogenous genomic sequence on chromosome IV (strain 1200) (Kitamura, Blow et al. 2006), while the second has two tagged loci flanking 30 kb of endogenous genomic sequence, integrated at the same locus on chromosome IV (strain 1252, unpublished). The genomic distances separating the fluorescent spots in these strains are within the range of distances used in previous chromatin compaction studies, making the strains likely candidates for the present study, both for comparative purposes, and also as these genomic spot separation distances are known to be of appropriate dimensions for use in yeast. Furthermore, examination of the genes and other sequences in the intervening regions failed to identify any criteria by which to exclude the strains. The genes flanked by these tags are presented in Table A.1 in the appendix.

4.4 Optimization of fluorescent tags

A challenge of live cell 3D fluorescence microscopy is the production of a fluorescent signal with sufficient intensity that it may be detected on a rapid time scale even after extensive bleaching. This may be partially addressed through improvements in the microscope, by adjustment of the copy number of the repressor binding sites, adjustment of the copy number of the fluorescent tags in the repressor protein fusions, by choice of fluorescent tags in the fusions, or by choice of the promoter used to express the fusions. Adjustment of the duration which the cells have to express the fusions can also have an effect on signal to noise.

3D live cell fluorescence video microscopy was performed with the OMX microscope on strain 1200, which is a 70 kb strain that contains a GFP-tagged spot and a CFP-tagged spot, and though the GFP-tagged locus was found to be of satisfactory intensity, the CFP-tagged locus was inadequate. The 405 nm laser excites CFP sub-optimally, and requires use of a neutral density filter setting of 100% to generate an adequate signal to noise ratio. This results in the complete loss by photobleaching of the CFP signal after two 9-image stacks (data not shown).

To remedy this, 3xGFP was cloned into this strain replacing the 3xCFP. 3D live cell fluorescence video microscopy was performed on the resulting strain, but the levels of unbound tetR-3xGFP and GFP-lacI were such that the background nuclear GFP signal masked the spots (data not shown).

tetR-1xmCherry was then cloned into strain 1200 replacing the tetR-3xCFP, and 3D live cell fluorescence video microscopy was performed. The mCherry signal was found to bleach almost entirely during the acquisition of a single stack of nine images.

TetR-1xGFP was then cloned into strain 1200, replacing the tetR-3xCFP, and 3D live cell fluorescence video microscopy was performed. This configuration was found to generate adequate signal from both arrays to allow for the generation of at least 50 stacks. This new strain was called 1300. Strain 1252 was transformed with tetR-1xGFP as well and again adequate signal was detected. This new strain was called 1301. Strains 1300 and 1301 were verified by PCR across the junctions of the tetR-1xGFP integration sites, as well as by observation under the microscope for the appropriate phenotype.

4.5 Viability study

Live cell fluorescence microscopy must be performed without excessive light exposure to the sample as it can eliminate the fluorescent signal through photobleaching or kill the cell. This becomes a significant problem with 3D imaging as multiple exposures, and thus multiple bleach events, are required for each time point. Additionally, due to constraints of fluorescent chromosomal tagging, the spots themselves are near the intensity threshold of the camera and therefore have a low threshold for bleaching before they are reduced to background levels.

These challenges can be addressed through the implementation of state of the art electronics such as high-sensitivity cameras which can efficiently detect low intensity

signals, by improvements in the light path by, for example, by using state of the art band-pass filters which optimize passage of desired wavelengths, and through establishment of samples with high intensity photostable fluorescent tags.

The OMX microscope is a new system which incorporates such high-sensitivity cameras and custom band-pass filters. Testing of high-intensity fluorescently tagged strains for viability after photobleaching informs us about the experimental parameters which are appropriate for yeast. Strain 1295, which has a W303 background and was derived from the parent strain used to generate strains 1200, 1252, 1300, and 1301, was used to test for the viability of cells after overbleaching using the OMX microscope. Cells were found to be viable, based on ability to form new buds, after 100 stacks of 9 images per stack at 10msec exposures using a neutral density filter setting of 10%. At most, experiments performed during the course of this thesis utilized only 50 such stacks.

4.6 Optimization of acquisition settings

Videos were generated using strain 1300, a 70 kb strain where both spots are labelled with GFP, with exposure times ranging from 1 msec to 15 msec, ND filter settings of either 10% or 31.6%, a step heights of 200, 300, or 400 nm, and stack heights ranging from 3 to 5 μm resulting in from 7 to 11 images per stack. From these initial tests, working experimental conditions were found to be 5 or 10 msec exposures, 10% ND setting, a step height of 400 nm, and stack heights of from 3-5 μm, depending on the orientation of the spots in adjacent nuclei. There is some natural variation in the intensity of the spots and the nuclear background from cell to cell, and on occasion

videos with 5 msec exposure times were found to generate adequate signal to noise ratios for tracking. The step height of 400 nm typically resulted in a visible spot in 3-5 of the images in the stack.

In order to for any analysis of data obtained to be possible, it is necessary to track the positions of tagged loci. Several different software packages perform this task. Spot tracking software developed by the Danuser Lab, and Imaris spot tracking software developed by Bitplane (see Materials and Methods) were used to analyze the same 3D videos generated on the OMX microscope, as means of comparison. Imaris is one of the leading commercial spot tracking programs available, and is generally efficient at accurate automated tracking, but the Danuser program was found to be far superior in correctly tracking spots which were in close proximity (Figure 4.2). The Gasser Lab Spot Tracker software (see Materials and Methods) was used for some 2D analysis as the version of the Danuser software in our possession is currently limited to 3D.

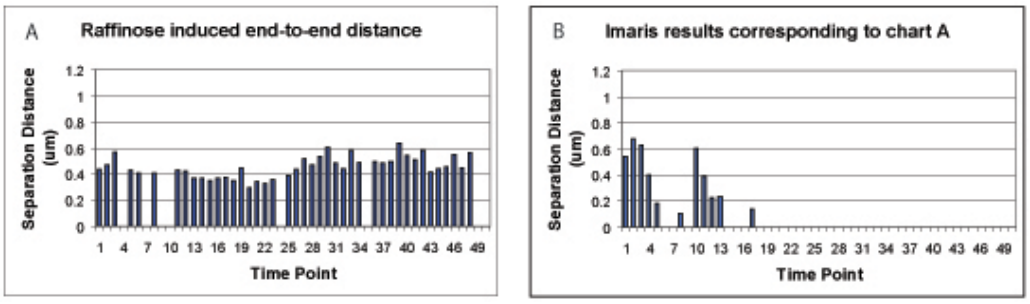

Figure 4.2. Example of differences in Danuser software versus Imaris software analysis. Graphs A and B depict the same video, analyzed with the Danuser software in A, and with Imaris in B. The missing measurements between time points 6 and 27 in B were judged to be colocalized spots by the Imaris software, and spots in the remaining time points were not detected, possibly due to differences in background subtraction by the two programs.

4.7 Establishing performance of the OMX microscope

A number of tests were carried out on the OMX microscope to determine its working specifications. One goal of the microscopy field is to be able to make 3-dimensional videos at a rate such that fluorescently tagged objects do not measurably diffuse during the time necessary to generate a stack. In order to test whether the OMX microscope can acquire images at this rate, videos were generated using the fastest possible image acquisition settings, the spots were tracked with the Gasser Lab Spot Tracker software, and mean squared displacement analysis was performed. The strain used for this test, 1280, contained a single GFP-tagged locus, and with this strain exposure times of 5 msec were achieved, with an overall time between images of 26 msec. 2D video microscopy was used for this analysis as this setting permits the fastest acquisition rate. If oversampling occurred, that is, if the microscope can acquire images fast enough that the spot has no time to diffuse from frame to frame, and instead is detected to move on a time scale of two or more frames, then the slope of the MSD curve will be zero near the origin. The MSD curve generated is presented in Figure 4.3, and inspection of the curve near the origin shows that the slope is positive, which indicates that oversampling did not occur, and that the temporal resolution of the OMX microscope is not within a time scale that is sub-diffusional for GFP-tagged non-immobilized chromosomal loci in cerevisiae in its fastest setting. Since oversampling did not occur while performing 2D microscopy, it ruled out the possibility that oversampling could occur using the slower 3D acquisition conditions.

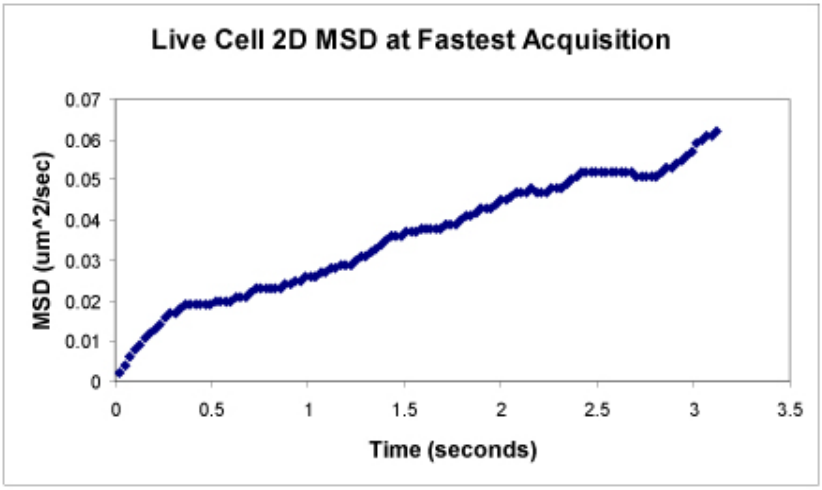

Figure 4.3. OMX fastest acquisition settings. Fluorescence video microscopy was performed on strain 1280, which contains a single tet operator array tagged with tetR-GFP, at the fastest possible acquisition settings in order to determine if the OMX microscope can image fast enough such that tagged genomic loci have no time to diffuse between two successive images. Fastest acquisition occurs in 2D analysis, as changes in stage height introduce a rate limiting factor. The single fluorescent spot in strain 1280 has sufficient intensity to permit 5 msec exposure times at 10% ND with a field of view of 128x128, the smallest setting. Image acquisition rate with these settings is one per 26 msec. The MSD curve was generated from 240 time points, of which 120 were graphed. Analysis indicates that the spot moves with a diffusion constant of D=7.69x10^-12. If oversampling occurred it would be apparent as a slope of 0 near the origin, which is not observed, thus the spot does measurably diffuse from image to image.

In order to estimate the degree of intensity fluctuation from a typical experiment on the OMX, 2D fluorescence video microscopy was performed on paraformaldehyde-fixed strain 1280, which contains a single tet operator array tagged with GFP, and is the parent strain of the Gal1p-MDN1 strain which is used later. Microscope settings included 50 ms exposure times and 10% ND setting, and spot intensities were graphed over time, as presented in Figure 4.4. Analysis of the graph indicates that there is a mean 3.1% variation in intensity from image to image under these conditions, with a standard deviation of 2.3%. This degree of fluctuation is significant; however, calculation of the RMS measurement error, as presented below, indicates that the overall error in z is within acceptable limits.

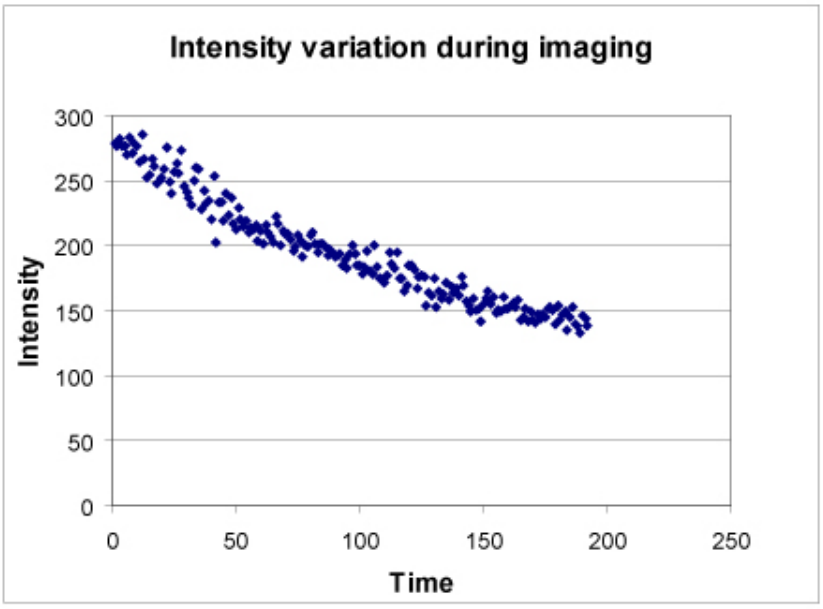

Figure 4.4. Variation in spot intensity. Variation in spot intensity during 2D video acquisition with the OMX microscope was measured using strain 1280, which contains a tet operator array and tetR-GFP, was fixed with formaldehyde and then imaged using 50 ms exposure times with 10% ND setting. Spot intensities were graphed over time and then analyzed. The results indicate a mean 3.1% variation in intensity from image to image, with a standard deviation of 2.3%.

A challenge to the study of chromatin in yeast arises from the effect of Brownian motion on chromosomal loci and the limitations it places on 3D live cell fluorescent video microscopy (Marshall, Straight et al. 1997; Heun, Laroche et al. 2001; Vazquez, Belmont et al. 2001). Fluorescently tagged yeast chromosomal loci have been reported to undergo a diffusive random walk which is capable of sampling a large fraction of the nucleus on a time scale of <5 minutes, and are further characterized by rapid displacements on the order of up to 0.5 μm in a <10 second interval (Heun, Laroche et al. 2001). In order to accurately track such loci in living cells in 3D, a microscope must be able to acquire stacks of images at a rate which does not allow for significant spot diffusion to occur during the acquisition of a single stack, as any such motion increases measurement error.

In order to determine the measurement error of the OMX microscope, as described in chapter 2 under "RMS measurement error determination", single GFP-spot strain 1280 was fixed with formaldehyde and 2D fluorescence video microscopy was performed. Images were collected every 71 msec, which was the fastest rate possible given the intensity of the spots post-fixation. Spots were tracked using Gasser Lab Spot Tracker software (see Materials and Methods), and MSD analysis was performed using the results. The 2D RMS measurement error for the OMX microscope when tracking spots in fixed strain 1280 was calculated to be 45 nm.

Similar calculations were made for 3D live cell videos of strain 1300, which is a 70 kb strain flanked by two GFP tagged loci on chromosome IV. Acquisition settings included using a step size of 400 nm, a stack size of 4 μm, exposure times of 10 msec, an acquisition rate of one image per 40 msec, and utilizing the Danuser spot tracking software (see Materials and Methods) for analysis. Four videos met the criterion of both spots being >400 nm apart for almost the entire duration of the video, and all four of these were used for this analysis. The RMS measurement error results from these videos, as well as the number of usable consecutive time points, are presented in Table 4.1. These mean RMS measurement error generated by averaging the values of the four videos is 81 nm. When calculating the distance between two spots, this error value must be applied to both spots, and is therefore additive, and the total RMS measurement error for the distance measurement is 162 nm. This value indicates that the OMX microscope can generate stacks of images at a rate which results in a significant introduction of measurement error, but which is still useful for making live

cell 3D measurements on a scale smaller than the yeast nucleus, and represents a significant advance in fluorescence microscopy.

Video	RMS error	Diffusion Constant	Usable time points
11	67	2.27E-11	50
17	103	5.31E-11	46
25	69	2.37E-11	41
35	50	1.26E-11	37

Table 4.1. RMS measurement error values from 70 kb strain data sets. RMS measurement error units are nm. Diffusion constant units are cm^2/sec.

Spot resolution is orientation dependent when two spots of the same fluor are analyzed, as was the case here. When oriented laterally, spots imaged with the OMX microscope and tracked with the Danuser software often could be resolved when <250 nm apart, although when oriented axially this dropped to <~400 nm.

One consideration for 3D tracking of strains with two spots is that the spots may not have the same z coordinates at any given time during a video. Spots which do have the same z coordinate are imaged simultaneously. Spots which have different z coordinates necessarily are imaged at slightly different times, and therefore the second spot has a small amount of time in which to diffuse after the first spot has been imaged. This lag time between spot imaging is a source of RMS measurement error, and the error increases the further apart two spots are in z. This problem is spot-orientation-dependent, and therefore the amount of error changes during the course of a given video as the spots re-orient themselves with respect to z.

Since x and y coordinate information from the calibration videos was acquired with high resolution for a given spot in every image of a video, while the z coordinate was

calculated by averaging intensity information from several images with 400 nm z step between them, it is expected that there is a higher degree of error with respect to the z coordinate. Furthermore, resolution of spots depended of their orientation, for timing reasons as well as with the problem of using two spots of the same wavelength, as mentioned above. To compare the relative amounts of error introduced from the x and y measurements to that introduced from the z measurement, RMS error was determined for analysis limited to x and y, x and z, or y and z information using the same 3D data set as used to obtain the 103 nm RMS error value. The RMS error in x and y was calculated to be 64 nm, while the error in x and z was determined to be 106 nm and the error in y and z was determined to be 99 nm. This indicates a 57% increase in error when the z dimension is considered in the 3D RMS error calculation.

4.8 Estimation of drift during live cell imaging of fluorescently tagged loci

RMS measurement error analysis was also performed individually on the spots from the video with the highest RMS error in order to estimate drift. The two spots were found to have RMS values of 155 nm and 151 nm, with a mean value of 153 nm. For determination of the drift inherent in the measurement of the distance between two spots, this value is doubled to arrive a drift-inclusive RMS measurement error of 306 nm. When compared to the RMS analysis of pairs of spots, this should indicate the amount of drift compensated for by the pair-wise analysis. The results of this analysis indicate that, on average, 144 nm worth of drift per time point is unaccounted for in the 2 spot RMS error analysis method.

An attempt was made to perform similar analysis using a 200 nm step size to estimate RMS measurement error at this setting; however, the videos collected using this setting either had low signal intensity at later time points in the videos, contained colocalized spots, both of which prevented analysis with the Danuser software. Spots in stacks acquired at this step size were observed by eye to diffuse during single stack acquisition. This step size may prove to be useful for generating videos, and Applied Precision has proposed fixes for rate limiting steps in the functioning of the OMX microscope, which should limit diffusion during stack acquisition.

4.9 Collection of data from the 40 kb and 70 kb strains

Strains 1300 and 1301, the 70 kb and 40 kb strains with two GFP spots, were prepared as discussed in the Materials and Methods. Live cell 3D fluorescence video microscopy was performed with the OMX microscope, typically with 10 msec exposures, 10% ND, stack heights of 4 μm, a step height of 400 nm, and 50 time points. Under these conditions, individual images were 40 msec apart, and each stack, and thus each time point, was 539 msec apart. Analysis was performed with the Danuser tracking software.

4.10 Data analysis

Videos were analyzed with proprietary software developed by the Danuser Lab and it was determined that this software could resolve spots which were further apart than roughly 250 nm laterally or 400 nm axially. As mentioned above, both spots in strains 1300 and 1301 were tagged with GFP which placed limitations on the

resolution. Ideally, the limit of resolution of two spots of the same wavelength is the distance from the central maximum of one spot to its first minimum. In practice, the separation distance by which the Danuser software could correctly locate two spots was inconsistent from stack to stack. It could often correctly locate spots at a given proximity, but would obviously mislocate spots at a slightly greater separation distance. Because of this, it was necessary to manually examine all location calls made by the software, and a judgement call was then made on spots in close proximity in regard to their location accuracy. Data from time points where spots were mislocated were dropped.

Distance measurements from multiple time points from multiple (15-20) videos were calculated, and the resulting spot separation profiles for the 40 kb and 70 kb strains are presented as histograms in Figure 4.5. Spots which were in close proximity (<400 nm) often could not be resolved, which is problematic as it is not possible to analyze incomplete histograms. To address this, the histogram bins were set to 400 nm in order to include these close-proximity time points. A chi squared test for independence determined that the 70 kb and 40 kb spot separation histograms are statistically different (Table 4.2). Bin sizes of 10 nm resulted in histograms with large gaps in the data corresponding to un-resolvable close-proximity spots. These histograms show empirically that the 70 kb strain shows larger spot separations than the 40 kb strain. These histograms are presented in Figure 4.6.

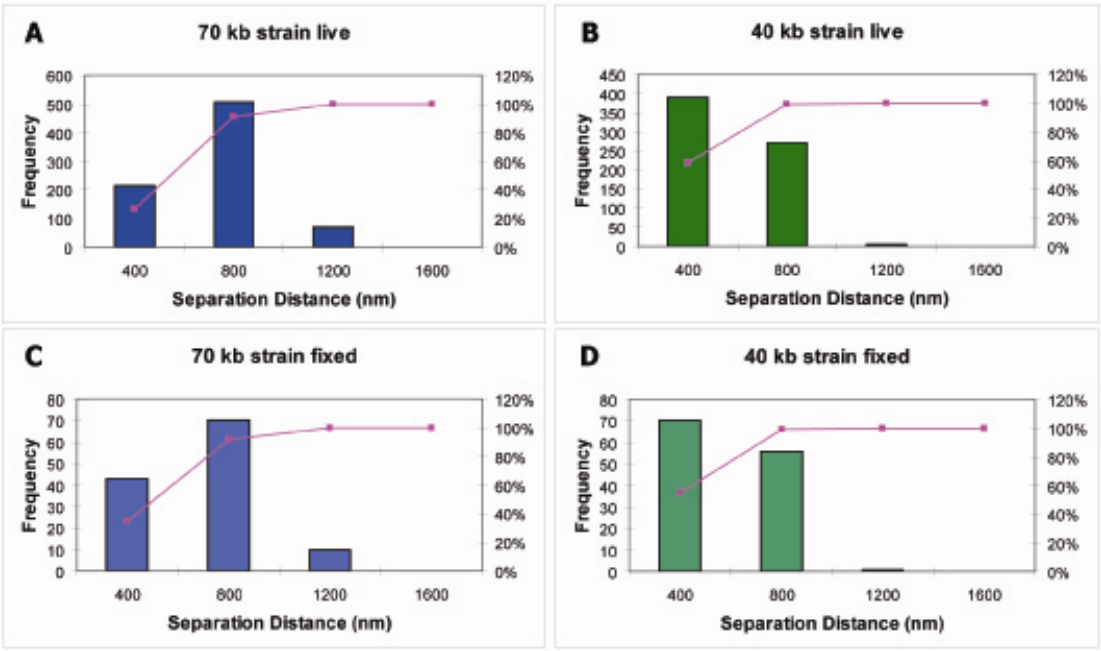

Figure 4.5 40 kb and 70 kb spot separation histograms. Spot separation distance were measured in the 40 and 70 kb strains with flurescence video microscopy by the OMX microscope, the data was analyzed using the Danuser tracking software, and the results are presented here as histograms of the frequency which a particular spot separation value is found within the 400 nm bin size. The line graph and values on the right-hand axis represent the cumulative percent of all time points. A. 70 kb strain separation distance histogram from live cells using 3D tracking with the OMX microscope. B. 40 kb strain separation distance histogram from live cells using 3D tracking with the OMX microscope. C. 70 kb strain separation distance histogram from fixed cells using 3D tracking with the Deltavision microscope. D. 40 kb strain separation distance histogram from fixed cells using 3D tracking with the Deltavision microscope.

	Chi^2	p	n vs n
40 live vs 70 live	35.5	9.00E-08	1176 1154
40 fix vs 70 fix	18.4	3.69E-04	127 123
40 live vs 40 fix	.49	7.82E-01	1176 127
70 live vs 70 fix	3.4	3.34E-01	1154 123

Table 4.2. Chi square tests for independence were performed on the 40 kb and 70 kb strain fixed and live data sets. Histogram bins were set to 400 nm to include data from spots which were in close proximity but which the software failed to resolve. Outliers were excluded from the 70 kb fixed-cell data set. Both the 40 kb live vs 40 kb fixed and 70 kb live vs 70 kb fixed comparisons were found to be statistically similar. Whether comparing fixed or live data sets, the 40 kb strain was found to be statistically different from the 70 kb strain.

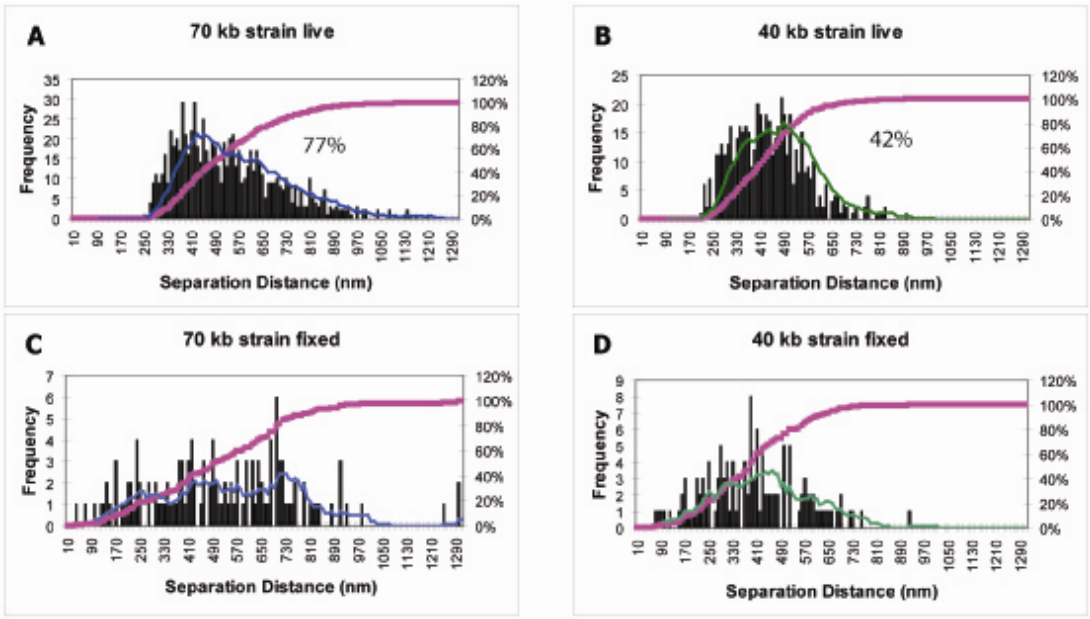

Figure 4.6. The 40 kb and 70 kb live- and fixed-cell histograms with bin sizes of 10 nm. Separation distance data from the live cell data is incomplete as close proximity spots could not be resolved. The percentages of time points where the spots could be resolved are listed as 77% for the 70 kb live cell data set, and 42% for the 40 kb live cell data set. The fixed cell data sets were analyzed in 40 and 70 kb strains which contained a blue (CFP) and a green (GFP) spot, and therefore do not have this proximity constraint. Blue and green lines indicate moving average analysis with a period of 10. Pink lines indicate cumulative percentage of time points, with corresponding annotation shown on right-hand axis. A. 70 kb strain separation distance histogram from live cells using 3D tracking with the OMX microscope. B. 40 kb strain separation distance histogram from live cells using 3D tracking with the OMX microscope. C. 70 kb strain separation distance histogram from fixed cells using 3D tracking with the Deltavision microscope. D. 40 kb strain separation distance histogram from fixed cells using 3D tracking with the Deltavision microscope.

4.11 Estimation of compaction ratios

A chromatin fiber within a living nucleus is subject to Brownian motion, and its effect can be directly observed under the microscope by the constant random motion of a fluorescently tagged chromosomal locus. It would be expected that a length of chromatin which is flanked by fluorescent spots would sometimes be found with the spots in their closest possible conformation, while at other times the spots would

diffuse to their furthest possible separation distance, and that the likelihood of finding the chromatin in any given state would follow the laws of probability. We would thus expect that, as there is only one fully extended conformation for the chromatin fiber, while there are multiple ways that it could be compacted into a less-extended conformation, it would be least likely that the chromatin would be found in its most-extended state. With this in mind we chose to examine the mean of the top 5% separation distances from the histograms with 10 nm bins as a method for estimating the compaction of fibers as they approach a linear conformation. The mean of the top 5% of distances were calculated. The expected linear end-to-end distance for B-form DNA of either 40 kb or 70 kb was calculated using the knowledge that one base in B-form DNA has linear dimensions of 0.34 nm. This value was then divided by the mean of the top 5% of distance values to estimate the compaction ratio.

This approach estimated the compaction ratio for the live 70 kb data to be 21.1-fold, and for the live 40 kb data to be 15.5-fold (Table 4.3), for an average of 18.3-fold. As it is possible that some of the largest end-to-end measurements result from random forces in the nucleus stretching the chromatin fibers, this result may be inflated. Similar top 5% calculations were made for the corresponding fixed cell data sets, resulting in compaction ratios of 22.3-fold for the 70 kb strain, and 13.6-fold for the 40 kb strain, for a mean of 18-fold (Table 15). The mean values from the live and fixed cell data sets are within 98% of one another. The difference between the 70 kb and 40 kb results may be due to the transcriptional status of the genes flanked by the two spots, which we were not able to determine.

	40 kb	70 kb	Mean	Porod-Kratky
Live	15.5	21.1	18.3	NA
Fixed	13.6	22.3	18.0	12.6

Table 4.3. Compaction ratios estimated from top 5% method for determining mean end-to-end spot separation distance. Units are –fold compaction.

Compaction ratio calculations were also made with modal end-to-end measurements from our fixed samples. As these cells contained a blue (CFP) and a green (GFP) spot, measurements were possible when the spots were in close proximity, and there were no binning restrictions as with the live cell measurements. Fitting the Porod-Kratky chain equation to the modal end-to-end data from our 40 kb and 70 kb fixed cell analysis results in a compaction ratio of 12.6-fold (+/-1.4-fold), a persistence length of 89 nm (+/-10 nm), and a linear mass density of 37 bp/nm (+/-4 bp/nm) (Figure 4.7).

The 40 kb and 70 kb fixed cell data sets were also compared using the Chi square test for independence, which indicated that, when chemically fixed, the strains still have statistically different spot separation profiles (Table 4.2). When the 40 kb strain live and fixed data sets were compared via the Chi square test they were calculated to be statistically similar. Likewise, the 70 kb live and fixed cell data sets were found to be statistically similar (Table 4.2).

4.12 Observations of changes in end-to-end distance

Empirically, the spots exhibited a variety of motion profiles which differed from nucleus to nucleus and from spot to spot. Some spots appeared to have high rates of

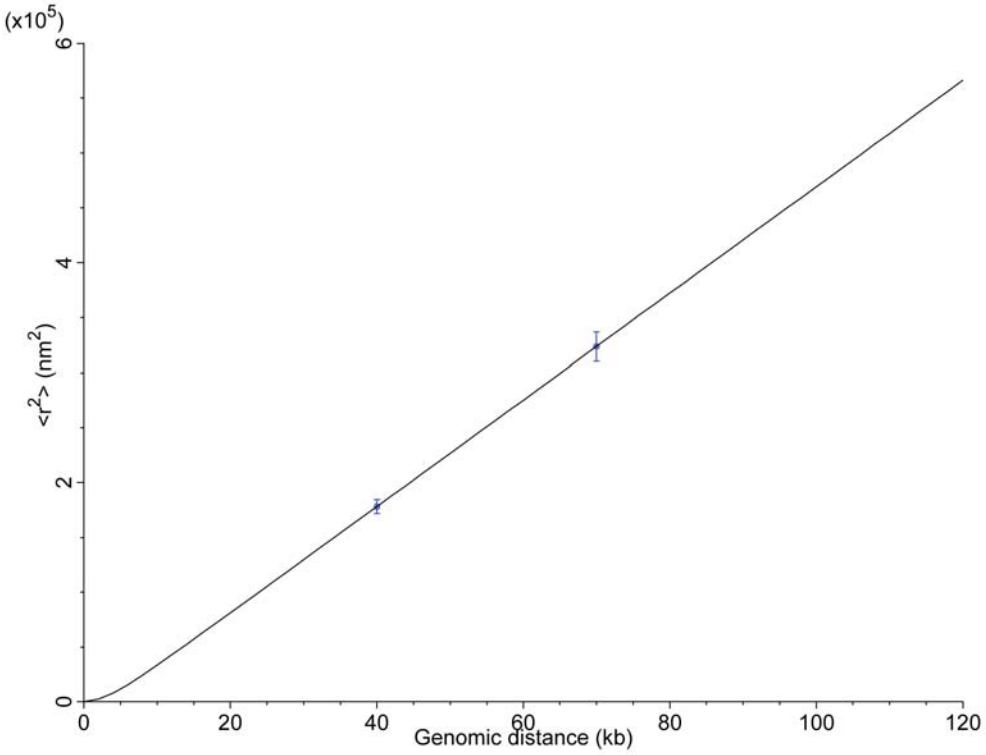

Figure 4.7. Porod-Kratky fitting. Fixed cell end-to-end spot distance analysis of 40 kb and 70 kb strains produced modal distance measurements which were graphed and a best-fit was made with the Porod-Kratky chain equation. As this analysis is based on only two data points the confidence in the results is low; however, estimates of a persistence length of 89 nm, a linear mass density of 37 bp/nm, and a compaction ratio of 12.6 were generated.

diffusion, others had less, and most tracking data sets from individual videos were missing time points due to the use of two GFP spots. Due to photobleaching constraints, videos were limited to 50 time points. Because of these factors it was not possible to perform meaningful MSD analysis on every spot, nor was it fair to combine tracking data from different videos in order to average their MSDs. Some spots were observed to localize to the nuclear periphery, although in most cases there was no concurrent reduction in motion which might be evidence of physical association with nuclear envelope. Some pairs of spots appeared to have similar rates of diffusion, while others did not.

In order to analyze changes in end-to-end distances over time increments of roughly half a second, graphs were generated from 40 and 70 kb videos with the fewest missing data points, as presented in Figure 4.8. Changes in separation on the order of >300 nm in this time scale appear to be common for tags separated by either 70 kb or 40 kb. Changes in end-to-end distance of 550 nm can occur on a time scale of <6 seconds in the 70 kb strain, and <15 seconds for the 40 kb strain. As the RMS measurement error under these conditions is estimated to be 103 nm, there is a degree of uncertainty regarding these values; however, duplicate measurements in consecutive time points were used as a means of increasing confidence in the measured end-to-end distances.

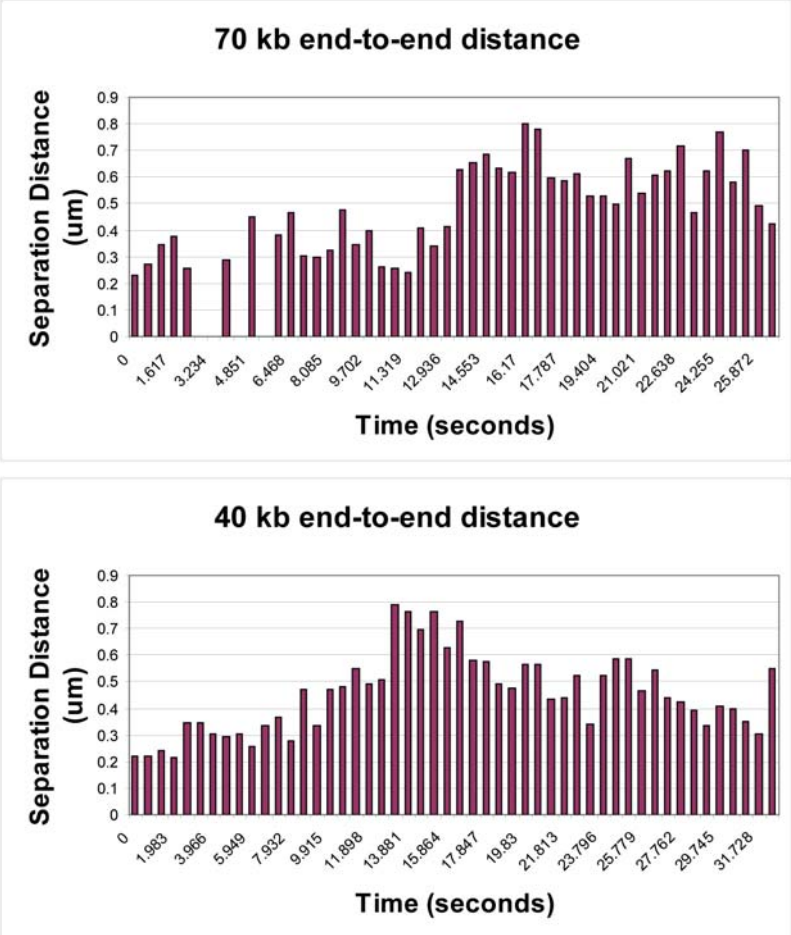

Figure 4.8. 40 kb and 70 kb spot separation distance graphs. Spot separation distance versus time for two individual videos of 40 kb and 70 kb separation distances.

4.13 Discussion

Proof of principle experiments demonstrate that this system for measuring chromatin compaction in yeast using the OMX microscope and the Danuser tracking software is viable. We find that image acquisition is rapid enough to measure the distance between two fluorescently tagged genomic loci in live yeast cells in 3D with a RMS measurement error of 162 nm that, while significant, permits meaningful analysis of chromatin structure. Chi square analysis of end-to-end separation histograms from 40 kb and 70 kb strains indicates that the OMX microscope can distinguish between the two strains whether they are live or fixed. Although the fixed-cell data sets are relatively small at n=123 and n=127, the data shows that in two different data sets, the 40 kb live versus the 40 kb fixed, and the 70 kb live versus the 70 kb fixed, fixed cell analysis can recapitulate live cell 3D results with accuracy. Such agreement improves confidence in both methods.

We observed three-fold changes in end-to-end distance on a time scale of <6 seconds in the 70 kb strain, and 3.75-fold in <15 seconds for the 40 kb strain. Two consecutive time points with the same separation distance were used for this analysis to improve confidence in the measurements. Previous studies have analyzed 3D motion of individually tagged genetic loci (Marshall, Straight et al. 1997) or multiple adjacent tagged loci (Robinett, Straight et al. 1996), but this is the first such study to analyze two adjacently tagged loci in such close proximity at such small time scales. The absolute change in separation of these measurements is on the order of 550 nm.

It has been observed by us and others that strains with adjacent fluorescently tagged genomic loci exhibit a wide distribution of end-to-end distance measurements, in live cells as well as pools of fixed cells (Marshall, Straight et al. 1997; Bystricky, Heun et al. 2004). One method of using these measurements to estimate chromatin compaction ratios involves the Porod-Kratky chain equation, which models chromatin as a semi-flexible polymer. Bystricky et al use the Porod-Kratky chain equation to generate chromatin compaction estimates from maximum frequency (mode) end-to-end 2D distance measurements from FISH data from multiple strains with spots separated by different genomic distances (Figure 4.9) (Bystricky, Heun et al. 2004). The Bystricky fixed-cell FISH results from diploid yeast cells estimated a 40-fold compaction ratio for chromatin of genomic lengths between 14 kb and 103 kb. This value is comparable to the expected compaction ratio of the 30 nm fiber *in vivo* (Bystricky, Heun et al. 2004). Our fixed cell results generated with the Porod-Kratky chain equation are one-third of either of this value at 12.6-fold, though again, confidence in this result is low as only two data points were analyzed. Use of the top 5% method on our live- and fixed-cell data sets gave compaction ratio estimates which, at 18-fold, are roughly half that of the Bystricky result. These results are summarized in Table 4.2.

Top 5%	MDN1+gal	MDN1+raf	30 kb/60 kb mean	30 kb/60 kb Porod-Kratky
Live	9.8	18	18.3	NA
Fixed	NA	NA	18	12.6

Table 4.2 Chromatin compaction ratio estimations. The chromatin compaction ratio estimations from the mean top 5% method and the Porod-Kratky chain equation-fitting method (last column only). Units are fold-compaction. By comparison, the theoretical compaction ratio for the 30 nm fiber in vivo is estimated to be 40-fold, as is the estimation reported by Bystricky et al, while the theoretical compaction ratio for nucleosomal DNA is estimated to be at minimum 6-fold.

It should be noted that for our fixation technique we followed the method described by Bressan (Bressan, Vazquez et al. 2004), and while Bystricky also performed formaldehyde fixation, it was followed by a FISH protocol which involves dehydration and rehydration of the samples (Bystricky, Heun et al. 2004). Such differences in methodologies may affect chromatin structure and result in the differences in our compaction ratio estimates. Additionally, Bystricky made measurements in diploid cells, while the 40 kb strain and the 70 kb strain were

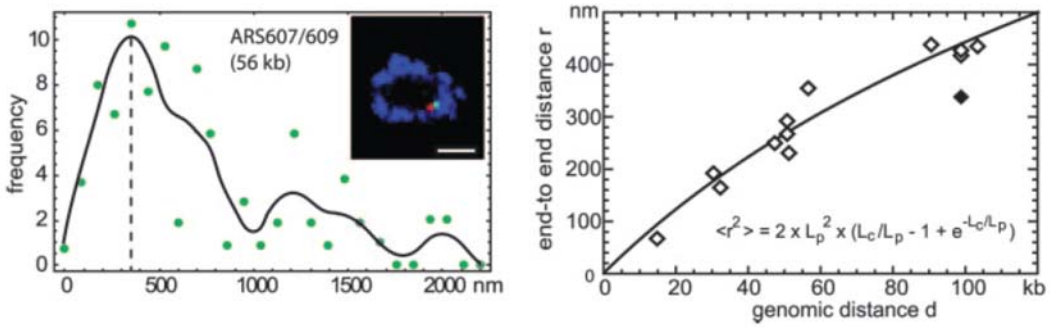

Figure 4.9. Graphs from the Bystricky data set. Yeast strains with fluorescent spots flanking genomic regions of from 14 to 103 kb were imaged in 3D by FISH and the modal end-to-end spot separation distances were determined. The dataset from the 56 kb strain is depicted in A. The modal end-to-end spot separation distances from all data sets were plotted as distance r versus genomic distance d in graph B, and the Porod-Kratky chain equation (inset) was fitted to the resulting data set. From this the persistence length was calculated to be 170-220 nm, the linear mass density was calculated to be 110-150 bp/nm, and the compaction ratio was calculated to be 40-fold (Bystricky K, 2004).

haploid. Bystricky also analyzed haploid cells for comparative purposes, and reported that end-to-end distance measurements were the same in diploids and haploids (Bystricky, Heun et al. 2004). Finally, Bystricky relied on 2D microscopy analysis while the present study relied on 3D analysis. Interestingly, the histograms from the Bystricky fixed diploid cell data show separation distances of 1.7-1.9 μm for genomic distances ranging from 32 to 103 kb, which is just under the 2.4 μm diameter

measured for the diploid yeast nucleus. Sample populations ranged from n=65 to n=93 for the different genomic distances. During the acquisition of our 70 kb live-cell data the furthest separation distance we saw was under 1.3 μm from a sample number of n>1000. We did, however, see some outlying separation distances from cells thought to be in S-phase due to observed temporary doublet formation from what were initially thought to be individual spots, and these videos were dropped from the data set. It was not possible to check for S-phase cells in this manner during the fixed-cell experiments, which raises concern for us regarding outliers in both our and the Bystricky fixed-cell data. Also, it would not make sense to apply our top 5% method for compaction ratio estimation to the Bystricky data set as the presence of the outliers would result in compaction ratios which decrease linearly with genomic distance.

As previously mentioned, *in vitro* techniques which rely on chemical fixation, 2-dimensional imaging, or the introduction of salts to the sample may result in artificial distortion of chromatin structure. For example, mono- and divalent cations such as sodium (chloride) and magnesium (chloride) have been shown to cause the condensation of 30 nm fibers into a higher order of structural organization in solution in a concentration-dependent manner (Paulson and Laemmli 1977; Marsden and Laemmli 1979; Thoma, Koller et al. 1979; Gerchman and Ramakrishnan 1987). While physiological NaCl concentrations are thought to be near 150 mM, and $MgCl_2$ concentrations are thought to be near 0.6 mM, it cannot be assumed that chromatin fibers will have identical properties in these concentrations outside the cell.

There is evidence that the nucleosomal fiber, as opposed to the 30 nm fiber, predominates in yeast. It has been demonstrated that H4K16 acetylation inhibits formation of 30 nm fibers *in vitro* (Shogren-Knaak, Ishii et al. 2006) and over 80% of histones in *Saccharomyces cerevisiae* are acetylated at this site (Shogren-Knaak and Peterson 2006). Estimations from 3C data from yeast predicted that, *in vivo*, chromatin has a mass density of 1.2-2.4 nucleosomes per 11nm turn, and a persistence length of 28 nm, shorter than that expected from a 30 nm fiber (Dekker, Rippe et al. 2002). That study arrived at those estimates through mathematical modelling of the association of different genomic loci in chemically fixed cells, as opposed to measuring fiber sizes directly, and thus avoiding potential artefacts introduced by non-physiological cation concentration. Additionally, cryo-EM studies of mammalian ES cells in close-to-native state have found little evidence for structure larger than nucleosomal fibers (Bazett-Jones, Li et al. 2008; Eltsov, Maclellan et al. 2008). Our data also supports lower figures for linear mass density, persistence length, and compaction ratio, and thus supports the theory that yeast interphase chromatin primarily has dimensions smaller than 30 nm. Fitting our 40 kb and 70 kb fixed cell data with the Porod-Kratky chain equation results in a compaction ratio estimation of 12.6-fold, a persistence length estimation of 89 nm, a linear mass density estimation of 37 bp/nm, and 2-3 nucleosomes per 11 nm turn in the chromatin fiber. Our live- and fixed-cell top 5% method estimates yield 18-fold compaction and 3.5-5 nucleosomes per 11 nm turn. The results of both methods describe a fiber that would be slightly more compact than nucleosomal DNA, which is estimated to be compacted 6-fold, and one-half to one-quarter as compact than the estimated 40-fold of the 30 nm fiber. Due to limitations to the resolution of the system, we can not rule out the 1.5 to 3-fold decrease in compaction associated with transcription that has been

reported previously using 2D live cell microscopy of fluorescently tagged chromosomal loci in hamster (Hu, Kireev et al. 2009). As we only have two data points with which to fit the Porod-Kratky chain equation, and as our top 5% method includes an assumption that the structure of the chromatin is never stretched by mechanical forces, confidence in these estimations is low. It is hoped that in future it will be possible to acquire additional data to substantiate our initial observations.

CHAPTER 5

Effects of Transcription on Chromatin Compaction

5.1 Introduction

Having established a system suitable for the measurement chromatin compaction, we were interested to apply it to the study of factors that might regulate the level of compaction. Based on evidence that chromatin adopts a configuration consistent with a 30 nm fiber, it might be anticipated that factors influencing chromatin structure at this level would also influence chromatin compaction. An ideal candidate in this respect might be to examine the role of the H4 tail in compaction. *In vitro* the H4 tail has been demonstrated to be important for transcriptional repression through the formation of heterochromatin (Roth, Shimizu et al. 1992; Lenfant, Mann et al. 1996). Attempts were made to cross an H4 tail truncation strain with strain 1200, a 70 kb strain, in order to determine if an effect on chromatin compaction could be measured microscopically. This cross proved to be problematic and was not successful. As an alternative a number of ATP-dependent chromatin remodeling enzymes were deleted in strain 1200 and their effects on chromatin compaction were studied. However, no significant effects were observed in these deletion strains (see Appendix I), possibly due in part to the inherent dynamic properties of chromatin structure which would mask a minor effect, and possibly due in part to the redundancy of function known to exist among chromatin remodeling enzymes (Barbaric, Luckenbach et al. 2007).

We chose as an alternative to characterize the effects of transcription on chromatin structure. There are reports that coding regions of highly transcribed genes are depleted of nucleosomes (Schwabish and Struhl 2004; Govind, Zhang et al. 2007; Schwabish and Struhl 2007), which should have a powerful effect on chromatin compaction. Taking advantage of high performance microcopy might enable the detection of the separation of tagged loci flanking a single gene. For this reason we decided to study chromatin compaction between tags flanking a Gal1-inducible copy of the largest yeast gene, *MDN1*. Further explanation for this choice is provided below.

5.1.1 The *GAL* locus

Transcription from the *Gal* locus in yeast is regulated by the bi-directional, galactose inducible, glucose inhibited Gal1 promoter, which drives expression of both the *GAL1* and *GAL10* genes, which have roles in galactose metabolism (St John and Davis 1981; Johnston and Davis 1984; West, Chen et al. 1987). The Gal1 promoter is among the strongest promoters in cerevisiae (St John and Davis 1981) and real time studies which utilized GFP as reporter indicate that a minimum 0.05 g/L galactose can double GFP fluorescence signal over background, while 0.1 g/L gave the highest specific GFP yield (Li, Wang et al. 2000). Pol II occupancy at the Gal1 promoter has been demonstrated to be correlated with galactose (Schwabish and Struhl 2004). Additionally, RT-PCR analysis has shown that Gal1, Gal7, and Gal10 polyadenylated mRNAs represent 0.25-1% of total polyadenylated mRNA when galactose is the carbon source (Lohr, Venkov et al. 1995). The Gal1 promoter has been used extensively as a non-leaky, strongly inducing promoter to drive expression of a host

of genes in a variety of studies (Yocum, Hanley et al. 1984; Kontoyiannis 1999; Li, Wang et al. 2000; Mason and Struhl 2003; Govind, Zhang et al. 2007; Schwabish and Struhl 2007).

Transcription from the Gal1 promoter is repressed when non-galactose carbon sources are present, through the activity of the Gal80p protein, which binds Gal4p and prevents it from activating transcription (Peng and Hopper 2002). When glucose is present, GAL4 mRNA levels drop, the amount of Gal4p at the Gal1 promoter drops, Gal80 binds and inhibits Gal4p from activating transcription, and GAL1 and GAL10 are not detectably expressed (Lohr, Venkov et al. 1995).

Gal1 transcription is reported to be repressed by the trisaccharide raffinose, as Gal80p remains bound to Gal4p in this instance, although the gene is described as poised for transcription since Gal4p remains bound to the Gal1 promoter (Kundu, Horn et al. 2007).

When galactose is present, the Gal3p protein binds the Gal80p repressor, sequestering it in the cytoplasm and preventing it from inhibiting Gal4p (Peng and Hopper 2002). Also when galactose is present, Gal4p, which is bound to UASs in the Gal1 promoter in the absence of Gal80p, induces transcription at the locus (Lohr, Venkov et al. 1995) through its recruitment of the SAGA complex, and then the Mediator complex, in that order, though independently (Bryant and Ptashne 2003).

Looping which results in the physical association of the Gal10 promoter and terminator in a TFIIB-dependent manner associated with transcriptional memory has

been reported in yeast (Singh and Hampsey 2007; Laine, Singh et al. 2009). This looping effect is also dependent on subunits of the pre-mRNA 3'-end processing machinery, including Ssu72 and Rna15 (Singh and Hampsey 2007; El Kaderi, Medler et al. 2009).

Transcription from the Gal1 promoter is implicated in the eviction of nucleosomes along the length of downstream ORFs in a SWI/SNF-dependent manner (Schwabish and Struhl 2004; Govind, Zhang et al. 2007; Schwabish and Struhl 2007). Upon glucose repression, H3 levels at the endogenous Gal1 ORF were shown to increase within one minute (Schwabish and Struhl 2004), reaching pre-initiation levels within four minutes (Govind, Zhang et al. 2007), and a 20- to 30-fold reduction in Pol II occupancy is seen within four minutes as well (Schwabish and Struhl 2004).

Upon activation, the Gal locus is recruited to the nuclear periphery in a SAGA-dependent manner where it interacts with nuclear pore protein Nup1 to up-regulate transcription from the gene (Cabal, Genovesio et al. 2006).

The properties of promoter-terminator looping, nucleosome eviction along the ORF, and recruitment of the locus to the nuclear periphery upon induction have been shown to be preserved when the Gal promoter is cloned upstream of other genes elsewhere in the genome, although in the case of looping this is possibly due to the functions of specific terminators used in the assays (Govind, Zhang et al. 2007; Luthra, Kerr et al. 2007; Laine, Singh et al. 2009).

These studies have established in some detail that a series of dramatic chromatin transitions occur in response to the induction of GAL, and considering its high transcription rate and nucleosome depletion effect, it represents a system with a good chance of detecting transcription-related alterations in compaction.

5.1.2 The *MDN1* gene

The *MDN1* gene is the longest gene in the yeast genome at 15 kb. It codes for a 4910 amino acid, 560 kiloDalton (kDa) AAA-type ATPase called midasin which is linked to the modification and nuclear export of the pre-60S ribosomal subunit (Garbarino and Gibbons 2002; Nissan, Galani et al. 2004; Ulbrich, Diepholz et al. 2009). It is essential for viability and, despite being a pre-ribosomal protein, it has been shown to be transcribed in its entirety as a single mRNA by PolII in yeast (Winzeler, Shoemaker et al. 1999; Joshi and Struhl 2005). When expressed from the endogenous promoter, the MDN1 mRNA is present in roughly 6 copies per cell, as determined by a method of transcript counting called transcription fluctuation analysis (Daniel Larson, personal communication), while MDN1p is present in roughly 540 copies per cell (Ghaemmaghami, Huh et al. 2003). The large size of the *MDN1* gene is an advantage, as changes in its compaction might be readily detected by light microscopy.

A strain containing the Gal1p-MDN1 flanked by operator arrays and expressing DNA-binding domain-GFP fusion proteins was created with the aim of studying transcription-induced changes in chromatin compaction (see Materials and Methods). Samples cultured overnight in the presence of different carbon sources were imaged

with the OMX microscope , the raw data was analyzed with the Danuser tracking software (see Materials and Methods), and the results were compared.

5.2 Results

5.2.1 Strain construction

In order to create a strain in which the MDN1 Gene was flanked by operator sites, three plasmids were constructed. The first, plasmid 202, included the tetOx256 operator array flanked on one side by the Cyc1 terminator, and on the other by a ~300 bp *MDN1* downstream sequence for subsequent cloning purposes, and also included URA3 sequence which permitted the linearized plasmid to stably integrate at the *URA3* locus. The second, plasmid 206, contained the *MDN1* gene and URA3 sequence allowing the linearized plasmid to integrate adjacent to the first plasmid. The third, plasmid 207, contained the lacOx224 array, as well as the TEF1 terminator, the Gal1 promoter, the 5' end of *MDN1*, and URA3 sequence to allow it to integrate adjacent to the second plasmid. The construction of these plasmids, as well as the generation of strain 1295, are described in detail in the Materials and Methods and are outlined in Figure 2.2.

5.2.2 Confirmation that MDN1 expression is galactose-inducible

Several RT-PCR primer sets were tested for this analysis. Attempts were made to PCR across the junction spanning the 3' end of the *MDN1* transgene and the Cyc1 terminator in order to avoid amplification of the endogenous *MDN1*, but these were

unsuccessful. The final set of primers used for this analysis, including both the 5' and 3' primer pairs, had sequence homology to the endogenous gene as well as the transgene. RT-PCR analysis of the glucose-cultured samples detects what is presumed to be the background level of MDN1 transcripts (Figure 5.1). The 3' end of

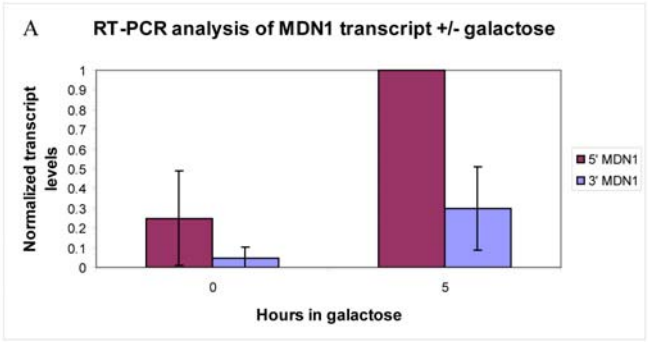

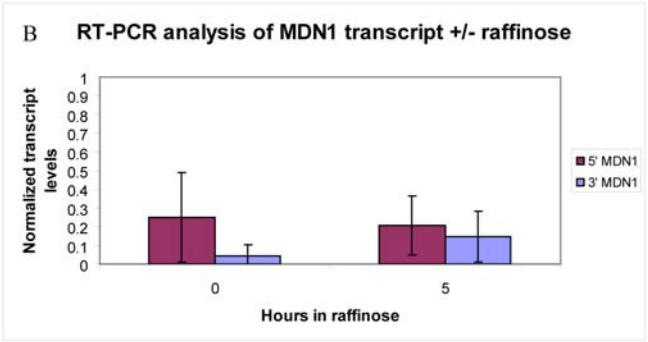

C	5'	3'
Galactose	4.0	6.8
Raffinose	0.8	3.4

Fold upregulation of MDN1 transcript after 5 hours

Figure 5.1. RT-PCR results. The Gal1p-MDN1 strain was grown overnight in YPA+2% glucose, washed 4x with deionized water, re-fed with YPA plus either 2% glucose, 2% raffinose, or 2% raffinose plus 2% galactose, incubated for 5 hours, and then total RNA was harvested as described, with a total of 6 samples per carbon source. Primers designed to amplify a 662 bp region within the 5' end of the cDNA, a 770 bp region spanning the 3' end of the cDNA, or a 561 bp region within the Act1 cDNA were used in single-plex PCR reactions (n=9), which were electrophoresed, stained with SYBR gold, and analyzed on a Fujifilm FLA-5100 fluorescent image analyzer using an excitation wavelength of 473 nm and the LPB detection filter setting. Band intensities were measured using Aida Advanced Image Data Analyzer software version 3.27.001. Sample band intensities were normalized to the Act1 internal control, and then normalized to the intensity of the galactose-induced 5' end band intensity. Analysis indicates that MDN1 transcripts are present in glucose conditions, and full length transcripts are upregulated upon incubation with either raffinose or galactose (A and B). 5 hours of galactose induction produces a 4-fold increase in detection of the 5' end of the transcript and a 6.8-fold increase in detection of full length transcripts, while 5 hours raffinose induction produces roughly 2/3 full length transcripts compared to galactose (C).

the MDN1 transcripts are upregulated 3.4-fold upon incubation with raffinose, and both the 3' and 5' ends of the *MDN1* gene are detected to a 6.8- and a 4-fold larger extent in the raffinose plus galactose samples, respectively. These values would presumably be higher if endogenous MDN1 transcripts could be eliminated.

5.2.3 Measuring compaction of the Gal1-MDN1 gene

Strain 1295 was cultured in either 2% glucose, 2% raffinose, or 2% raffinose+ 2% galactose overnight and imaged with the OMX microscope as described in the Materials and Methods. Virtually all spots were observed to be adjacent to the nuclear periphery by eye, although we did not verify physical association with the nuclear envelope or nuclear pore proteins. Videos were analyzed using the Danuser tracking software as described in the Materials and Methods.

Analysis of the glucose-inhibited strain show that the two tagged loci were predominantly colocalized, and were only resolvable as individual spots in 2% of the time points examined. This percentage of resolved spots was insufficient for the Danuser software to generate accurate tracking results, and for this reason there is no histogram for the 2% glucose experimental condition.

Cells grown overnight in 2% raffinose showed spot colocalization in 91% of the time points examined. However, a minority of the videos contained sufficient spot separation that the Danuser software was able to track the spots. A minority of videos showed spots which remained separated through all 50 time points.

Cells grown overnight in 2% raffinose plus 2% galactose showed spot colocalization in 75% of the time points examined, and again this was sufficient in some videos to permit Danuser tracking analysis. A minority of videos showed spots which remained separated through almost all 50 time points. Overall, the percentage of time spots were apart was observed to be correlated with the carbon source, and thus with transcription.

5.2.4 Statistical analysis of carbon source-dependent differences in spot separation

Histograms of the observed end-to-end spot distances with bins of 10 nm were generated for the raffinose and galactose samples, and although these histograms are missing the close-proximity data, they still show empirically that there is a difference in spot separation profiles dependent on the carbon source. This data is presented in Figure 5.2.

The histograms from the raffinose and galactose samples were generated with bins of 400 nm. This bin size ensures that close proximity spots which could not be tracked by the Danuser software are still accounted for. Comparison of the raffinose and galactose data sets using the Chi square test indicates that the two spot separation profiles are statistically different. The end-to-end distance results are presented as

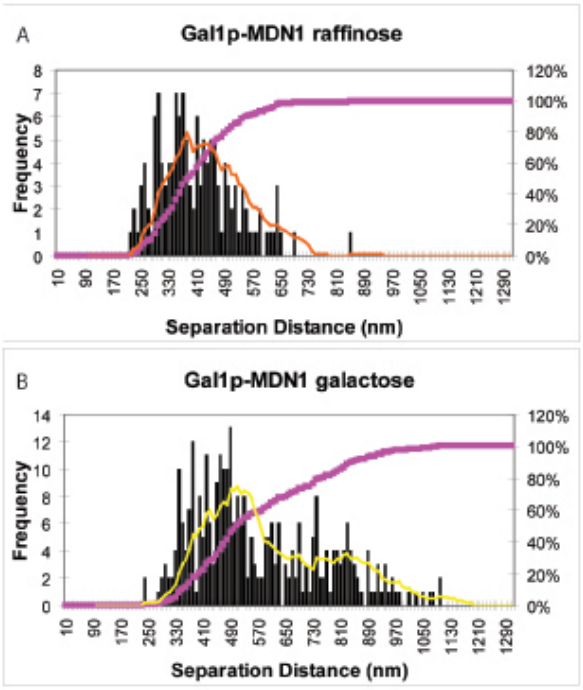

Figure 5.2. Gal1p-MDN1 10 nm histograms. Live cell 3D end-to-end spot distance analysis of the MDN1 gene in different transcriptional states. A. Gal1p-MDN1 + raffinose sample. N=136. B. Gal1p-MDN1 + raffinose + galactose sample. N=309. Bin size=10 nm. Pink lines show cumulative percent, with corresponding annotation on right side of graph.

Strain 1300, a 70 kb strain, was cultured overnight in YPA + 2% raffinose + 2% galactose and videos were generated following the protocol in the Materials and Methods in order to rule out a non-specific effect of these carbon sources on chromatin compaction. The intensities of the spots were poor and the data was unusable. This experiment will be repeated later.

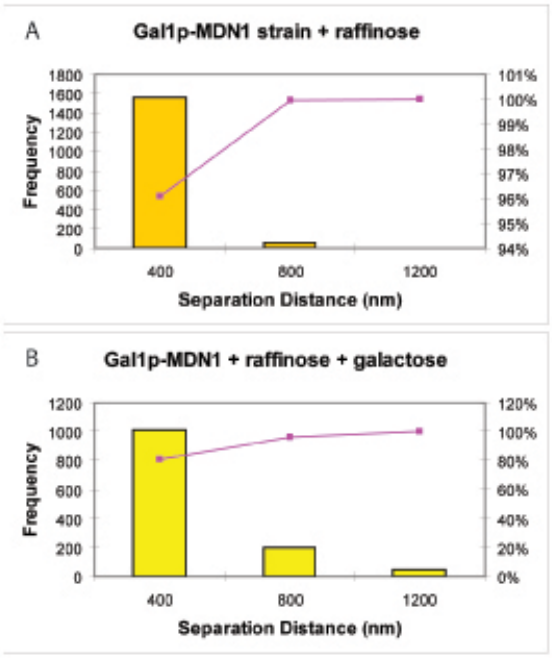

C

Comparison at bin=400	Chi^2	p	n vs n
15 raf vs 15 raf gal	187	0	1628 1263

Figure 5.3. Gal1p-MDN1 400 nm histograms. The Gal1p-MDN1 strain was cultured overnight in either YPA + 2% glucose, YPA + 2% raffinose, or YPA + 2% raffinose + 2%galactose. Live cells were imaged in 3D with the OMX microscope, analyzed with the Danuser tracking software, and the spot separation distances are presented as histograms above. The spots in the 2% glucose sample predominantly were found to colocalize, and thus distance measurements could not be calculated and a histogram could not be generated. A. The raffinose sample. B. The raffinose + galactose sample. C. Chi square analysis indicates that the two histograms are significantly different. N refers to the number of data points.

5.2.5 Observations of changes in end-to-end spot separation distance

In order to analyze changes in end-to-end distances over time increments of roughly half a second, graphs were generated from videos with the fewest missing time points, as presented in Figure 5.4. Reversible changes in end-to-end separation on the order of ~500 nm in two seconds are possible for the galactose-induced strain. Analysis of sequences of time points from a 3D video from this induced strain show two consecutive time points where spot separation is measured at ~900 nm, then two

seconds later the spots are determined to be co-localized for several consecutive time points, and then half a second later spot separation is measured at ~800 nm for two consecutive time points (Figure 5.4D). Again, the RMS measurement error is on the order of 103 nm, and thus the observed changes in end-to-end separation are significant. In a subset of videos, spots were observed to either start together and move apart and stay apart, or start separated and then come together and stay together, over the course of the ~25 sec duration of the videos. An example of a possible transcription initiation event is presented in Figure 5.5. Transcription termination event videos were of insufficient quality for Danuser software analysis and are not presented. Due to the relatively short duration of the videos it is not possible to determine

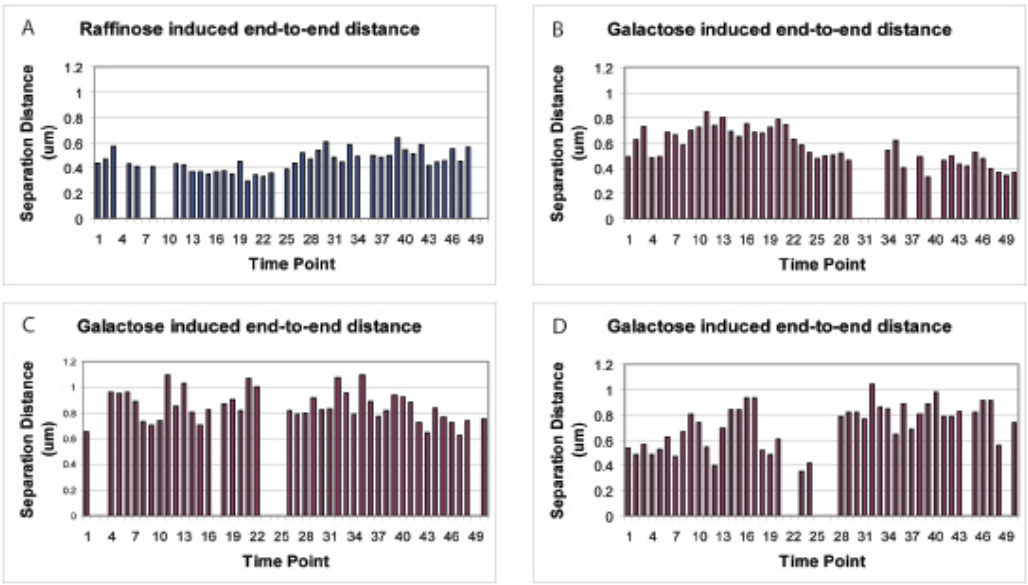

Figure 5.4. Gal1p-MDN1 end-to-end graphs. Spot separation distance versus time for videos of the Gal1p-MDN1 strain cultured overnight in raffinose (A) or galactose (B-D). Missing measurements from time points 20-27 from graph D were verified to contain colocalized spots, and thus represent the extremes in rapid conformational changes from this study.

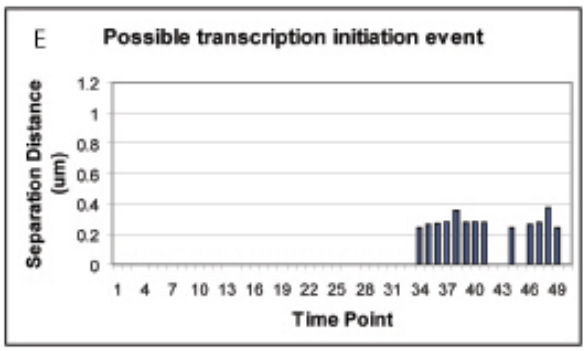

Figure 5.5. Possible transcription initiation event. Spots are initially colocalized, but move apart and remain apart. This sample was cultured in raffinose.

the duration between separation events. It is possible that these videos represent the beginning or end of individual transcriptional events, and while it was not possible to verify if this was the case, nonetheless the observed spot behaviours are intriguing, and they justify further long time course analysis.

5.4 Discussion

We have established that the MDN1 gene undergoes a change in conformation depending on its transcriptional status. The ends of the MND1 locus could seldom be resolved as distinct spots when the strain was cultured in glucose. Under these conditions, multiple pathways act to maintain the GAL1 promoter in a repressed state. These include a decrease in levels of the Gal4p activator and the galactose permease enzyme (Gal2p), and activation of several glucose repressor proteins that act at the *GAL1* promoter (Johnston, Flick et al. 1994; Carlson 1998). Following growth in neutral carbon sources such as raffinose, these repressive pathways are not deployed and the GAL1 promoter is considered to be held in a poised state with activation prevented only by the inactivation of the Gal4 protein through its interaction with the

Gal80 repressor. Under these conditions, 9% of spots were distinguishable. However, following growth in galactose, this increased to 25%. Thus, spot separation was observed to be correlated with the carbon source as well as the transcription status anticipated from previous studies (Gilbert, Kristjuhan et al. 2004) and our own measurements by RT-PCR. There are several different potential explanations for the observed changes in conformation of this locus. In principle, spot separation profiles could result from changes in chromatin structure occurring independently of transcription. For example, in the glucose repressed state chromatin may be highly condensed, and some remodeling of chromatin may occur when glucose is removed prior to induction of substantial levels of transcription. An alternative explanation is that the changes in conformation reflect alterations coincident with bursts of transcription from the gal1 promoter. Given that nucleosomes have been observed to be depleted from a gal inducible MND1 gene (Schwabish and Struhl 2007), this latter explanation is attractive.

5.4.1 Separation distance is associated with full length transcripts and carbon source

Videos of the sample cultured in glucose, which is expected to inhibit transcription of the tagged copy of the *MDN1* gene, showed only 2% of all spots were measurably separate. The sample cultured in raffinose showed an intermediate spot separation profile where a low level of separation was seen in 9% of time points analyzed. The third sample, which was cultured in raffinose and galactose and was expected to transcribe the tagged *MDN1* gene, showed a third spot separation profile with 25% of cells showing separation. Thus, spot separation was observed to be correlated with

the carbon source as well as full length transcripts, and thus likely provides a real-time readout for transcription, in agreement with the model that transcription induced by the Gal1 promoter elicits a decrease in chromatin compaction. Additionally, raffinose exhibited a low level transcription spot separation profile, confirmed by RT-PCR and microscopy.

As mentioned previously, the Gal1 promoter has been observed to participate in promoter-terminator looping in a TFIIB-dependent manner during transcription .(Laine, Singh et al. 2009). It is possible that looping is occurring in the induced Gal1p-MDN1 strain, and that the percentage of cells transcribing is thus higher than 25%. This could be verified by making point mutations in proteins associated with the looping activity, such as Ssu72 and Rna15 (Singh and Hampsey 2007; El Kaderi, Medler et al. 2009).

The fact that this technique can detect three spot separation profiles from three carbon sources indicates that the RMS measurement error, while significant, is not great enough to render the approach unusable.

5.4.2 Observed changes in end-to-end spot separation distances

Reversible changes in end-to-end distance of ~500 nm within two seconds were detected in the galactose-induced strain, and this is the first time that such changes have been detected at this temporal resolution. These motions could reflect the flexibility of a molecule which can fold back on itself as well as the dynamic nature of chromatin subject to Brownian motion, or reflect random forces within the nucleus

acting on local chromatin, although there is no way for us to distinguish between these two possibilities.

A subset of the videos made of the Gal1p-MDN1 strain which show spots that either were initially colocalized and moved apart and stayed apart, or were initially separated and then came together and stayed together, may have captured either transcriptional initiation or termination events. A phenomenon known as transcriptional pulsing has been reported previously in *Dictyostelium*, yeast, and human, using independent methods including ChIP time courses (Metivier, Penot et al. 2003), FISH (Tan and van Oudenaarden 2010), and single molecule mRNA detection analysis (Chubb, Trcek et al. 2006). These studies indicate that, in a subset of genes at least, transcription does not occur non-stop, but rather in bursts separated by periods of inactivity. Our method may provide independent verification of such studies, as it is expected that discrete transcriptional events will be detectable through spot separation profiles using long time course analysis.

CLOSURE

To date, studies of chromatin structure have relied on chemical fixation of cells, analysis in non-physiological conditions, or 2D analysis, which may introduce measurement artefact, and have resulted in significant variation in interphase chromatin measurements from a number of different techniques.

A system of analysis of chromatin structure in 3D in living cells using the OMX microscope and the Danuser Lab tracking software has been developed, and proof of principle experiments demonstrate that the system is viable.

The results of the OMX live cell 3D fluorescence video microscopy experiments indicate that the system is sensitive enough to distinguish strains with two fluorescent spots which differ in their intervening genomic sequences by 30 kb, or with two spots separated by only 15 kb when the intervening gene is strongly induced. Additionally, using two separate methods, the live cell analysis has generated estimates for chromatin compaction in yeast that are on the order of at least one-half that calculated using FISH techniques (Guacci, Hogan et al. 1994; Bystricky, Heun et al. 2004), while corroborating estimates based on 3C (Dekker, Rippe et al. 2002).

Furthermore, the system finds no fixation artefact regarding the Bressan formaldehyde fixation method (Bressan, Vazquez et al. 2004) when comparing end-to-end separation using the top 5% method, although the data sets analyzed are small and the resolution of the system was suboptimal.

Similar experiments on the inducible *MDN1* strain, when considered in light of RTPCR analysis, indicate that the system likely provides a real-time readout for transcription. The system is sensitive enough to distinguish between subtle transcriptional spot separation profiles resulting from different carbon sources, and can detect changes in 3D end-to-end distance on a sub-second time scale.

Models for possible chromatin states described by the various experiments are presented in Figure 5.6.

The inducible strain system in its current form could be used to study the timing of initiation of transcriptional events post induction, the duration of transcriptional events, the latency period between transcriptional events, and the frequency of transcriptional events on a per-cell basis. With the addition of MS2 repeat sequences to the inducible gene, which would allow visualization of the transcript (Bertrand, Chartrand et al. 1998), the system could also potentially be used to study transcription and chromatin compaction simultaneously.

Several areas in the system have been identified where the spatial and temporal resolution of the system may be improved. By switching one of the fluors to a different wavelength the orientation-dependent limitation in resolution will be eliminated, and thus histogram bin sizes could be decreased. This would allow more accurate comparison of live versus fixed samples through the Chi Square test for independence, and could potentially allow detection of fixation artefact. Additionally, by switching a fluor, background GFP signal will drop, permitting shorter exposure

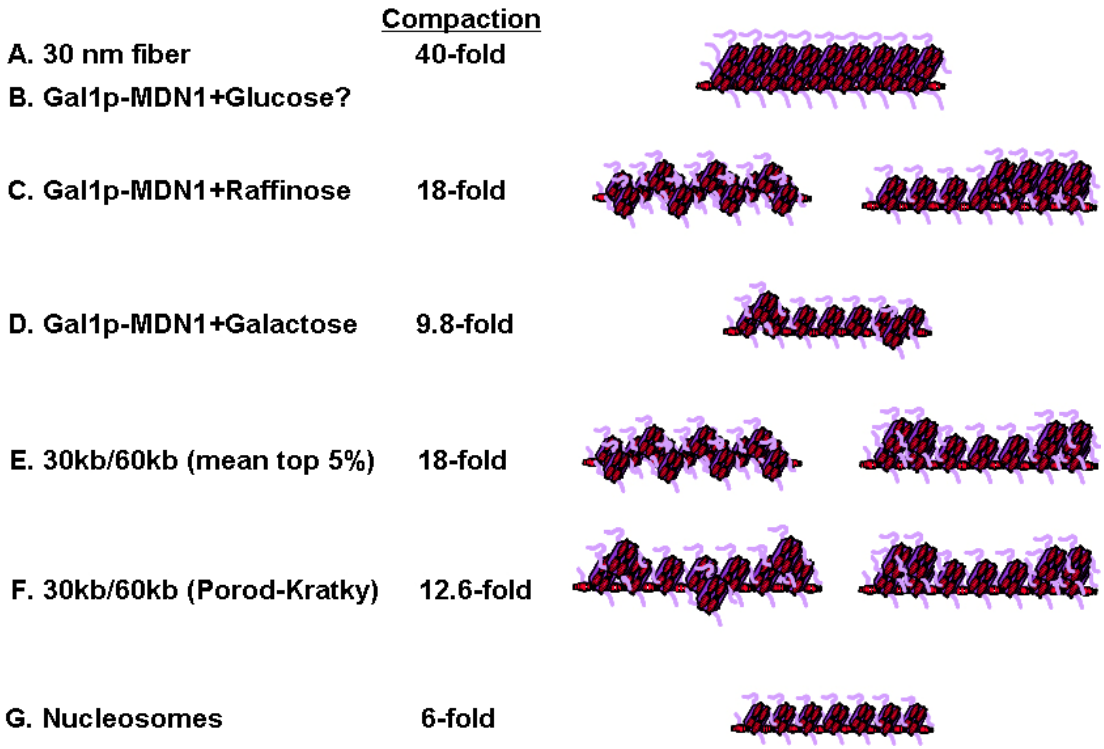

Figure 5.6 Chromatin state models. A. the 30 nm fiber, with 40-fold compaction. B. The Gal1p-MDN1 strain inhibited with glucose had colocalizing spots the majority of the time, which did not result in a compaction ratio estimate, although it can not be ruled out that the compaction ratio was as high as 40-fold, and thus can not rule out that the chromatin structure was that of the 30 nm fiber. C. The Gal1p-MDN1 strain cultured with raffinose exhibited an 18-fold compaction. The system was not able to determine whether this represents a new chromatin state (C, left cartoon), or whether this represents abortive transcription, where the first portion of the gene is transcribed, and thus remodeled, and the remainder is not (C, right cartoon), although the latter is most likely considering the 15 kb length of the transcription unit. D. The Gal1p-MDN1 strain cultured with galactose exhibited 9.8-fold compaction, which is similar to the compaction ratio expected for nucleosomal DNA. E. The compaction of chromatin as determined by the mean top 5% method. The cartoon at the left is meant to represent a novel state of chromatin with 18-fold compaction, although the cartoon at right, which represents sequences of condensed chromatin with higher compaction interspersed with sequences of less compact, transcribed chromatin, is more likely to be representative of the true chromatin state. Again, the system can not distinguish between these possibilities. F. The compaction of chromatin as determined by fitting of the Porod-Kratky chain equation. A similar rationale may be applied to F as to E. G. Nucleosomal DNA with 6-fold compaction.

times or increasing the signal to noise ratio, and thus improving resolution. Shorter exposure times could benefit the system in either of two ways: it would limit sample photobleaching, allowing for more time points to be acquired without affecting the viability of the sample, or it would permit the use of smaller step sizes, which could

increase resolution in z and could potentially reduce the RMS measurement error. Use of smaller step sizes would necessitate an increase in the number of images per stack. CFP is a likely candidate for a new fluor; however, switching to this color would require the purchase of a new laser and filter set. Anther possible choice is the DsRed derivative mTomato which is reported to be relatively photostable, although it has been characterized as having low quantum yields and thus reduced brightness, and multiple copies may need to be cloned in tandem to address this (Hoffman 2008).

A final possible improvement in the system would be to improve the image acquisition rate of the OMX microscope. Applied Precision has indicated that it has identified specific areas where such changes could be made which would optimize the data transfer rate from the cameras. Such changes would permit faster image acquisition, which would decrease the amount of diffusion from image to image during the generation of a stack and improve the RMS measurement error.

Such improvements would be useful in the study of chromatin compaction, the effects of transcription on chromatin compaction, and the study of the effects of individual factors, such as ATP-dependent chromatin remodeling enzymes, on chromatin compaction. For example, a change in fluors would permit the application of the Porod-Kratky chain equation to the live cell data sets and allow more accurate characterization of chromatin structure *in vivo*, perhaps providing independent verification of whether nucleosomal DNA is the predominant chromatin fiber in yeast or eukaryotic ES cells, or allowing more accurate characterization of the changes in chromatin fibers which occur during transcription.

REFERENCES

Abbott, D. W., V. S. Ivanova, et al. (2001). "Characterization of the stability and folding of H2A.Z chromatin particles: implications for transcriptional activation." J Biol Chem **276**(45): 41945-9.

Abrams, E., L. Neigeborn, et al. (1986). "Molecular analysis of SNF2 and SNF5, genes required for expression of glucose-repressible genes in Saccharomyces cerevisiae." Mol Cell Biol **6**(11): 3643-51.

Adams, C. C. and J. L. Workman (1995). "Binding of disparate transcriptional activators to nucleosomal DNA is inherently cooperative." Mol Cell Biol **15**(3): 1405-21.

Adolph, K. W. (1980). "Isolation and structural organization of human mitotic chromosomes." Chromosoma **76**(1): 23-33.

Ahmed, S., D. G. Brickner, et al. (2010). "DNA zip codes control an ancient mechanism for gene targeting to the nuclear periphery." Nat Cell Biol **12**(2): 111-8.

Andersson, K., R. Mahr, et al. (1982). "Rapid reformation of the thick chromosome fiber upon completion of RNA synthesis at the Balbiani ring genes in Chironomus tentans." Chromosoma **87**(1): 33-48.

Andrulis, E. D., A. M. Neiman, et al. (1998). "Perinuclear localization of chromatin facilitates transcriptional silencing." Nature **394**(6693): 592-5.

Aragon-Alcaide, L. and A. V. Strunnikov (2000). "Functional dissection of in vivo interchromosome association in Saccharomyces cerevisiae." Nat Cell Biol **2**(11): 812-8.

Ardehali, M. B. and J. T. Lis (2009). "Tracking rates of transcription and splicing in vivo." Nat Struct Mol Biol **16**(11): 1123-4.

Arents, G., R. W. Burlingame, et al. (1991). "The nucleosomal core histone octamer at 3.1 A resolution: a tripartite protein assembly and a left-handed superhelix." Proc Natl Acad Sci U S A **88**(22): 10148-52.

Auble, D. T., D. Wang, et al. (1997). "Molecular analysis of the SNF2/SWI2 protein family member MOT1, an ATP- driven enzyme that dissociates TATA-binding protein from DNA." Mol Cell Biol **17**(8): 4842-51.

Auble, D. T., D. Wang, et al. (1997). "Molecular analysis of the SNF2/SWI2 protein family member MOT1, an ATP-driven enzyme that dissociates TATA-binding protein from DNA." Mol Cell Biol **17**(8): 4842-51.

Awad, S., D. Ryan, et al. "The Snf2 homolog Fun30 acts as a homodimeric ATP-dependent chromatin-remodeling enzyme." J Biol Chem **285**(13): 9477-84.

Axelrod, D., Koppel, D., Schlessinger, J., Elson, E., Webb, W. (1976). "Mobility measurements by analysis of fluorescence photo-bleaching recovery kinetics." Biophys J **16**: 1055-1069.

Baker, T. A. and S. P. Bell (1998). "Polymerases and the replisome: machines within machines." Cell **92**(3): 295-305.

Barbaric, S., T. Luckenbach, et al. (2007). "Redundancy of chromatin remodeling pathways for the induction of the yeast PHO5 promoter in vivo." J Biol Chem **282**(38): 27610-21.

Basehoar, A. D., S. J. Zanton, et al. (2004). "Identification and distinct regulation of yeast TATA box-containing genes." Cell **116**(5): 699-709.

Bates, D. L., P. J. Butler, et al. (1981). "Stability of the higher-order structure of chicken-erythrocyte chromatin in solution." Eur J Biochem **119**(3): 469-76.
Bazett-Jones, D. P., R. Li, et al. (2008). "Elucidating chromatin and nuclear domain architecture with electron spectroscopic imaging." Chromosome Res **16**(3): 397-412.
Becker, P. B. and W. Horz (2002). "ATP-dependent nucleosome remodeling." Annu Rev Biochem **71**: 247-73.
Bednar, J., R. A. Horowitz, et al. (1998). "Nucleosomes, linker DNA, and linker histone form a unique structural motif that directs the higher-order folding and compaction of chromatin." Proc Natl Acad Sci U S A **95**(24): 14173-8.
Belmont, A. S. and K. Bruce (1994). "Visualization of G1 chromosomes: a folded, twisted, supercoiled chromonema model of interphase chromatid structure." J Cell Biol **127**(2): 287-302.
Berg, H. (1993). Random Walks in Biology. Princeton, Princeton University Press.
Bertrand, E., P. Chartrand, et al. (1998). "Localization of ASH1 mRNA particles in living yeast." Mol Cell **2**(4): 437-45.
Bhoite, L. T., Y. Yu, et al. (2001). "The Swi5 activator recruits the Mediator complex to the HO promoter without RNA polymerase II." Genes Dev **15**(18): 2457-69.
Bingham, N. H., Dunham, B. (1996). "Estimating Diffusion Coefficients from Count Data: Einstein-Smoluchowski Theory Revisited." Ann. Inst. Statist. Math. **49**(4): 667-679.
Bobola, N., R. P. Jansen, et al. (1996). "Asymmetric accumulation of Ash1p in postanaphase nuclei depends on a myosin and restricts yeast mating-type switching to mother cells." Cell **84**(5): 699-709.
Bode, J., C. Benham, et al. (2000). "Transcriptional augmentation: modulation of gene expression by scaffold/matrix-attached regions (S/MAR elements)." Crit Rev Eukaryot Gene Expr **10**(1): 73-90.
Bode, J., T. Schlake, et al. (1995). "Scaffold/matrix-attached regions: structural properties creating transcriptionally active loci." Int Rev Cytol **162A**: 389-454.
Bon, M., S. J. McGowan, et al. (2006). "Many expressed genes in bacteria and yeast are transcribed only once per cell cycle." FASEB J **20**(10): 1721-3.
Boulard, M., P. Bouvet, et al. (2007). "Histone variant nucleosomes: structure, function and implication in disease." Subcell Biochem **41**: 71-89.
Boy de la Tour, E. and U. K. Laemmli (1988). "The metaphase scaffold is helically folded: sister chromatids have predominantly opposite helical handedness." Cell **55**(6): 937-44.
Brazas, R. M. and D. J. Stillman (1993). "The Swi5 zinc-finger and Grf10 homeodomain proteins bind DNA cooperatively at the yeast HO promoter." Proc Natl Acad Sci U S A **90**(23): 11237-41.
Bressan, D. A., J. Vazquez, et al. (2004). "Mating type-dependent constraints on the mobility of the left arm of yeast chromosome III." J Cell Biol **164**(3): 361-71.
Bruno, M., A. Flaus, et al. (2003). "Histone H2A/H2B dimer exchange by ATP-dependent chromatin remodeling activities." Mol Cell **12**(6): 1599-606.
Bryant, G. O. and M. Ptashne (2003). "Independent recruitment in vivo by Gal4 of two complexes required for transcription." Mol Cell **11**(5): 1301-9.
Bulger, M. and M. Groudine (1999). "Looping versus linking: toward a model for long-distance gene activation." Genes Dev **13**(19): 2465-77.
Burke, D., Dawson, D., Stearns, T. (2000). Methods in Yeast Genetics. Cold Spring Harbor, Cold Spring Harbor Laboratory Press.

Bystricky, K., P. Heun, et al. (2004). "Long-range compaction and flexibility of interphase chromatin in budding yeast analyzed by high-resolution imaging techniques." Proc Natl Acad Sci U S A **101**(47): 16495-500.
Bystricky, K., T. Laroche, et al. (2005). "Chromosome looping in yeast: telomere pairing and coordinated movement reflect anchoring efficiency and territorial organization." J Cell Biol **168**(3): 375-87.
Cabal, G. G., A. Genovesio, et al. (2006). "SAGA interacting factors confine sub-diffusion of transcribed genes to the nuclear envelope." Nature **441**(7094): 770-3.
Cairns, B. R., H. Erdjument-Bromage, et al. (1998). "Two actin-related proteins are shared functional components of the chromatin-remodeling complexes RSC and SWI/SNF." Mol Cell **2**(5): 639-51.
Cairns, B. R., R. S. Levinson, et al. (1996). "Essential role of Swp73p in the function of yeast Swi/Snf complex." Genes Dev **10**(17): 2131-44.
Carlson, M. (1998). "Regulation of glucose utilization in yeast." Curr Opin Genet Dev **8**(5): 560-4.
Carmo-Fonseca, M. (2002). "New clues to the function of the Cajal body." EMBO Rep **3**(8): 726-7.
Carmo-Fonseca, M. (2007). "How genes find their way inside the cell nucleus." J Cell Biol **179**(6): 1093-4.
Carretero, M., S. Remeseiro, et al. (2010). "Cohesin ties up the genome." Curr Opin Cell Biol.
Carruthers, L. M., J. Bednar, et al. (1998). "Linker histones stabilize the intrinsic salt-dependent folding of nucleosomal arrays: mechanistic ramifications for higher-order chromatin folding." Biochemistry **37**(42): 14776-87.
Champoux, J. J. (2001). "DNA topoisomerases: structure, function, and mechanism." Annu Rev Biochem **70**: 369-413.
Chen, C. C., J. J. Carson, et al. (2008). "Acetylated lysine 56 on histone H3 drives chromatin assembly after repair and signals for the completion of repair." Cell **134**(2): 231-43.
Chuang, C. H., A. E. Carpenter, et al. (2006). "Long-range directional movement of an interphase chromosome site." Curr Biol **16**(8): 825-31.
Chubb, J. R., T. Trcek, et al. (2006). "Transcriptional pulsing of a developmental gene." Curr Biol **16**(10): 1018-25.
Clapier, C. R. and B. R. Cairns (2009). "The biology of chromatin remodeling complexes." Annu Rev Biochem **78**: 273-304.
Cloutier, T. E. and J. Widom (2004). "Spontaneous sharp bending of double-stranded DNA." Mol Cell **14**(3): 355-62.
Corey, L. L., C. S. Weirich, et al. (2003). "Localized recruitment of a chromatin-remodeling activity by an activator in vivo drives transcriptional elongation." Genes Dev **17**(11): 1392-401.
Cosgrove, M. S., J. D. Boeke, et al. (2004). "Regulated nucleosome mobility and the histone code." Nat Struct Mol Biol **11**(11): 1037-43.
Cosma, M. P. (2004). "Daughter-specific repression of Saccharomyces cerevisiae HO: Ash1 is the commander." EMBO Rep **5**(10): 953-7.
Cosma, M. P., S. Panizza, et al. (2001). "Cdk1 triggers association of RNA polymerase to cell cycle promoters only after recruitment of the mediator by SBF." Mol Cell **7**(6): 1213-20.

Cosma, M. P., T. Tanaka, et al. (1999). "Ordered recruitment of transcription and chromatin remodeling factors to a cell cycle- and developmentally regulated promoter." Cell **97**(3): 299-311.
Cote, J., J. Quinn, et al. (1994). "Stimulation of GAL4 derivative binding to nucleosomal DNA by the yeast SWI/SNF complex." Science **265**(5168): 53-60.
Cremer, T. and C. Cremer (2001). "Chromosome territories, nuclear architecture and gene regulation in mammalian cells." Nat Rev Genet **2**(4): 292-301.
Daganzo, S. M., J. P. Erzberger, et al. (2003). "Structure and function of the conserved core of histone deposition protein Asf1." Curr Biol **13**(24): 2148-58.
Davidson, M. W. (2010). "MicroscopyU." Resolution, 2010, from http://www.microscopyu.com/articles/formulas/formulasresolution.html.
Dechassa, M. L., B. Zhang, et al. (2008). "Architecture of the SWI/SNF-nucleosome complex." Mol Cell Biol **28**(19): 6010-21.
Dekker, J., K. Rippe, et al. (2002). "Capturing chromosome conformation." Science **295**(5558): 1306-11.
Donaldson, A. D. (2005). "Shaping time: chromatin structure and the DNA replication programme." Trends Genet **21**(8): 444-9.
Dorigo, B., T. Schalch, et al. (2003). "Chromatin fiber folding: requirement for the histone H4 N-terminal tail." J Mol Biol **327**(1): 85-96.
Dorigo, B., T. Schalch, et al. (2004). "Nucleosome arrays reveal the two-start organization of the chromatin fiber." Science **306**(5701): 1571-3.
Dorn, J. F., K. Jaqaman, et al. (2005). "Yeast kinetochore microtubule dynamics analyzed by high-resolution three-dimensional microscopy." Biophys J **89**(4): 2835-54.
Drew, H. R. and A. A. Travers (1985). "DNA bending and its relation to nucleosome positioning." J Mol Biol **186**(4): 773-90.
Drubin, D. A., A. M. Garakani, et al. (2006). "Motion as a phenotype: the use of live-cell imaging and machine visual screening to characterize transcription-dependent chromosome dynamics." BMC Cell Biol **7**: 19.
Duan, Z., M. Andronescu, et al. (2010). "A three-dimensional model of the yeast genome." Nature **465**(7296): 363-7.
Durand-Dubief, M., J. Persson, et al. (2010). "Topoisomerase I regulates open chromatin and controls gene expression in vivo." Embo J.
Eberharter, A. and P. B. Becker (2002). "Histone acetylation: a switch between repressive and permissive chromatin. Second in review series on chromatin dynamics." EMBO Rep **3**(3): 224-9.
El Kaderi, B., S. Medler, et al. (2009). "Gene looping is conferred by activator-dependent interaction of transcription initiation and termination machineries." J Biol Chem **284**(37): 25015-25.
Eltsov, M., K. M. Maclellan, et al. (2008). "Analysis of cryo-electron microscopy images does not support the existence of 30-nm chromatin fibers in mitotic chromosomes in situ." Proc Natl Acad Sci U S A **105**(50): 19732-7.
English, C. M., M. W. Adkins, et al. (2006). "Structural basis for the histone chaperone activity of Asf1." Cell **127**(3): 495-508.
English, C. M., N. K. Maluf, et al. (2005). "ASF1 binds to a heterodimer of histones H3 and H4: a two-step mechanism for the assembly of the H3-H4 heterotetramer on DNA." Biochemistry **44**(42): 13673-82.

Fan, X., Z. Moqtaderi, et al. (2010). "Nucleosome depletion at yeast terminators is not intrinsic and can occur by a transcriptional mechanism linked to 3'-end formation." Proc Natl Acad Sci U S A.

Faro-Trindade, I. and P. R. Cook (2006). "Transcription factories: structures conserved during differentiation and evolution." Biochem Soc Trans **34**(Pt 6): 1133-7.

Felsenfeld, G. and M. Groudine (2003). "Controlling the double helix." Nature **421**(6921): 448-53.

Fillingham, J., J. Recht, et al. (2008). "Chaperone control of the activity and specificity of the histone H3 acetyltransferase Rtt109." Mol Cell Biol **28**(13): 4342-53.

Finch, J. T. and A. Klug (1976). "Solenoidal model for superstructure in chromatin." Proc Natl Acad Sci U S A **73**(6): 1897-901.

Fisher-Adams, G. and M. Grunstein (1995). "Yeast histone H4 and H3 N-termini have different effects on the chromatin structure of the GAL1 promoter." Embo J **14**(7): 1468-77.

Fitzgerald D., A. J. (1999). "DNA structural and sequence determinants for nucleosome positioning." Gene Ther Mol Biol **4**: 349-362.

Flaus, A., D. M. Martin, et al. (2006). "Identification of multiple distinct Snf2 subfamilies with conserved structural motifs." Nucleic Acids Res **34**(10): 2887-905.

Flaus, A. and T. Owen-Hughes (2001). "Mechanisms for ATP-dependent chromatin remodelling." Curr Opin Genet Dev **11**(2): 148-54.

Fletcher, T. M. and J. C. Hansen (1996). "The nucleosomal array: structure/function relationships." Crit Rev Eukaryot Gene Expr **6**(2-3): 149-88.

Fletcher, T. M., N. Xiao, et al. (2002). "ATP-dependent mobilization of the glucocorticoid receptor during chromatin remodeling." Mol Cell Biol **22**(10): 3255-63.

Floer, M., X. Wang, et al. (2010). "A RSC/nucleosome complex determines chromatin architecture and facilitates activator binding." Cell **141**(3): 407-18.

Freeman, L., L. Aragon-Alcaide, et al. (2000). "The condensin complex governs chromosome condensation and mitotic transmission of rDNA." J Cell Biol **149**(4): 811-24.

Freitas, M. A., A. R. Sklenar, et al. (2004). "Application of mass spectrometry to the identification and quantification of histone post-translational modifications." J Cell Biochem **92**(4): 691-700.

Ganster, R. W., R. R. McCartney, et al. (1998). "Identification of a calcineurin-independent pathway required for sodium ion stress response in Saccharomyces cerevisiae." Genetics **150**(1): 31-42.

Garbarino, J. E. and I. R. Gibbons (2002). "Expression and genomic analysis of midasin, a novel and highly conserved AAA protein distantly related to dynein." BMC Genomics **3**(1): 18.

Gasser, S. M. (2001). "Positions of potential: nuclear organization and gene expression." Cell **104**(5): 639-42.

Gasser, S. M., T. Laroche, et al. (1986). "Metaphase chromosome structure. Involvement of topoisomerase II." J Mol Biol **188**(4): 613-29.

Gerchman, S. E. and V. Ramakrishnan (1987). "Chromatin higher-order structure studied by neutron scattering and scanning transmission electron microscopy." Proc Natl Acad Sci U S A **84**(22): 7802-6.

Ghaemmaghami, S., W. K. Huh, et al. (2003). "Global analysis of protein expression in yeast." Nature **425**(6959): 737-41.
Gietz, D., A. St Jean, et al. (1992). "Improved method for high efficiency transformation of intact yeast cells." Nucleic Acids Res **20**(6): 1425.
Gilbert, C., A. Kristjuhan, et al. (2004). "Elongator interactions with nascent mRNA revealed by RNA immunoprecipitation." Mol Cell **14**(4): 457-64.
Gkikopoulos, T., K. M. Havas, et al. (2009). "SWI/SNF and Asf1p cooperate to displace histones during induction of the saccharomyces cerevisiae HO promoter." Mol Cell Biol **29**(15): 4057-66.
Goldman, R., J. Swedlow, et al., Eds. (2010). Live Cell Imaging, A Laboratory Manual. Cold Spring Harbor, John Inglis.
Gondor, A. and R. Ohlsson (2009). "Chromosome crosstalk in three dimensions." Nature **461**(7261): 212-7.
Gong, Y., Y. Kakihara, et al. (2009). "An atlas of chaperone-protein interactions in Saccharomyces cerevisiae: implications to protein folding pathways in the cell." Mol Syst Biol **5**: 275.
Govind, C. K., F. Zhang, et al. (2007). "Gcn5 promotes acetylation, eviction, and methylation of nucleosomes in transcribed coding regions." Mol Cell **25**(1): 31-42.
Grant, P. A., D. E. Sterner, et al. (1998). "The SAGA unfolds: convergence of transcription regulators in chromatin-modifying complexes." Trends Cell Biol **8**(5): 193-7.
Guacci, V., E. Hogan, et al. (1994). "Chromosome condensation and sister chromatid pairing in budding yeast." J Cell Biol **125**(3): 517-30.
Guelen, L., L. Pagie, et al. (2008). "Domain organization of human chromosomes revealed by mapping of nuclear lamina interactions." Nature **453**(7197): 948-51.
Guillemette, B. and L. Gaudreau (2006). "Reuniting the contrasting functions of H2A.Z." Biochem Cell Biol **84**(4): 528-35.
Gutierrez, J. L., M. Chandy, et al. (2007). "Activation domains drive nucleosome eviction by SWI/SNF." Embo J **26**(3): 730-40.
Hajjoul, H., S. Kocanova, et al. (2009). "Lab-on-Chip for fast 3D particle tracking in living cells." Lab Chip **9**(21): 3054-8.
Hampsey, M. (1998). "Molecular genetics of the RNA polymerase II general transcriptional machinery." Microbiol Mol Biol Rev **62**(2): 465-503.
Hansen, J. C. (2002). "Conformational dynamics of the chromatin fiber in solution: determinants, mechanisms, and functions." Annu Rev Biophys Biomol Struct **31**: 361-92.
Hansen, J. C., C. Tse, et al. (1998). "Structure and function of the core histone N-termini: more than meets the eye." Biochemistry **37**(51): 17637-41.
Hassan, A. H., S. Awad, et al. (2006). "The Swi2/Snf2 bromodomain is required for the displacement of SAGA and the octamer transfer of SAGA-acetylated nucleosomes." J Biol Chem **281**(26): 18126-34.
Hassan, A. H., P. Prochasson, et al. (2002). "Function and selectivity of bromodomains in anchoring chromatin-modifying complexes to promoter nucleosomes." Cell **111**(3): 369-79.
Havas, K., A. Flaus, et al. (2000). "Generation of superhelical torsion by ATP-dependent chromatin remodeling activities." Cell **103**(7): 1133-42.
Heard, E. and W. Bickmore (2007). "The ins and outs of gene regulation and chromosome territory organisation." Curr Opin Cell Biol.

Heng, H. H., S. Goetze, et al. (2004). "Chromatin loops are selectively anchored using scaffold/matrix-attachment regions." J Cell Sci **117**(Pt 7): 999-1008.
Henikoff, S. (2009). "Labile H3.3+H2A.Z nucleosomes mark 'nucleosome-free regions'." Nat Genet **41**(8): 865-6.
Heun, P., T. Laroche, et al. (2001). "The positioning and dynamics of origins of replication in the budding yeast nucleus." J Cell Biol **152**(2): 385-400.
Heun, P., T. Laroche, et al. (2001). "Chromosome dynamics in the yeast interphase nucleus." Science **294**(5549): 2181-6.
Hiraga, S., S. Botsios, et al. (2008). "Histone H3 lysine 56 acetylation by Rtt109 is crucial for chromosome positioning." J Cell Biol **183**(4): 641-51.
Hirano, T. and T. J. Mitchison (1994). "A heterodimeric coiled-coil protein required for mitotic chromosome condensation in vitro." Cell **79**(3): 449-58.
Hirschhorn, J. N., S. A. Brown, et al. (1992). "Evidence that SNF2/SWI2 and SNF5 activate transcription in yeast by altering chromatin structure." Genes Dev **6**(12A): 2288-98.
Hizume, K., S. Araki, et al. (2007). "Topoisomerase II, scaffold component, promotes chromatin compaction in vitro in a linker-histone H1-dependent manner." Nucleic Acids Res **35**(8): 2787-99.
Hoffman, R. M. (2008). "A better fluorescent protein for whole-body imaging." Trends Biotechnol **26**(1): 1-4.
Holm, C. (1994). "Coming undone: how to untangle a chromosome." Cell **77**(7): 955-7.
Horvath, A. and H. Riezman (1994). "Rapid protein extraction from Saccharomyces cerevisiae." Yeast **10**(10): 1305-10.
Hoskins, L. (1997). "Yeast Genomic DNA Prep." from http://labs.fhcrc.org/hahn/Methods/mol_bio_meth/yeast_genom_dna.html.
Houtsmuller, A. B. (2005). "Fluorescence recovery after photobleaching: application to nuclear proteins." Adv Biochem Eng Biotechnol **95**: 177-99.
Hozak, P. and P. R. Cook (1994). "Replication factories." Trends Cell Biol **4**(2): 48-52.
Hu, Y., I. Kireev, et al. (2009). "Large-scale chromatin structure of inducible genes: transcription on a condensed, linear template." J Cell Biol **185**(1): 87-100.
Hunter, T. and M. Karin (1992). "The regulation of transcription by phosphorylation." Cell **70**(3): 375-87.
Hyland, E. M., M. S. Cosgrove, et al. (2005). "Insights into the role of histone H3 and histone H4 core modifiable residues in Saccharomyces cerevisiae." Mol Cell Biol **25**(22): 10060-70.
Iborra, F. J., A. Pombo, et al. (1996). "Active RNA polymerases are localized within discrete transcription "factories' in human nuclei." J Cell Sci **109 (Pt 6)**: 1427-36.
Ikeda, K., T. Mizutani, et al. (2010). "Intermediate structure between chromatin fibers and chromosome revealed by mechanical stretching and SPM measurement." Biochem Biophys Res Commun **400**(1): 181-6.
Jackson, D. A., S. J. McCready, et al. (1984). "Replication and transcription depend on attachment of DNA to the nuclear cage." J Cell Sci Suppl **1**: 59-79.
Jackson, D. A., A. Pombo, et al. (2000). "The balance sheet for transcription: an analysis of nuclear RNA metabolism in mammalian cells." FASEB J **14**(2): 242-54.

Jaskelioff, M., I. M. Gavin, et al. (2000). "SWI-SNF-mediated nucleosome remodeling: role of histone octamer mobility in the persistence of the remodeled state." Mol Cell Biol **20**(9): 3058-68.
Jensen, R., G. F. Sprague, Jr., et al. (1983). "Regulation of yeast mating-type interconversion: feedback control of HO gene expression by the mating-type locus." Proc Natl Acad Sci U S A **80**(10): 3035-9.
Jin, C., C. Zang, et al. (2009). "H3.3/H2A.Z double variant-containing nucleosomes mark 'nucleosome-free regions' of active promoters and other regulatory regions." Nat Genet **41**(8): 941-5.
Johnson, A. and M. O'Donnell (2005). "Cellular DNA replicases: components and dynamics at the replication fork." Annu Rev Biochem **74**: 283-315.
Johnston, M. and R. W. Davis (1984). "Sequences that regulate the divergent GAL1-GAL10 promoter in Saccharomyces cerevisiae." Mol Cell Biol **4**(8): 1440-8.
Johnston, M., J. S. Flick, et al. (1994). "Multiple mechanisms provide rapid and stringent glucose repression of GAL gene expression in Saccharomyces cerevisiae." Mol Cell Biol **14**(6): 3834-41.
Joshi, A. A. and K. Struhl (2005). "Eaf3 chromodomain interaction with methylated H3-K36 links histone deacetylation to Pol II elongation." Mol Cell **20**(6): 971-8.
Kabani, M., K. Michot, et al. (2005). "Anc1 interacts with the catalytic subunits of the general transcription factors TFIID and TFIIF, the chromatin remodeling complexes RSC and INO80, and the histone acetyltransferase complex NuA3." Biochem Biophys Res Commun **332**(2): 398-403.
Kagey, M., Newman, J., Bilodeau, S., Zhan, Y., Orlando, D., van Berkum, N., Ebmeier, C., Goossens, J., Rahl, P., Levine, S., Taatjes, D., Dekker, J., Young, R. (2010). "Mediator and cohesin connect gene expression and chromatin architecture." Nature **466**(7309).
Kaplan, N. (2010). "Nucleosome sequence preferences influence *in vivo* nucleosome organization." Nat Struct Mol Biol **17**(8): 918-920.
Kassabov, S. R., B. Zhang, et al. (2003). "SWI/SNF unwraps, slides, and rewraps the nucleosome." Mol Cell **11**(2): 391-403.
Kia, S. K., M. M. Gorski, et al. (2008). "SWI/SNF mediates polycomb eviction and epigenetic reprogramming of the INK4b-ARF-INK4a locus." Mol Cell Biol **28**(10): 3457-64.
Kireev, I., M. Lakonishok, et al. (2008). "In vivo immunogold labeling confirms large-scale chromatin folding motifs." Nat Methods **5**(4): 311-3.
Kitamura, E., J. J. Blow, et al. (2006). "Live-cell imaging reveals replication of individual replicons in eukaryotic replication factories." Cell **125**(7): 1297-308.
Knezetic, J. A. and D. S. Luse (1986). "The presence of nucleosomes on a DNA template prevents initiation by RNA polymerase II in vitro." Cell **45**(1): 95-104.
Knoepfler, P. S. and R. N. Eisenman (1999). "Sin meets NuRD and other tails of repression." Cell **99**(5): 447-50.
Kontoyiannis, D. P., Sagar, N., Hirschi, K. (1999). "Overexpression of Erg11p by the Regulatable GAL1 Promoter Confers Fluconazole Resistance in Saccharomyces cerevisiae." Antimicrobial Agents and Chemotherapy **43**(11): 2798-2800.
Kornberg, R. (1974). "Chromatin structure: a repeating unit of histones and DNA." Science **184**: 868-871.

Kornberg, R. D. and Y. Lorch (1999). "Twenty-five years of the nucleosome, fundamental particle of the eukaryote chromosome." Cell **98**(3): 285-94.
Kornberg, R. D. and J. O. Thomas (1974). "Chromatin structure; oligomers of the histones." Science **184**(139): 865-8.
Kortschak, R. D., P. W. Tucker, et al. (2000). "ARID proteins come in from the desert." Trends Biochem Sci **25**(6): 294-9.
Kouzarides, T. (2007). "Chromatin modifications and their function." Cell **128**(4): 693-705.
Kratky, O. and G. Porod (1949). "Diffuse small-angle scattering of X-rays in colloid systems." J Colloid Sci **4**(1): 35-70.
Krebs, J. E., M. H. Kuo, et al. (1999). "Cell cycle-regulated histone acetylation required for expression of the yeast HO gene." Genes Dev **13**(11): 1412-21.
Krogan, N. J., M. C. Keogh, et al. (2003). "A Snf2 family ATPase complex required for recruitment of the histone H2A variant Htz1." Mol Cell **12**(6): 1565-76.
Kundu, S., P. J. Horn, et al. (2007). "SWI/SNF is required for transcriptional memory at the yeast GAL gene cluster." Genes Dev **21**(8): 997-1004.
Kunkel, G. R. and H. G. Martinson (1981). "Nucleosomes will not form on double-stranded RNa or over poly(dA).poly(dT) tracts in recombinant DNA." Nucleic Acids Res **9**(24): 6869-88.
Kwon, H., A. N. Imbalzano, et al. (1994). "Nucleosome disruption and enhancement of activator binding by a human SW1/SNF complex." Nature **370**(6489): 477-81.
Laine, J. P., B. N. Singh, et al. (2009). "A physiological role for gene loops in yeast." Genes Dev **23**(22): 2604-9.
Langowski, J. S., H (2004). Chromatin Structure and Dynamics: State of the Art. New York, Elsevier.
Lawrence, J. B., R. H. Singer, et al. (1990). "Interphase and metaphase resolution of different distances within the human dystrophin gene." Science **249**(4971): 928-32.
Lee, T. I. and R. A. Young (2000). "Transcription of eukaryotic protein-coding genes." Annu Rev Genet **34**: 77-137.
Lee, W., D. Tillo, et al. (2007). "A high-resolution atlas of nucleosome occupancy in yeast." Nat Genet **39**(10): 1235-44.
Lenfant, F., R. K. Mann, et al. (1996). "All four core histone N-termini contain sequences required for the repression of basal transcription in yeast." Embo J **15**(15): 3974-85.
Leung, K. N., R. O. Vallero, et al. (2009). "Imprinting regulates mammalian snoRNA-encoding chromatin decondensation and neuronal nucleolar size." Hum Mol Genet **18**(22): 4227-38.
Li, B., M. Carey, et al. (2007). "The role of chromatin during transcription." Cell **128**(4): 707-19.
Li, J., S. Wang, et al. (2000). "Green fluorescent protein in Saccharomyces cerevisiae: real-time studies of the GAL1 promoter." Biotechnol Bioeng **70**(2): 187-96.
Li, Q., H. Zhou, et al. (2008). "Acetylation of histone H3 lysine 56 regulates replication-coupled nucleosome assembly." Cell **134**(2): 244-55.
Lippencott-Schwartz, J. (1998). *GFP Biofluorescence:* Imaging Gene Expression and Protein Dynamics in Living Cells, Academic Press.
Lleres, D., J. James, et al. (2009). "Quantitative analysis of chromatin compaction in living cells using FLIM-FRET." J Cell Biol **187**(4): 481-96.

Lohr, D., P. Venkov, et al. (1995). "Transcriptional regulation in the yeast GAL gene family: a complex genetic network." FASEB J **9**(9): 777-87.
Lorch, Y., J. W. LaPointe, et al. (1987). "Nucleosomes inhibit the initiation of transcription but allow chain elongation with the displacement of histones." Cell **49**(2): 203-10.
Lorch, Y., M. Zhang, et al. (1999). "Histone octamer transfer by a chromatin-remodeling complex." Cell **96**(3): 389-92.
Luger, K. (2006). "Dynamic nucleosomes." Chromosome Res **14**(1): 5-16.
Luger, K., T. J. Rechsteiner, et al. (1997). "Characterization of nucleosome core particles containing histone proteins made in bacteria." J Mol Biol **272**(3): 301-11.
Luger, K. and T. J. Richmond (1998). "DNA binding within the nucleosome core." Curr Opin Struct Biol **8**(1): 33-40.
Luger, K. and T. J. Richmond (1998). "The histone tails of the nucleosome." Curr Opin Genet Dev **8**(2): 140-6.
Luthra, R., S. C. Kerr, et al. (2007). "Actively transcribed GAL genes can be physically linked to the nuclear pore by the SAGA chromatin modifying complex." J Biol Chem **282**(5): 3042-9.
Maeshima, K., M. Eltsov, et al. (2005). "Chromosome structure: improved immunolabeling for electron microscopy." Chromosoma **114**(5): 365-75.
Mahy, N. L., P. E. Perry, et al. (2002). "Gene density and transcription influence the localization of chromatin outside of chromosome territories detectable by FISH." J Cell Biol **159**(5): 753-63.
Marsden, M. P. and U. K. Laemmli (1979). "Metaphase chromosome structure: evidence for a radial loop model." Cell **17**(4): 849-58.
Marshall, W. F., A. Straight, et al. (1997). "Interphase chromosomes undergo constrained diffusional motion in living cells." Curr Biol **7**(12): 930-9.
Mason, P. B. and K. Struhl (2003). "The FACT complex travels with elongating RNA polymerase II and is important for the fidelity of transcriptional initiation in vivo." Mol Cell Biol **23**(22): 8323-33.
McBryant, S. J., X. Lu, et al. (2010). "Multifunctionality of the linker histones: an emerging role for protein-protein interactions." Cell Res **20**(5): 519-28.
Meneghini, M. D., M. Wu, et al. (2003). "Conserved histone variant H2A.Z protects euchromatin from the ectopic spread of silent heterochromatin." Cell **112**(5): 725-36.
Mersfelder, E. L. and M. R. Parthun (2006). "The tale beyond the tail: histone core domain modifications and the regulation of chromatin structure." Nucleic Acids Res **34**(9): 2653-62.
Metivier, R., G. Penot, et al. (2003). "Estrogen receptor-alpha directs ordered, cyclical, and combinatorial recruitment of cofactors on a natural target promoter." Cell **115**(6): 751-63.
Michaelis, C., R. Ciosk, et al. (1997). "Cohesins: chromosomal proteins that prevent premature separation of sister chromatids." Cell **91**(1): 35-45.
Mizuguchi, G., X. Shen, et al. (2004). "ATP-driven exchange of histone H2AZ variant catalyzed by SWR1 chromatin remodeling complex." Science **303**(5656): 343-8.
Morse, R. H. (1992). "Transcribed chromatin." Trends Biochem Sci **17**(1): 23-6.
Munkel, C., R. Eils, et al. (1999). "Compartmentalization of interphase chromosomes observed in simulation and experiment." J Mol Biol **285**(3): 1053-65.

Natsume, R., M. Eitoku, et al. (2007). "Structure and function of the histone chaperone CIA/ASF1 complexed with histones H3 and H4." Nature **446**(7133): 338-41.
Neely, K. E., A. H. Hassan, et al. (2002). "Transcription activator interactions with multiple SWI/SNF subunits." Mol Cell Biol **22**(6): 1615-25.
Neigeborn, L. and M. Carlson (1984). "Genes affecting the regulation of SUC2 gene expression by glucose repression in Saccharomyces cerevisiae." Genetics **108**(4): 845-58.
Neves-Costa, A., W. R. Will, et al. (2009). "The SNF2-family member Fun30 promotes gene silencing in heterochromatic loci." PLOS One **4**(12): e8111.
Nissan, T. A., K. Galani, et al. (2004). "A pre-ribosome with a tadpole-like structure functions in ATP-dependent maturation of 60S subunits." Mol Cell **15**(2): 295-301.
Nunez, E., Y. S. Kwon, et al. (2008). "Nuclear receptor-enhanced transcription requires motor- and LSD1-dependent gene networking in interchromatin granules." Cell **134**(1): 189.
Ohlsson, R. and A. Gondor (2007). "The 4C technique: the 'Rosetta stone' for genome biology in 3D?" Curr Opin Cell Biol **19**(3): 321-5.
Ohniwa, R. L., K. Morikawa, et al. (2007). "Atomic force microscopy dissects the hierarchy of genome architectures in eukaryote, prokaryote, and chloroplast." Microsc Microanal **13**(1): 3-12.
Olave, I. A., S. L. Reck-Peterson, et al. (2002). "Nuclear actin and actin-related proteins in chromatin remodeling." Annu Rev Biochem **71**: 755-81.
Olins, A. L., D. E. Olins, et al. (1986). "DNA compaction during intense transcription measured by electron microscope tomography." Eur J Cell Biol **40**(1): 105-10.
Osborne, C. S., L. Chakalova, et al. (2004). "Active genes dynamically colocalize to shared sites of ongoing transcription." Nat Genet **36**(10): 1065-71.
Owen-Hughes, T. and J. L. Workman (1996). "Remodeling the chromatin structure of a nucleosome array by transcription factor-targeted trans-displacement of histones." Embo J **15**(17): 4702-12.
Paulson, J. R. and U. K. Laemmli (1977). "The structure of histone-depleted metaphase chromosomes." Cell **12**(3): 817-28.
Peckham, H. E., R. E. Thurman, et al. (2007). "Nucleosome positioning signals in genomic DNA." Genome Res **17**(8): 1170-7.
Pederson, D. S. and R. H. Morse (1990). "Effect of transcription of yeast chromatin on DNA topology in vivo." Embo J **9**(6): 1873-81.
Peng, G. and J. E. Hopper (2002). "Gene activation by interaction of an inhibitor with a cytoplasmic signaling protein." Proc Natl Acad Sci U S A **99**(13): 8548-53.
Peterson, C. L., Y. Zhao, et al. (1998). "Subunits of the yeast SWI/SNF complex are members of the actin-related protein (ARP) family." J Biol Chem **273**(37): 23641-4.
Petesch, S. J. and J. T. Lis (2008). "Rapid, transcription-independent loss of nucleosomes over a large chromatin domain at Hsp70 loci." Cell **134**(1): 74-84.
Phatnani, H. P. and A. L. Greenleaf (2006). "Phosphorylation and functions of the RNA polymerase II CTD." Genes Dev **20**(21): 2922-36.
Phelan, M. L., G. R. Schnitzler, et al. (2000). "Octamer transfer and creation of stably remodeled nucleosomes by human SWI-SNF and its isolated ATPases." Mol Cell Biol **20**(17): 6380-9.

Phillips, D. M. and E. W. Johns (1965). "A Fractionation of the Histones of Group F2a from Calf Thymus." Biochem J **94**: 127-30.
Platani, M., R. Santarella-Mellwig, et al. (2009). "The Nup107-160 nucleoporin complex promotes mitotic events via control of the localization state of the chromosome passenger complex." Mol Biol Cell **20**(24): 5260-75.
Pray-Grant, M. G., J. A. Daniel, et al. (2005). "Chd1 chromodomain links histone H3 methylation with SAGA- and SLIK-dependent acetylation." Nature **433**(7024): 434-8.
Prochasson, P., K. E. Neely, et al. (2003). "Targeting activity is required for SWI/SNF function in vivo and is accomplished through two partially redundant activator-interaction domains." Mol Cell **12**(4): 983-90.
Pugh, B. F. (2010). "A preoccupied position on nucleosomes." Nat Struct Mol Biol **17**(8): 923.
Qian, H., M. P. Sheetz, et al. (1991). "Single particle tracking. Analysis of diffusion and flow in two-dimensional systems." Biophys J **60**(4): 910-21.
Quinn, J., A. M. Fyrberg, et al. (1996). "DNA-binding properties of the yeast SWI/SNF complex." Nature **379**(6568): 844-7.
Rabl, C. (1885). "Uber Zellteilung." Morph Jb. **10**.
Raisner, R. M., P. D. Hartley, et al. (2005). "Histone variant H2A.Z marks the 5' ends of both active and inactive genes in euchromatin." Cell **123**(2): 233-48.
Rando, O. J. (2007). "Global patterns of histone modifications." Curr Opin Genet Dev **17**(2): 94-9.
Rando, O. J., K. Zhao, et al. (2000). "Searching for a function for nuclear actin." Trends Cell Biol **10**(3): 92-7.
Rattner, J. B. and C. C. Lin (1985). "Radial loops and helical coils coexist in metaphase chromosomes." Cell **42**(1): 291-6.
Richmond, E. and C. L. Peterson (1996). "Functional analysis of the DNA-stimulated ATPase domain of yeast SWI2/SNF2." Nucleic Acids Res **24**(19): 3685-92.
Richmond, T. J. and C. A. Davey (2003). "The structure of DNA in the nucleosome core." Nature **423**(6936): 145-50.
Ringrose, L., S. Chabanis, et al. (1999). "Quantitative comparison of DNA looping in vitro and in vivo: chromatin increases effective DNA flexibility at short distances." Embo J **18**(23): 6630-41.
Rino, J., T. Carvalho, et al. (2007). "A stochastic view of spliceosome assembly and recycling in the nucleus." PLoS Comput Biol **3**(10): 2019-31.
Rippe, K. (2001). "Making contacts on a nucleic acid polymer." Trends Biochem Sci **26**(12): 733-40.
Robinett, C. C., A. Straight, et al. (1996). "In vivo localization of DNA sequences and visualization of large-scale chromatin organization using lac operator/repressor recognition." J Cell Biol **135**(6 Pt 2): 1685-700.
Robinson, P. J. and D. Rhodes (2006). "Structure of the '30 nm' chromatin fibre: a key role for the linker histone." Curr Opin Struct Biol **16**(3): 336-43.
Roca, J. (2009). "Topoisomerase II: a fitted mechanism for the chromatin landscape." Nucleic Acids Res **37**(3): 721-30.
Rosa, A. and R. Everaers (2008). "Structure and dynamics of interphase chromosomes." PLoS Comput Biol **4**(8): e1000153.
Roth, S. Y., M. Shimizu, et al. (1992). "Stable nucleosome positioning and complete repression by the yeast alpha 2 repressor are disrupted by amino-terminal mutations in histone H4." Genes Dev **6**(3): 411-25.

Russo, P. and F. Sherman (1989). "Transcription terminates near the poly(A) site in the CYC1 gene of the yeast Saccharomyces cerevisiae." Proc Natl Acad Sci U S A **86**(21): 8348-52.
Sage, D., F. R. Neumann, et al. (2005). "Automatic tracking of individual fluorescence particles: application to the study of chromosome dynamics." IEEE Trans Image Process **14**(9): 1372-83.
Saha, A., J. Wittmeyer, et al. (2002). "Chromatin remodeling by RSC involves ATP-dependent DNA translocation." Genes Dev **16**(16): 2120-34.
Saha, A., J. Wittmeyer, et al. (2005). "Chromatin remodeling through directional DNA translocation from an internal nucleosomal site." Nat Struct Mol Biol **12**(9): 747-55.
Sambrook, J., E. F. Fritsch, et al. (1989). Molecular Cloning, A Laboratory Manual. Cold Spring Harbor, Cold Spring Harbor Laboratory Press.
Santisteban, M. S., T. Kalashnikova, et al. (2000). "Histone H2A.Z regulats transcription and is partially redundant with nucleosome remodeling complexes." Cell **103**(3): 411-22.
Sarma, N. J., T. M. Haley, et al. (2007). "Glucose-responsive regulators of gene expression in Saccharomyces cerevisiae function at the nuclear periphery via a reverse recruitment mechanism." Genetics **175**(3): 1127-35.
Satchwell, S. C., H. R. Drew, et al. (1986). "Sequence periodicities in chicken nucleosome core DNA." J Mol Biol **191**(4): 659-75.
Saxton, M. J. (1994). "Anomalous diffusion due to obstacles: a Monte Carlo study." Biophys J **66**(2 Pt 1): 394-401.
Scheer, U. (1987). "Structure of lampbrush chromosome loops during different states of transcriptional activity as visualized in the presence of physiological salt concentrations." Biol Cell **59**: 33-42.
Schoenfelder, S., T. Sexton, et al. (2010). "Preferential associations between co-regulated genes reveal a transcriptional interactome in erythroid cells." Nat Genet **42**(1): 53-61.
Schwabish, M. A. and K. Struhl (2004). "Evidence for eviction and rapid deposition of histones upon transcriptional elongation by RNA polymerase II." Mol Cell Biol **24**(23): 10111-7.
Schwabish, M. A. and K. Struhl (2006). "Asf1 mediates histone eviction and deposition during elongation by RNA polymerase II." Mol Cell **22**(3): 415-22.
Schwabish, M. A. and K. Struhl (2007). "The Swi/Snf Complex is important for histone eviction during transcriptional activation and RNA polymerase II elongation in vivo." Mol Cell Biol.
Sedat, J. and L. Manuelidis (1978). "A direct approach to the structure of eukaryotic chromosomes." Cold Spring Harb Symp Quant Biol **42 Pt 1**: 331-50.
Segal, E., Y. Fondufe-Mittendorf, et al. (2006). "A genomic code for nucleosome positioning." Nature **442**(7104): 772-8.
Shah, P. P., X. Zheng, et al. (2010). "Swi2/Snf2-Related Translocases Prevent Accumulation of Toxic Rad51 Complexes during Mitotic Growth." Mol Cell **39**(6): 862-72.
Shen, X., G. Mizuguchi, et al. (2000). "A chromatin remodelling complex involved in transcription and DNA processing." Nature **406**(6795): 541-4.
Shi, X., T. Hong, et al. (2006). "ING2 PHD domain links histone H3 lysine 4 methylation to active gene repression." Nature **442**(7098): 96-9.
Shiratori, A., T. Shibata, et al. (1999). "Systematic identification, classification, and characterization of the open reading frames which encode novel helicase-

related proteins in Saccharomyces cerevisiae by gene disruption and Northern analysis." Yeast **15**(3): 219-53.
Shogren-Knaak, M., H. Ishii, et al. (2006). "Histone H4-K16 acetylation controls chromatin structure and protein interactions." Science **311**(5762): 844-7.
Shogren-Knaak, M. and C. L. Peterson (2006). "Switching on chromatin: mechanistic role of histone H4-K16 acetylation." Cell Cycle **5**(13): 1361-5.
Simic, R., D. L. Lindstrom, et al. (2003). "Chromatin remodeling protein Chd1 interacts with transcription elongation factors and localizes to transcribed genes." Embo J **22**(8): 1846-56.
Singh, B. N. and M. Hampsey (2007). "A transcription-independent role for TFIIB in gene looping." Mol Cell **27**(5): 806-16.
Smith, C. L., R. Horowitz-Scherer, et al. (2003). "Structural analysis of the yeast SWI/SNF chromatin remodeling complex." Nat Struct Biol **10**(2): 141-5.
Spadafora, C., M. Bellard, et al. (1976). "The DNA repeat lengths in chromatins from sea urchin sperm and gastrule cells are markedly different." FEBS Lett **69**(1): 281-5.
Spector, D. L. (2003). "The dynamics of chromosome organization and gene regulation." Annu Rev Biochem **72**: 573-608.
Spencer, V. A. and J. R. Davie (1999). "Role of covalent modifications of histones in regulating gene expression." Gene **240**(1): 1-12.
Sprague, B. L., F. Muller, et al. (2006). "Analysis of binding at a single spatially localized cluster of binding sites by fluorescence recovery after photobleaching." Biophys J **91**(4): 1169-91.
Spring, H. and W. W. Franke (1981). "Transcriptionally active chromatin in loops of lampbrush chromosomes at physiological salt concentrations as revealed by electron microscopy of sections." Eur J Cell Biol **24**(2): 298-308.
St John, T. P. and R. W. Davis (1981). "The organization and transcription of the galactose gene cluster of Saccharomyces." J Mol Biol **152**(2): 285-315.
Stavreva, D. A. and J. G. McNally (2004). "Fluorescence recovery after photobleaching (FRAP) methods for visualizing protein dynamics in living mammalian cell nuclei." Methods Enzymol **375**: 443-55.
Staynov, D. Z. (2008). "The controversial 30 nm chromatin fibre." Bioessays **30**(10): 1003-9.
Sterner, D. E., P. A. Grant, et al. (1999). "Functional organization of the yeast SAGA complex: distinct components involved in structural integrity, nucleosome acetylation, and TATA-binding protein interaction." Mol Cell Biol **19**(1): 86-98.
Strahl, B. D. and C. D. Allis (2000). "The language of covalent histone modifications." Nature **403**(6765): 41-5.
Straight, A. F., A. S. Belmont, et al. (1996). "GFP tagging of budding yeast chromosomes reveals that protein-protein interactions can mediate sister chromatid cohesion." Curr Biol **6**(12): 1599-608.
Strukov, Y. G. and A. S. Belmont (2009). "Mitotic chromosome structure: reproducibility of folding and symmetry between sister chromatids." Biophys J **96**(4): 1617-28.
Studitsky, V. M., D. J. Clark, et al. (1994). "A histone octamer can step around a transcribing polymerase without leaving the template." Cell **76**(2): 371-82.
Sudarsanam, P., V. R. Iyer, et al. (2000). "Whole-genome expression analysis of snf/swi mutants of Saccharomyces cerevisiae." Proc Natl Acad Sci U S A **97**(7): 3364-9.

Sudarsanam, P. and F. Winston (2000). "The Swi/Snf family nucleosome-remodeling complexes and transcriptional control." Trends Genet **16**(8): 345-51.
Sullivan, E. K., C. S. Weirich, et al. (2001). "Transcriptional activation domains of human heat shock factor 1 recruit human SWI/SNF." Mol Cell Biol **21**(17): 5826-37.
Swedlow, J. (2010). In Vivo Imaging of Mammalian Cells. Live Cell Imaging, A Laboratory Manual. R. Goldman. Cold Spring Harbor, Cold Spring Harbor Laboratory Press.
Swedlow, J. R. and T. Hirano (2003). "The making of the mitotic chromosome: modern insights into classical questions." Mol Cell **11**(3): 557-69.
Taddei, A., G. Van Houwe, et al. (2006). "Nuclear pore association confers optimal expression levels for an inducible yeast gene." Nature **441**(7094): 774-8.
Takahata, S., Y. Yu, et al. (2009). "FACT and Asf1 regulate nucleosome dynamics and coactivator binding at the HO promoter." Mol Cell **34**(4): 405-15.
Talbert, P. B. and S. Henikoff (2010). "Histone variants--ancient wrap artists of the epigenome." Nat Rev Mol Cell Biol **11**(4): 264-75.
Tan, R. Z. and A. van Oudenaarden (2010). "Transcript counting in single cells reveals dynamics of rDNA transcription." Mol Syst Biol **6**: 358.
Tang, L., E. Nogales, et al. (2010). "Structure and function of SWI/SNF chromatin remodeling complexes and mechanistic implications for transcription." Prog Biophys Mol Biol **102**(2-3): 122-8.
Taylor, I. C., J. L. Workman, et al. (1991). "Facilitated binding of GAL4 and heat shock factor to nucleosomal templates: differential function of DNA-binding domains." Genes Dev **5**(7): 1285-98.
Thastrom, A., P. T. Lowary, et al. (1999). "Sequence motifs and free energies of selected natural and non-natural nucleosome positioning DNA sequences." J Mol Biol **288**(2): 213-29.
Thastrom, A., P. T. Lowary, et al. (2004). "Measurement of histone-DNA interaction free energy in nucleosomes." Methods **33**(1): 33-44.
Thoma, F., T. Koller, et al. (1979). "Involvement of histone H1 in the organization of the nucleosome and of the salt-dependent superstructures of chromatin." J Cell Biol **83**(2 Pt 1): 403-27.
Thomann, D., J. Dorn, et al. (2003). "Automatic fluorescent tag localization II: Improvement in super-resolution by relative tracking." J Microsc **211**(Pt 3): 230-48.
Thrash, C., A. T. Bankier, et al. (1985). "Cloning, characterization, and sequence of the yeast DNA topoisomerase I gene." Proc Natl Acad Sci U S A **82**(13): 4374-8.
Tirosh, I., N. Sigal, et al. "Divergence of nucleosome positioning between two closely related yeast species: genetic basis and functional consequences." Mol Syst Biol **6**: 365.
Tran, H. G., D. J. Steger, et al. (2000). "The chromo domain protein chd1p from budding yeast is an ATP-dependent chromatin-modifying factor." Embo J **19**(10): 2323-31.
Treich, I., B. R. Cairns, et al. (1995). "SNF11, a new component of the yeast SNF-SWI complex that interacts with a conserved region of SNF2." Mol Cell Biol **15**(8): 4240-8.
Tremethick, D. J. (2007). "Higher-order structures of chromatin: the elusive 30 nm fiber." Cell **128**(4): 651-4.

Trifonov, E. N. (1980). "Sequence-dependent deformational anisotropy of chromatin DNA." Nucleic Acids Res **8**(17): 4041-53.
Tumbar, T., G. Sudlow, et al. (1999). "Large-scale chromatin unfolding and remodeling induced by VP16 acidic activation domain." J Cell Biol **145**(7): 1341-54.
Turner, B. M. (2000). "Histone acetylation and an epigenetic code." Bioessays **22**(9): 836-45.
Ulbrich, C., M. Diepholz, et al. (2009). "Mechanochemical removal of ribosome biogenesis factors from nascent 60S ribosomal subunits." Cell **138**(5): 911-22.
Ushinsky, S. C., H. Bussey, et al. (1997). "Histone H1 in Saccharomyces cerevisiae." Yeast **13**(2): 151-61.
Utley, R. T., J. Cote, et al. (1997). "SWI/SNF stimulates the formation of disparate activator-nucleosome complexes but is partially redundant with cooperative binding." J Biol Chem **272**(19): 12642-9.
Uzunova, K., K. Gottsche, et al. (2007). "Ubiquitin-dependent proteolytic control of SUMO conjugates." J Biol Chem **282**(47): 34167-75.
Valouev, A., J. Ichikawa, et al. (2008). "A high-resolution, nucleosome position map of C. elegans reveals a lack of universal sequence-dictated positioning." Genome Res **18**(7): 1051-63.
van den Engh, G., R. Sachs, et al. (1992). "Estimating genomic distance from DNA sequence location in cell nuclei by a random walk model." Science **257**(5075): 1410-2.
van Holde, K. E. (1988). Chromatin. New York, Springer-Verlag.
Van Holde, K. E., J. R. Allen, et al. (1980). "DNA-histone interactions in nucleosomes." Biophys J **32**(1): 271-82.
van Vugt, J. J., M. Ranes, et al. (2007). "The ins and outs of ATP-dependent chromatin remodeling in budding yeast: biophysical and proteomic perspectives." Biochim Biophys Acta **1769**(3): 153-71.
Vazquez, J., A. S. Belmont, et al. (2001). "Multiple regimes of constrained chromosome motion are regulated in the interphase Drosophila nucleus." Curr Biol **11**(16): 1227-39.
Visa, N. and P. Percipalle (2010). "Nuclear functions of actin." Cold Spring Harb Perspect Biol **2**(4): a000620.
Volpi, E. V., E. Chevret, et al. (2000). "Large-scale chromatin organization of the major histocompatibility complex and other regions of human chromosome 6 and its response to interferon in interphase nuclei." J Cell Sci **113 (Pt 9)**: 1565-76.
Waga, S. and B. Stillman (1998). "The DNA replication fork in eukaryotic cells." Annu Rev Biochem **67**: 721-51.
Wang, L., R. A. Haeusler, et al. (2005). "Silencing near tRNA genes requires nucleolar localization." J Biol Chem **280**(10): 8637-9.
Wang, Y. M., J. O. Tegenfeldt, et al. (2005). "Single-molecule studies of repressor-DNA interactions show long-range interactions." Proc Natl Acad Sci U S A **102**(28): 9796-801.
Weake, V. M. and J. L. Workman (2008). "Clearing the way for unpaused polymerases." Cell **134**(1): 16-8.
Weake, V. M. and J. L. Workman (2010). "Inducible gene expression: diverse regulatory mechanisms." Nat Rev Genet **11**(6): 426-37.
West, R. W., Jr., S. M. Chen, et al. (1987). "GAL1-GAL10 divergent promoter region of Saccharomyces cerevisiae contains negative control elements in addition to

functionally separate and possibly overlapping upstream activating sequences." Genes Dev **1**(10): 1118-31.
White, C. L., R. K. Suto, et al. (2001). "Structure of the yeast nucleosome core particle reveals fundamental changes in internucleosome interactions." Embo J **20**(18): 5207-18.
White, R. (2001). Gene Transcription Mechanisms and Control. London, Blackwell Science Ltd**:** 4-7.
Whitehouse, I., A. Flaus, et al. (1999). "Nucleosome mobilization catalysed by the yeast SWI/SNF complex." Nature **400**(6746): 784-7.
Whitehouse, I. and T. Tsukiyama (2006). "Antagonistic forces that position nucleosomes in vivo." Nat Struct Mol Biol **13**(7): 633-40.
Widom, J. (2001). "Role of DNA sequence in nucleosome stability and dynamics." Q Rev Biophys **34**(3): 269-324.
Wiggins, P. A., T. van der Heijden, et al. (2006). "High flexibility of DNA on short length scales probed by atomic force microscopy." Nat Nanotechnol **1**(2): 137-41.
Winzeler, E. A., D. D. Shoemaker, et al. (1999). "Functional characterization of the S. cerevisiae genome by gene deletion and parallel analysis." Science **285**(5429): 901-6.
Wippo, C. J., B. S. Krstulovic, et al. (2009). "Differential cofactor requirements for histone eviction from two nucleosomes at the yeast PHO84 promoter are determined by intrinsic nucleosome stability." Mol Cell Biol **29**(11): 2960-81.
Wood, A. J., A. F. Severson, et al. (2010). "Condensin and cohesin complexity: the expanding repertoire of functions." Nat Rev Genet **11**(6): 391-404.
Wood, C. M., J. M. Nicholson, et al. (2005). "High-resolution structure of the native histone octamer." Acta Crystallogr Sect F Struct Biol Cryst Commun **61**(Pt 6): 541-5.
Woodcock, C. L. and S. Dimitrov (2001). "Higher-order structure of chromatin and chromosomes." Curr Opin Genet Dev **11**(2): 130-5.
Woodcock, C. L., A. I. Skoultchi, et al. (2006). "Role of linker histone in chromatin structure and function: H1 stoichiometry and nucleosome repeat length." Chromosome Res **14**(1): 17-25.
Workman, J. L. and R. E. Kingston (1998). "Alteration of nucleosome structure as a mechanism of transcriptional regulation." Annu Rev Biochem **67**: 545-79.
Wu, W. H., C. H. Wu, et al. (2009). "N Terminus of Swr1 Binds to Histone H2AZ and Provides a Platform for Subunit Assembly in the Chromatin Remodeling Complex." J Biol Chem **284**(10): 6200-7.
Xella, B., C. Goding, et al. (2006). "The ISWI and CHD1 chromatin remodelling activities influence ADH2 expression and chromatin organization." Mol Microbiol **59**(5): 1531-41.
Yanagida, M. (1990). "Higher-order chromosome structure in yeast." J Cell Sci **96 (Pt 1)**: 1-3.
Yang, J. G. and G. J. Narlikar (2007). "FRET-based methods to study ATP-dependent changes in chromatin structure." Methods **41**(3): 291-5.
Yocum, R. R., S. Hanley, et al. (1984). "Use of lacZ fusions to delimit regulatory elements of the inducible divergent GAL1-GAL10 promoter in Saccharomyces cerevisiae." Mol Cell Biol **4**(10): 1985-98.
Yokota, H., G. van den Engh, et al. (1995). "Evidence for the organization of chromatin in megabase pair-sized loops arranged along a random walk path in the human G0/G1 interphase nucleus." J Cell Biol **130**(6): 1239-49.

Yu, Q., H. Kuzmiak, et al. (2009). "Saccharomyces cerevisiae linker histone Hho1p functionally interacts with core histone H4 and negatively regulates the establishment of transcriptionally silent chromatin." J Biol Chem **284**(2): 740-50.
Yu, Y., Y. Teng, et al. (2005). "UV irradiation stimulates histone acetylation and chromatin remodeling at a repressed yeast locus." Proc Natl Acad Sci U S A **102**(24): 8650-5.
Yuan, G. C., Y. J. Liu, et al. (2005). "Genome-scale identification of nucleosome positions in S. cerevisiae." Science **309**(5734): 626-30.
Yudkovsky, N., J. A. Ranish, et al. (2000). "A transcription reinitiation intermediate that is stabilized by activator." Nature **408**(6809): 225-9.
Zhang, B. (2010). "Evidence against a genomic code for nucleosome positioning." Nat Struct Mol Biol **17**(8): 920-922.
Zhang, H., D. N. Roberts, et al. (2005). "Genome-wide dynamics of Htz1, a histone H2A variant that poises repressed/basal promoters for activation through histone loss." Cell **123**(2): 219-31.
Zhang, Y., Z. Moqtaderi, et al. (2009). "Intrinsic histone-DNA interactions are not the major determinant of nucleosome positions in vivo." Nat Struct Mol Biol **16**(8): 847-52.
Zhang, Z. and A. R. Buchman (1997). "Identification of a member of a DNA-dependent ATPase family that causes interference with silencing." Mol Cell Biol **17**(9): 5461-72.
Zheng, C. and J. J. Hayes (2003). "Intra- and inter-nucleosomal protein-DNA interactions of the core histone tail domains in a model system." J Biol Chem **278**(26): 24217-24.
Zheng, C. and J. J. Hayes (2003). "Structures and interactions of the core histone tail domains." Biopolymers **68**(4): 539-46.
Zhou, B. O., S. S. Wang, et al. (2010). "SWR1 complex poises heterochromatin boundaries for antisilencing activity propagation." Mol Cell Biol **30**(10): 2391-400.
Zlatanova, J., T. C. Bishop, et al. (2009). "The nucleosome family: dynamic and growing." Structure **17**(2): 160-71.
Zofall, M., J. Persinger, et al. (2006). "Chromatin remodeling by ISW2 and SWI/SNF requires DNA translocation inside the nucleosome." Nat Struct Mol Biol **13**(4): 339-46.

APPENDIX

A.1 Determine whether ATP-dependent chromatin remodeling enzymes catalyze transitions in higher order chromatin structure on a scale detectable by light microscopy

Experiment rationale

Chromatin structure has been examined previously in fixed yeast strains containing two fluorescently tagged, syntenic loci with varying amounts of genomic DNA separating them using a method where the modal distances between two spots were determined microscopically via FISH, and the Porod-Kratky chain equation was employed to estimate various characteristics of the chromatin, including persistence length, linear mass density, and the compaction ratio (Bystricky, Heun et al. 2004).

We chose to adopt a similar approach to determine whether ATP-dependent chromatin remodeling enzyme-catalyzed transitions in the structure of higher order chromatin might be made on a scale which would be detectable through microscopy. Deletions of *ris1*, *chd1*, *fin30*, and *irc5*, as well as the chaperone protein *asf1,* were generated in a 70 kb strain with one GFP and one CFP spot, and were analyzed microscopically for changes in chromatin compaction. Previously yeast strains with truncations in the N-terminal tail of histone H4 have been characterized as having decreased chromatin compaction compared to wild type (Fisher-Adams and Grunstein 1995; Lenfant, Mann et al. 1996). These truncations could serve as positive controls for the proposed analysis.

A.1.1 Background

A.1.1.1 Ris1

The Ris1/Uls1 enzyme is a member of the Snf2 family of DNA-dependent ATP-ases which contains a RING finger domain thought to play a role in proteolytic control of sumoylated substrates (Uzunova, Gottsche et al. 2007). Ris1 has recently been implicated in eviction of Rad51p from sites of homologous recombination in yeast, an activity it shares with Rad54p and Rds54p (Shah, Zheng et al.). It has been shown to associate with Sir4, a telomeric protein, and has been implicated in antagonizing silencing during mating type switching (Zhang and Buchman 1997). It also is reported to associate with Ebp2p, a nucleolar protein, in a SUMO-mediated manner (Uzunova, Gottsche et al. 2007). GFP-tagged Ris1p localizes to the nucleus (Ghaemmaghami, Huh et al. 2003), but no punctate expression has been reported.

A.1.1.2 Chd1

Chd1 (chromo-ATPase.helicsase-DNA binding domain 1) is an ATP-dependent chromatin remodeling enzyme of the Snf2 family which plays a role in the regulation of transcription elongation (Simic, Lindstrom et al. 2003) and has been shown to maintain the ordered spacing of nucleosomes at a subset of genes (Xella, Goding et al. 2006). It is associated with the expression of 2-4% of genes in yeast and shows some overlap in function with SWI/SNF (Tran, Steger et al. 2000). Chd1 is a component of both the SAGA and SLIK complexes, and thus links histone H3 lysine 4 methylation

through one of its chromodomains with downstream histone tail acetylation (Pray-Grant, Daniel et al. 2005).

A.1.1.3 Fun30

Function unknown now 30 (Fun30) is a Snf2 family chromatin remodeling enzyme which exhibits ATP-dependent nucleosomal sliding and dimer exchange activities (Awad, Ryan et al.). It has been shown to exhibit a gene silencing activity at the boundaries of the mating type loci and a role in cell-cycle progression (Neves-Costa, Will et al. 2009).

A.1.1.4 Irc5

A largely uncharacterized, putative Snf2 family helicase which contains a DEAD/H helicase-related sequence motif that shares sequence homology with the mammalian helicase HELLS (Shiratori, Shibata et al. 1999).

A.1.1.5 Asf1

Asf is a chaperone protein known to bind H3-H4 tetramers (Daganzo, Erzberger et al. 2003; English, Maluf et al. 2005; English, Adkins et al. 2006; Natsume, Eitoku et al. 2007) that assists in the removal and deposition of nucleosomes during a variety of cellular processes, such as transcription, DNA repair, and replication [reviewed in (Gong, Kakihara et al. 2009)]. Asf1 travels with transcribing Pol II at some loci and plays a role in histone eviction as well as histone deposition in a manner which may

transfer histones from in front of elongating Pol II to behind it (Schwabish and Struhl 2006). Additionally, Asf1 has been shown to be associated with the eviction of nucleosomes as a role in transcriptional initiation at a subset of loci (Takahata, Yu et al. 2009).

A.1.2 Experimental design

The cloning steps involved in this project are presented in the Mateials and Methods.

Strains were cultured overnight in YPAD and fixed with 1.8% formaldehyde as described in the Mateials and Methods. Fixed cells were analyzed with 3-dimensional fluorescence microscopy on the Tanaka lab Deltavision microscope using 200 msec exposure times, 5 μm stack heights, 200 nm step heights. Spots were located using Imaris software, three-dimensional distances between the two spots were calculated, and their mean distances were compared to the 70 kb parent strain.

A.1.3 Results

These data are presented in Figure A.1. The results indicate show no significant change in chromatin compaction upon deletion of the various enzymes. All strains show a wide distribution of spot separation distances.

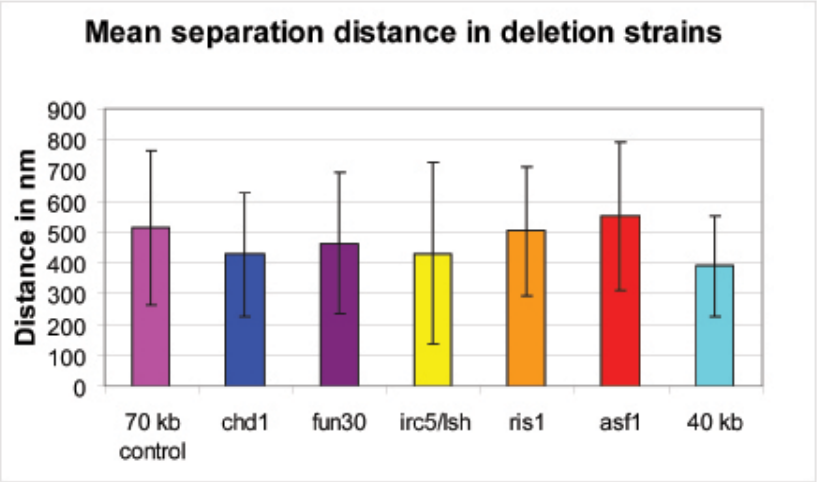

	Dist (nm)	Std Dev	n
70 kb control (n=126)	512	249	126
chd1 (n=38)	427	201	38
fun30 (n=46)	464	228	46
irc5/lsh (n=10)	431	294	10
ris1 (n=30)	502	211	30
asf1 (n=22)	552	241	22
40kb (n=127)	390	163	127

Figure A.1. The effects of deletion of individual ATP-dependent chromatin remodeling enzymes on spot separation distance in a 70 kb strain. Cells with one GFP spot and one CFP spot were fixed with 1.8% formaldehyde for 10 minutes at room temperature, then single stacks were taken with the Deltavision microscope. Spots were located with Imaris software (Bitplane), and the Pythagorean Theorum was used to calculate their separation distance in 3D. No significant effect on chromatin compaction was detected compared with the control. The asf1 chaperone deletion strain was also tested, and no significant change in chromatin compaction was detected. The 40 kb strain shows reduced standard deviation compared to the 70 kb strains.

A.1.4 Discussion of results

As can be seen from the graph, no significant differences in end-to-end distances were detected between the chromatin remodeling enzyme deletion strains and the wild type control strain. A great deal of variability was observed in the end-to-end distances of the various strains, and this is reflected in the large standard deviations found in Figure A.1 and was confirmed with 40 kb and 70 kb parent lines in live cell OMX analysis. Such variability confirms previous reports in the literature (Marshall,

Straight et al. 1997; Bystricky, Heun et al. 2004). It is likely that the deletions had no significant effect on higher order chromatin structure. This may be a consequence of the redundancy of function previously observed in chromatin remodeling enzymes (Barbaric, Luckenbach et al. 2007).

A.2

TetO	
ASM4	Nuclear pore complex subunit
LUC7	U1 snRNP complex subunit
YDL086W	Unchar, mitochondrial
YDL085C-A	Unchar
NDE2	Mitochondrial external NADH dehydrogenase
SUB2	Component of the TREX complex
RPS16B	40S ribosomal subunit
RPL13A	(60S) ribosomal subunit,
RPP1A	Ribosomal stalk protein
THI3	Protein involved in synthesis of HMP (thiamine precursor)
MRK1	Glycogen synthase kinase 3 (GSK-3) homolog
MDH3	Peroxisomal malate dehydrogenase
VAM6	Vacuolar protein
RXT3	Subunit of the RPD3L complex; involved in histone deacetylation
RPL31A	(60S) ribosomal subunit
SNR63	C/D box small nucleolar RNA (snoRNA)
BRE1	E3 ubiquitin ligase
YDL073W	Unchar
ARS413	Replication origin
YET3	Unchar, null mutant decreases the level of secreted invertase
YDL071C	Dubious
BDF2	involved in transcription initiation at TATA-containing promoters
CBS1	Mitochondrial translational activator
YDL068W	Dubious
COX9	Subunit VIIa of cytochrome c oxidase
IDP1	Mitochondrial NADP-specific isocitrate dehydrogenase
PEX19	Peroxisomal chaperone and import receptor
UBC9	SUMO conjugating enz
YDL063C	unchar, required for biogenesis of the large ribosomal subunit
YDL062W	dubious
RPS29B	40S ribosomal subunit
TSR1	Required for processing 20S pre-rRNA
RAD59	Double strand break repair
USO1	Involved in intracellular protein transport
YDL057W	Unchar
MBP1	Transcription factor involved in progression from G1 to S phase.
PSA1	GDP-mannose pyrophosphorylase (mannose-1-phosphate guanyltransferase), synthesizes GDP-mannose from GTP and mannose-1-phosphate in cell wall biosynthesis; required for normal cell wall structure.
LacO	

Table A.1. The 70 kb strains flank 36 genes with lac and tet operator arrays. The 40 kb strains share this lac operator array site, while the tet operator array is integrated between ARS413 and the YET3 gene, flanking 18 genes.

A.3 Plasmids, oligonucleotides, and yeast strains

The various plasmids, oligonucleotides, and yeast strains discussed in this study are presented in Tables A.2, A.3, and A.4, respectively.

Plasmid	Description	Origin
137	Shuttle	D. Dickerson
141	pFA13mycHIS3	Longtine
142	pC4N2RH5ZF3 FRB and FKBP plasmid	Ariad
145	Shuttle-SNF11	D. Dickerson
148	Shuttle-GGCN4	D. Dickerson
149	Shuttle-SNF6	D. Dickerson
153	Shuttle-FKBP	D. Dickerson
168	pRS416	D. Stillman
190	Yiplac204-Gal1Pro-MDN1	K. Struhl
196	pYCG-YLR106c MDN1	EUROSCARF
202	pRS416-TetO	D. Dickerson
206	pFA6-MDN1	D. Dickerson
207	pYiplac204-LacO	D. Dickerson

Table A.2. Plasmids used in this study. TOH Lab numbering system is used.

Primer	Sequence	Description
1487	ctgttcggagattaccgaatcaaa	TetO 5' jcn f
1488	ctgttgtaatcgttcttccacacggat	TetO 5' jcn r
1508	CTAGCAGATCTGACGCACTGCAACGCTTTAAATCCAATGGGTTTCTCACCATTG	TetR-GFP-GCN4 f
1509	ATGTCCCTAGGTCATTTAGCATCTTCTAGAACAGGAGTGGGTAA	TetR-GFP-GCN4 r
1516	CTAGTCCTAGGCGCCATGCAACGATGGGTGTCATCAAGAAGAAAAGATCGC	TetR-GFP-SNF6 f
1517	ATGTCTCCGGATTAAAAAAATACAGCATCAAGATCTCCAAATTCATC	TetR-GFP-SNF6 r
1518	CTAGTCCTAGGCGCCATGCAACGATGAGCAGTGAAATTGCCTACTCGAATAC	TetR-GFP-SNF11 f
1519	ATGTCTCCGGACTACCATATCTCGAACACTCTTGCCAAG	TetR-GFP-SNF11 r
1523	GGACAATTCAACGCGTCTGTGAGG	multi 5' check f
1524	Gcgttcaactagcagaccattatcaac	TetR-GFP fusions f
1526	ATCTGGGCAGATGATGTCGAGGC	TetR-GFP fusions r
1587	Tgttgactaatagcaataatggtagcagtaacaataacacacagaatacaggtcgacggatccccgggttaa	myc-tag Snf5 f
1588	CAAACCCGATTGCCAATCACACTGTTAC	Snf5-myc check f
1589	GACTACGTGTTCTTGTTATTCTCATGCTC	Snf5-myc check r
1610	TCCACGGTTATTTACATCTCCGGTATATTTTATATATGTGTATATATTTTTTAAACTGGATGGCGGCGTTAGTATCG	myc-tag Snf5 r
1634	Gtgctcctaccgtcaattaacatatcctg	SWI1-FRB check f
1635	TTAGTTGAGCCGCCCAAGATGTGAC	SWI1-FRB check r
1636	Ggaggaaatcaggtcgcagatagacc	SWI3-FRB check f
1637	CATGTACATAACATGTCTAGTCGAATCTAGAG	SWI3-FRB check r
1726	AGTCACATCAAGATCGTTTATGG	MAT f
1727	GCACGGAATATGGGACTACTTCG	MAT alpha r
1728	ACTCCACTTCAAGTAAGAGTTTG	MAT a r
1790	Ctatacactcatctttccgactactattggc	ash1 f
1792	Caagatgtttgaacgatttatgtcgtaagatcc	ash1 r
1795	GTTGGACGAGTCGGAATCGCAGAC	multi 3' check f
1796	CAAGATAAGCAAGCTTGCAGAAGTCAC	chd1 5' check r
1797	GGAAGGAACAATGGAAAATGTGGTGAAG	chd1 3' check r
1798	CTAAGAGGTCATCATCGCTATAATCGATG	CHD1 5' check r
1799	GAGATCATGAGCCCATCTCGCAATG	fun30 5' check r
1800	CTGAAATTGAAGCAGCACCACAAGATATC	fun30 3' check r
1802	CTATCTACTCTTTGCTTCTCTGCTCTAC	irc5 5' check r
1803	GAAAGTTATTTCTGAGAGGAACCGTCTGG	irc5 3' check r
1805	ACCGGACAGTTTACTTAGACTATGTAACG	ris1 check f
1805	ACCGGACAGTTTACTTAGACTATGTAACG	ris1 5' check r

Table A.3 Oligonucleotides

1806	GAGACGAGCTTCTTATATTGTATGTTACTAATGG	ris1 check r
1806	GAGACGAGCTTCTTATATTGTATGTTACTAATGG	ris1 3' check r
1808	CTCATCCTAAACGCGTAAATCTGTTCC	asf1 5' check r
1809	CGTGTGGCGTAGTCGGTAGC	asf1 3' check r
1957	CTATGCATCTAGAGAGGGCCGCATCATGTAATTAGTTATGTC	Cyc1 Terminator f
1958	TGAATCATGGATCCGGCCGCAAATTAAAGCCTTCGAG	Cyc1 Terminator r
1959	CTATGCAGAGCTCAGATCTagtctacgacTGATCACATTCCAGATCAGTATGGCAATCCGC	MDN1 3' end f
1960	CaggttTCTAGAttagctggatgccaggtctgtaaagtattgac	MDN1 3' end r
1988	GAAGCTGTAATCAATTCCAGAATCGCC	MDN1 5' RT-PCR f
1993	CTAACGGATCTCtgatcaTCTAGCCATTAGCCACGTGCATTCGTAATGTCTGCCCATTCTGC	URA3 promoter f
1994	GTCCTACGTCCGATGTAGTCGTAGGCGCCgggaatctcggtcgtaatgatttctataatgacg	URA3 downstream f
1995	CTGATTCATGCTTACAGCGAACATTcatatgCCAAGCCTTGTCCCAAGGCAGCG	URA3 downstream r
1996	GTCCTACGTCCGATGTAGTCGTAGTCGACGattcggtaatctccgaacagaaggaagaacg	URA3 promoter f
1997	CTGATTCATGCTTACAGCGAACATT**GGTGACC**GCGCGCGGCGCCTCTAGCATGCAGCCACGTGCATTCGTAATGTCTGCCCATTCTGC	URA3 promoter r
2003	GTGAAAGCATTTCGGGTAGTTCGCTTATATCG	MDN1 3' RT-PCR r
2004	GTCCTACGTCACGATCCGCGGGCATGCCTGATTCATGCTTACAGCGAACATT**C**ACGTGAAAGCATTTCGGGTAGTTCGCTTATATCGTGTACAAC	MDN1 fragment C f
2005	CCTCTAAAGTAGACATTAACTTAATCATTTTCGCG	MDN1 fragment A r
2008	GCATTCTACAAGCACATTCAACTAATTGG	MDN1 fragment C r
2013	GTCGTAGAGCTCGGCAAAGGAATAATCAGTACTGACAATAAAAAGATTC	TEF1 Terminator f
2014	CTGATTCATGCTTACAGCGAACATTCTCGAGTCGTTTTCGACACTGGATGGCGGC	TEF1 Terminator r
2015	GACACCGAGGTCACTAAGCTTGATTGTACTGAGAGTGCACCATACCACAGC	URA3 promoter r
2048	AGTCGTAGCGCGCatgtcccaggatagaattttgttagatttagacgtag	MDN1 fragment A f
2051	CGATTTAGTATCACGTCTTGGAGAAC	MDN1 3' RT-PCR f
2083	CATCGACATCACACTTCATGATGGAG	Act1 RT-PCR f
2084	CCCAGGATAGAATTTTGTTAGATTTAGACG	MDN1 5' RT-PCR r
2086	CTGTTCTTTTGACTGAAGCTCCAATG	Act1 RT-PCR r

Table A.3 Oligonucleotides cont.

Stock#	Mat Type	Description	Background	Source
1114	Mat a	GFP tagged HO, HIS::ahs1 LEU::cdc20 TRP::GALCDC20	W303	Trias Gkikopoulos
1115	Mat alpha	GFP tagged HO, LEU::cdc20 TRP::GALCDC20	W303	Trias Gkikopoulos
1154	Mat a	TetR-GFP at LEU2, TetO at 166K to 169K on chromosome XV	W303	Matt Renshaw
1160	Mat a	TetR-GFP at LEU2, TetO at 166K to 169K on chromosome XV, Snf5-myc	W303	David
1161	Mat a	TetR-GFP-GCN4 at LEU2, TetO at 166K to 169K on chromosome XV, Snf5-myc	W303	David
1168	Mat a	TetR-GFP-Snf11 at LEU2, TetO at 166K to 169K on chromosome XV, Snf5-myc	W303	David
1170	Mat a	TetR-GFP-Snf6 at LEU2, TetO at 166K to 169K on chromosome XV, Snf5-myc	W303	Hilary
1172	Mat a	TetR-GFP-FKBP at LEU2, TetO at 166K to 169K on chromosome XV, Snf5-myc	W303	Hilary
1182	Mat a	TetR-GFP-FKBP at LEU2, TetO at 166K to 169K on chromosome XV, Snf5-myc. SWI1-FRB	W303	Hilary
1194	Mat a	TetR-GFP-FKBP at LEU2, TetO at 166K to 169K on chromosome XV, Snf5-myc. SWI3-FRB	W303	Hilary
1196	Mat alpha	spc42::SPC42-GFP::KANMx6	W303	Tanaka Lab
1200	Mat a	TetR-3xCFP, GFP-LacI, TetOx224 at 298kb, LacOx256 at 358kb chromosome IV	W303	Etsushi Kitamura
1201	Mat a	TetR-3xCFP, GFP-LacI	W303	Toyoaki Natsume
1239	Mat a	Ris1-GFP	W303	Kim Nasmyth
1240	Mat a	Chd1-GFP	W303	Kim Nasmyth
1241	Mat	60kb with CFP/GFP hhf1::HIS3	W303	David
1242	Mat a	Fun30-GFP	W303	Kim Nasmyth
1243	Mat a	Irc5-GFP (lsh)	W303	Hilary Dewar
1331	Mat a	60kb with CFP/GFP, ris1	W303	David
1332	Mat a	60kb with CFP/GFP, chd1	W303	David
1333	Mat a	60kb with CFP/GFP, fun30	W303	David
1334	Mat a	60kb with CFP/GFP, irc5	W303	David
1335	Mat a	60kb with CFP/GFP, asf1	W303	David
1252	Mat a	30kb with GFP-LacI, TetR-2xCFP	W303	Toyoaki Natsume
1254	Mat alpha	Snf6-3xGFP, Snf11-3xGFP	W303	David
1255	Mat a	Net1-3xmyc::TRP1	W303	Ashwin Bhat
1256	Mat a	Net1-3HA::TRP1	W303	Ashwin Bhat
1260	Mat a	60kb with GFP-LacI, TetR-3xGFP	W303	David
1261	Mat a	TetR-3xGFP, GFP-LacI	W303	David
1262	Mat a	30kb with GFP-LacI, TetR-3xGFP	W303	David
1274	Mat alpha	cse4::Cse4-mCherry::kanNX4	W303	Tanaka Lab
1336	Mat a	60kb with GFP-LacI, TetR-mCherry	W303	David
1337	Mat a	30kb with GFP-LacI, TetR-mCherry	W303	David
1279	Mat a	TetR-GFP, GFP-LacI	W303	David
1280	Mat a	60kb with GFP-LacI, TetR-GFP	W303	David
1295	Mat a	15kb TetO-Gal1Pro-MDN1-LacO	W303	David
1300	Mat a	60kb with GFP-LacI, TetR-GFP	W303	David
1301	Mat a	30kb with GFP-LacI, TetR-GFP	W303	David

Table A.4 cont. Yeast strains